# EFFECT OF MEMANTINE ON RAT AND HUMAN NMDA RECEPTORS IN COMPARISON WITH HARMONIA AXYRIDIS EXTRACT

SUPERVISOR: DR IAN MELLOR

**Abdul Rehman 20400907**
**School of Life Sciences MRes Neuroscience**

## Table of Contents

# Acknowledgments

All praises to Allah the Almighty

I am very grateful and humbled to complete this research project under the supervision of Dr. Ian Mellor. Not only did I learn experimental approaches and lab protocols, but also had a deep understanding of the biophysics of Ion Channels. I am very thankful to Ian for his support and for providing me an opportunity to attend the GRC ion channels conference along with meeting fellow neuroscientists and sharing my research work. Moreover, I would like to pay thanks to Maryam Al Nasser for her support in helping us with DNA isolation and Mr. Liaque Latif for his help throughout the year in molecular biology techniques. I cannot forget the effort and cooperativeness of my lab colleagues and providing an open and cooperative lab environment and constant support.

## Abstract

Alzheimer's disease results in neuronal cell death, accumulation of amyloid-beta plaques, hyperphosphorylation of tau proteins, and ultimately, impairment of memory. Due to excessive glutamate in the synaptic cleft, NMDA receptor-dependent neurotransmission may be upregulated resulting in an excessive influx of $Ca^{2+}$ ions causing excitotoxicity. Currently, memantine is the only drug approved by the FDA targeting NMDA receptor-mediated excitotoxicity. NMDA receptors consist of combinations of two GluN1 and GluN2 subunits forming a hetero-tetrameric structure.

The purpose of this research was to analyze species-specific effects of memantine inhibition between humans and earlier research performed on rat NMDA receptors containing GluN1-1a subunits with GluN2A. We also compared the inhibition by an alkaloid extract from harlequin ladybirds containing 90% harmony (HAE), and memantine on human NMDA clones and the earlier performed experiments on rat clones. NMDA receptors were expressed in Xenopus oocytes and a two-electrode voltage clamp was used to measure responses to NMDA + glycine in the absence and presence of HAE and memantine. The $IC_{50}$ for memantine inhibition of rat GluN11a/GluN2A at holding potentials of -50mV, -75mV, and -100mV were 4.19µM, 1.45µM, and 1.84µM, respectively. The $IC_{50}$ for memantine at the same holding potentials in humanGluN11a/GluN2A were 3.4µM, 1.20µM, and 0.7µM respectively. The $IC_{50}$ for HAE inhibition of rat GluN1-1a/GluN2A at these holding potentials were 2.65µg/mL, 1.11µg/mL, and 1.75µg/mL, respectively. Whereas the $IC_{50}$ value for HAE inhibition of humanGluN1-GluN2a was 2.50µg/mL (8.80µM), 1.46µg/mL (5.16µM), and 0.86µg/mL (3.06µM), respectively.

In conclusion, memantine is effective at inhibiting human and rat NMDA receptors. Moreover, harmonine in HAE inhibits NMDA receptors with a similar mode of action as memantine. Memantine and HAE both showed voltage dependence inhibition. Moreover, the inhibition of HAE and memantine of NMDA receptors in rats and human NMDARs subtypes (GluN1-GluN2A) showed similarity in the terms of inhibition.

# Introduction

## 1.1 Background of Alzheimer's disease and NMDA Excitotoxicity:

Alzheimer's disease (AD) is a leading cause of death in the growing population, and the mortality rate has increased by 38% between 1990 and 2019 (Nichols and Vos, 2020). AD has two subtypes: early-onset AD (EOAD) and late-onset AD (LOAD) (Bekris et al., 2010). EOAD, which accounts for 1%-6% of all cases, occurs between the ages of 30-65 years. LOAD, which is the most common form of AD, starts after the age of 65. Around 60% of EOAD cases have familial AD, and 13% are inherited in an autosomal dominant pattern (Bekris et al., 2010).

The genetic aspect of EOAD has an autosomal dominant inheritance pattern. Three specific genes, including amyloid precursor protein (APP), presenilin 1 (PSEN1), and presenilin 2 (PSEN2), have been linked to neuropathic changes in the brain (Schellenberg and Montine, 2012). Among EOAD patients with onset before age 65 with an autosomal dominant pattern, 10%-15% of cases have an APP mutation, 20%-70% of cases are due to a PSEN1 mutation, and PSEN2 mutations are rare (Tsuang et al., 1999).

In 1984, Glenner and Wong identified a partial amino acid peptide sequence (Aβ peptide) on a cerebrovascular amyloid deposit from an AD patient, which allowed for the isolation and cloning of the APP gene by Kang et al on chromosome 21 in 1987 (Glenner and Wong, 1984). The discovery of APP on chromosome 21 explained why patients with Down syndrome develop amyloid deposits and AD neuropathological features at age 40 (Giaccone et al., 1989). APP is a single-pass transmembrane protein expressed ubiquitously, with Aβ peptides made from the proteolysis of APP by β-secretase and γ-secretase (Glenner and Wong, 1984). Aβ peptides are the main component of extracellular amyloid deposits, or plaques, that form in the brain parenchyma and the walls of cerebral vessels, leading to neuropathological changes in AD. The Swedish

mutation of APP involves a double substitution that increases Aβ peptide production, leading to the development of AD. The p. Val717Ile (V717I) mutation of Aβ peptides alters the activity of γ-secretase cleavage and is another cause of AD (Schellenberg and Montine, 2012).

The PSEN1 and PSEN2 genes are major components of the aspartyl protease complexes responsible for the γ-secretase cleavage of APP (Bekris et al., 2010). Missense mutations in PSEN1 cause 18% to 50% of autosomal dominant EOFAD and increase the ratio of Aβ42 to Aβ40 peptides. In contrast, missense mutations in the PSEN2 gene are a rare cause of EOFAD as it appears to be a less efficient producer of Aβ than PSEN1 (Theuns et al., 2000).

Late-onset AD (LOAD) is the second subtype associated with AD, and it involves apolipoprotein E (ApoE) genes. ApoE primarily functions in lipid metabolism and can act on Aβ trafficking, synaptic function, immune regulation, and intracellular signaling (Bekris et al., 2010). The APOE gene encodes 299 amino acid-containing protein isoforms, which include three common alleles called ε2, ε3, and ε4 (Bekris et al., 2010). These polymorphic alleles are haplotypes by two SNPs located in the coding region of the ε2 allele that has a cysteine (Cys) both at amino acid positions 112 and 158. Allele ε3 has a Cys at 112 and an arginine (Arg) at 158, while the ε4 allele has an Arg at 112 and 158. ApoE ε4 is a major risk factor for AD and has been linked to the progression of the disease and cognitive decline (Martins et al., 2005). The risk of AD in patients with a family history of AD increases with a higher number of ε4 alleles present in the patient, especially after age 65. Additionally, brain membranes with the ApoE ε4 subtype have shown more vulnerability to Aβ1-42-induced oxidative stress than brain membranes from the ε2 or ε3 subtypes. ApoE ε4-associated risk is also found in ethnic groups such as African Americans and Caribbean Hispanics (Yeung et al., 2019).

Moreover, the ε4 allele is the high-risk form of ApoE and developing AD, while the ε3 allele is the most common and considered a neutral allele (Romas et al., 2002). The ε2 allele of ApoE is associated with decreased risk of AD and having a genotype of ε4/ε4 is at higher risk than another person with an ε3/ε4 or ε2/ε4 genotype (Mahley and Rall, 1999). Women with an ApoE ε4/ε4

genotype have a 45% chance of developing AD by age 73 while men have a 25% risk of developing AD. However, the risk of AD is decreased for individuals with only one ApoE ε4 allele at age 87 or no ApoE ε4 allele at age 90. ApoE ε4 genotypes may also have an impact on certain onset ages in carriers of PSEN1 or PSEN2 mutations (Romas et al., 2002; Pastor et al., 2003).

To be diagnosed with AD, two distinct pathologies must be present such as the intracellular neurofibrillary tangles (NFTs) associated with microtubule binding tau protein and amyloid plaques from Aβ peptide (Murphy and LeVine, 2010). AD is characterized by the deposition of neurofibrillary tangles (NFTs) inside neurons. The human tau gene, located on chromosome 17, has six isoforms in the adult human brain. In normal physiology, the phosphorylation of tau protein maintains the cytoskeleton structure of microtubules, which plays a crucial role in the intracellular transport system and maintaining axoplasmic flow. (Goedert, Klug, and Crowther, 2006). The equilibrium of phosphorylated tau from protein kinases and unphosphorylated tau from protein phosphatases regulates the stability of microtubules in the cytoskeleton. However, in AD, an imbalance of the system occurs, causing excessive tau phosphorylation, which accumulates inside the cell and forms an insoluble aggregated pair of helical filaments (Andorfer et al., 2003). Two protein kinases, Glycogen synthase kinase 3β (GSK-3β) and cell division protein kinase 5 (CDK5), may be involved in the hyperphosphorylation of tau. This aggregation impairs axonal transport and can prevent normal neuronal metabolism, causing progressive neurodegeneration. Moreover, tau aggregation in AD has been reported to correlate with clinical dementia and cell death (Gong and Iqbal, 2008; Iqbal et al., 2005).

AD is characterized by the extracellular plaque deposits of the Aβ peptide, which is derived from the larger amyloid precursor protein (APP) (Kang et al., 1987). APP can be processed by two pathways: the non-amyloidogenic pathway, created by α-secretase cleavage, and the amyloidogenic pathway, involving β- and γ-secretase that create Aβ peptides (Schellenberg and Montine, 2012; Chen et al., 2017). Aβ peptides are crosslinked by tissue transglutaminase (TTG) and form hydrogen-bonded, parallel β-sheets to aggregate and produce amyloid plaques. The

slightly longer forms of Aβ, specifically Aβ1-42, are more hydrophobic and fibrillogenic, causing an increase in amyloid plaque in AD patients (Murphy and LeVine, 2010).

Structural changes, such as the β-strand conformation of Aβ1-42 residues, allow for quicker aggregation (Murphy and LeVine, 2010). Although a decline of cognition can occur before plaque deposition or detection of insoluble amyloid fibrils, Aβ monomer's ability to aggregate into different configurations such as oligomers and amyloid fibrils can lead to neurodegeneration and impairment of synaptic function (Mucke et al., 2000). Soluble Aβ oligomers have been shown to cause memory impairment and are a cause of neurodegeneration and impairment of synaptic function. Studies have shown that soluble oligomer deposits, rather than the most known insoluble amyloid plaques, show significant progression in AD (Danysz and Parsons, 2012).

APP is normally cleaved by γ-secretase to form a majority of Aβ1-40, with smaller amounts of Aβ1-42. However, APP mutations cause an increased Aβ1-42/Aβ1-40 ratio due to more Aβ42 production. Aβ1-42 is more prone to aggregate than Aβ1-40 and is involved in oxidative stress, neurodegeneration, and pathological changes in the glutamatergic system in AD (Citron, 2010; Yeung et al., 2019). Aβ1-42 is a peptide that can form stable tetramers and hexamers, leading to the formation of calcium-permeable channels in lipid membranes. This dysregulates $Ca^{2+}$ homeostasis and increases $Ca^{2+,}$ which can activate NADPH oxidase and generate ROS in astrocytes. Additionally, Aβ peptide oligomers can trigger neuronal damage through NMDAR-dependent $Ca^{2+}$ influx by binding to or near NMDAR (Lin, Bhatia, and Lal, 2001; De Felice et al., 2007). Chronic treatment with Aβ peptide oligomers can cause mitochondrial overload, depolarization, oxidative stress, and cell death in entorhinal/hippocampal cultures. However, NMDAR antagonists such as memantine can reduce the increasing concentration of $Ca^{2+}$ and delay the $Ca^{2+}$ - induced toxicity in the mitochondria (De Felice et al., 2007; Bieschke et al., 2011).

Recent studies have shown that Aβ oligomers (Aβ1-40, Aβ1-42) enhance glutamate neurotoxicity in human cortical cell cultures, leading to compromised calcium influx and enhanced calcium response to Excitatory Amino Acid (EAA) (Mattson et al., 1992). Soluble Aβ oligomers are also

involved in the phosphorylation of Tau. Aβ1-42 binds to forebrain synaptosomes linked with the postsynaptic complexes of NMDAR subunits GluN1 and GluN2B. Under the effect of amyloid beta treatment, the surface expression of the NMDA receptor subunit GluN1 and GluN2B is reduced, either by escalating the endocytosis of NMDAR or preventing surface delivery (Lacor et al., 2007). Some studies found that the GluN1 mRNA was decreased in AD patients, whereas other studies found it remained unchanged. However, mostly the mRNA of GluN2A and GluN2B were decreased in AD patients, and this happened mostly in the hippocampus and the entorhinal cortex (Hynd et al., 2004; Bi and Sze, 2002; Sze et al., 2001; Jacob et al., 2007).

Excitotoxicity resulting from excessive calcium influx can cause neuronal cell death through glutamatergic neurotransmission (Liu et al., 2019). Under normal conditions, NMDA receptors are activated by millimolar concentrations of glutamate, which are not sustained for long periods (Feldmeyer et al., 2002). However, during pathological activation, NMDA receptors are activated by lower concentrations of glutamate for longer durations. This leads to synaptic dysfunction and an inability of neurons to communicate efficiently with each other (Liu et al., 2019). Presynaptic glutamate release is necessary for efficient NMDA receptor transmission, as it leads to calcium influx and long-term potentiation, a significant mechanism for memory and learning. NMDA receptors have modulatory sites, including a voltage-dependent magnesium $Mg^{2+}$ block, which regulates calcium influx. At resting membrane potential, $Mg^{2+}$ blocks the $Ca^{2+}$ channel of NMDA receptors, inactivating them (Mayer, Westbrook, and Guthrie, 1984). However, during depolarization, the $Mg^{2+}$ block is removed, and NMDA receptors are unblocked, allowing calcium influx (Kampa et al., 2004). The duration of the $Mg^{2+}$ block impacts the rate of depolarization and NMDA receptor activation. The presynaptic release of glutamate removes the $Mg^{2+}$ block and allows calcium influx, which activates calcium-dependent calmodulin kinases and ultimately induces long-term potentiation (Wang and Reddy, 2017).

Glutamate, an excitatory neurotransmitter, plays a crucial role in learning and memory. However, maintaining the homeostasis of these neurotransmitters is equally important for proper brain function. Excessive release of glutamate and subsequent calcium influx can cause excitotoxicity,

which disrupts the activation of enzymes and proteins involved in long-term potentiation (LTP) (Dong et al., 2009). Different subtypes of N-methyl-D-aspartate receptors (NMDARs) serve unique functions in neuronal physiology and excitotoxicity. Specifically, the GluN2A and GluN2B subunits of NMDARs are localized at different locations due to their distinct electrophysiological and pharmacological properties. GluN2B subunits are preferentially located extrasynaptically, so excessive spillover of glutamate beyond synapses can lead to excitotoxicity. As a result, GluN2B-mediated death signaling is strongly favored over GluN2A (Li and Wang, 2016).

At the resting state, the concentration of glutamate is 0.6µM. Whereas during glutamatergic signaling and neurotransmission, it goes beyond 10µM in the synaptic cleft. Consequently, the slight disruption in ionotropic glutamate receptors causes underlying molecular changes i.e., learning and memory. Such symptoms at the neuronal level are widely reported in Alzheimer's, Huntington's disease, and multiple sclerosis. Therefore, this makes the ionotropic glutamate receptors prime targets for Alzheimer's therapy (Wang and Reddy, 2017). Moreover, amyloid beta plaques, being one of the causes of Alzheimer's, intervenes with excitotoxicity, cell death, and synaptic disruption. Under normal physiological conditions, amyloid beta peptides play a significant role in the synaptic mechanism. They stimulate presynaptic α7-nicotinic acetylcholine receptors, whereas, under pathological conditions, it forms dimers and trimers and, therefore, have a toxic effect on synapses causing excitotoxicity and cell death (Esposito et al., 2013).

The previous treatments for Alzheimer's focused on targeting NMDARs excitotoxicity, but the clinical efficacy of AChR was not efficient as in memantine. The challenge has been to inhibit the pathological activation of NMDARs without impairing the normal physiological synaptic transmission (Parsons, Danysz, and Quack, 1999). The only approved drug to date is memantine. It has an IC50 of around 1µM at -70mV and increases as holding potential shifts to a more positive value. Memantine is not always therapeutically successful and is neither a multi-ligand drug that could efficiently act as an ACh esterase inhibitor nor an NMDR antagonist. Cholinergic neurons that form the nucleus basalis of Meynert which are in the basal forebrain, are severely lost in AD (Ferreira-Vieira et al., 2016). Research has shown that cholinergic synapses are particularly

affected by Aβ oligomer's early neurotoxicity (Wong et al., 1999). This research focused on a drug harmonine targeting NMDAR subunits GluN1 and GluN2A. Moreover, the previous results showed harmonine to be efficient on nAChRs as well which will make it a multi-ligand drug.

## 1.2 Role of Cholinergic Neurotransmission in Memory:

Acetylcholine plays a very significant role in neurotransmission, synaptic plasticity, and memory. According to Ferreira-Vieira et al (2016), the cholinergic system plays a crucial role in memory and learning. It is also responsible for executive functioning, attention, and wakefulness. Moreover, it is also involved in making new memories and retrieval of old memories. Therefore, the breakdown of acetylcholine by acetylcholinesterase has a severe impact on cholinergic neurotransmission. Talesa (2001) describes that the presence of AChE is linked with neurotoxicity and amyloid components get triggered in its presence. The acetylcholine neurotransmitter level drops during Alzheimer's disease. The results from Alzheimer's patients have shown a 50% reduction in the α4β2 subtype levels, and they are the major nicotinic acetylcholine receptor in the brain along with α7-nAChR (Cheng, Lin, and Lane, 2021). Moreover, α7-nAChR has a specific binding affinity to Aβ (1-42) and is found within the brains of AD patients with Aβ (1-42) (Nagele et al., 2002).

According to Mufson et al (2008), there is a decline of acetylcholine-containing cell bodies as Alzheimer's progresses. Furthermore, the loss is seen in long projection neurons which innervate the cerebral cortex and hippocampus. The cholinergic synapses crucial for memory and learning are present in the brain. There is a high density of cholinergic synapses from the neocortex to the limbic system, thalamus, and striatum (Hampel et al., 2018). This suggests the significance of the neurotransmitter acetylcholine in memory, learning, and higher brain functions. Therefore, it becomes evident that acetylcholine esterase inhibitors can be a prime target to increase the levels of ACh. Thus, research suggests that AChE inhibitors limit ACh decline and help in neuronal functioning (Sharma, 2019). Moreover, the adrenergic and cholinergic systems are localized on

the dendritic spines and are thought to be involved in regulating glutamatergic neurotransmission (Sharma, 2019).

As it is clear now that AD does not only target NMDA neurotransmission. But it may also target nicotinic acetylcholine receptors as well by reducing Ach availability. α7-nAChR are somehow related to NMDAR and have an impact on glutamatergic synaptic transmission. Recent immunocytochemical work has shown that α7-nAChR is localized at postsynaptic asymmetric synapses. Most of these synapses are excitatory in nature and it has been shown that NMDARs are located on most asymmetric synapses (Nusser et al., 1998).

As discussed previously, α7-nAChR is the most significant subtype having an impact on NMDAR currents. α7-nAChR is localized in glutamate synapses in dlPFC and required for NMDA action. This shows the simultaneous working of α7-nAChR with NMDA in dlPFC (Yang et al., 2013). According to Markram and Segal (1992), the relation and action of acetylcholine on NMDARs are dependent on the region. In the CA1 region of the hippocampus, the action of acetylcholine on NMDARs is through muscarinic receptors. AChE inhibitor like donepezil has been shown to cause a reduction in the expression of GluN1 and NMDAR-mediated excitotoxicity (Shen et al., 2010).

Memantine also targets nicotinic acetylcholine receptors along with NMDARs. Studies have shown that it caused a reduction in the amplitude of whole-cell currents by α7-nAChR. It was more potent against α7-nAChR than NMDA. It had $IC_{50}$ of 0.34μM against α7-nAChR at -60mV.

## 1.3 Structure and Physiology of NMDA Receptor and Subunits:

The NMDA receptor plays a significant role in excitatory post-synaptic potentials and neuronal plasticity, regulating the late phase of EPSP. Voltage-dependent $Mg^{2+}$ blocks the NMDA channel, which regulates activation and depolarization rate (Dravid et al., 2007). Activation of these receptors causes alterations in synaptic plasticity through $Mg^{2+}$ regulation of NMDAR channels (Berberich et al., 2007).

The receptors exhibit spatiotemporal variation, with GluN2B and GluN2D more abundant during early development and GluN2A and GluN2C more widely expressed during late development. NMDA receptors require glycine and glutamate/NMDA as agonists for activation. Glutamate release in the synaptic cleft regulates NMDAR activation, as extracellular glycine is usually present at high concentrations at the synapse. Seven genes encode NMDAR subunits, including a single GRIN1 (encoding GluN1), four GRIN2 (encoding GluN2A-D), and two GRIN3 genes (encoding GluN3A-3B) (Hansen et al., 2018). GluN1 combines with GluN2 subunits to form a functional receptor, and the GluN1 subunit is abundant at excitatory synapses (Iacobucci et al., 2021; Berberich et al., 2007). Alternate splicing in GluN1 and GluN2 encodes the sequence for extracellular and intracellular domains, resulting in eight isoforms for GluN1 (Vrajová et al., 2010).

NMDA subunits, like all ionotropic glutamate receptor subunits, consist of an extracellular amino-terminal domain (ATD), an extracellular ligand-binding domain (LBD), a transmembrane domain, and an intracellular carboxy-terminal domain (Karakas and Furukawa, 2014).

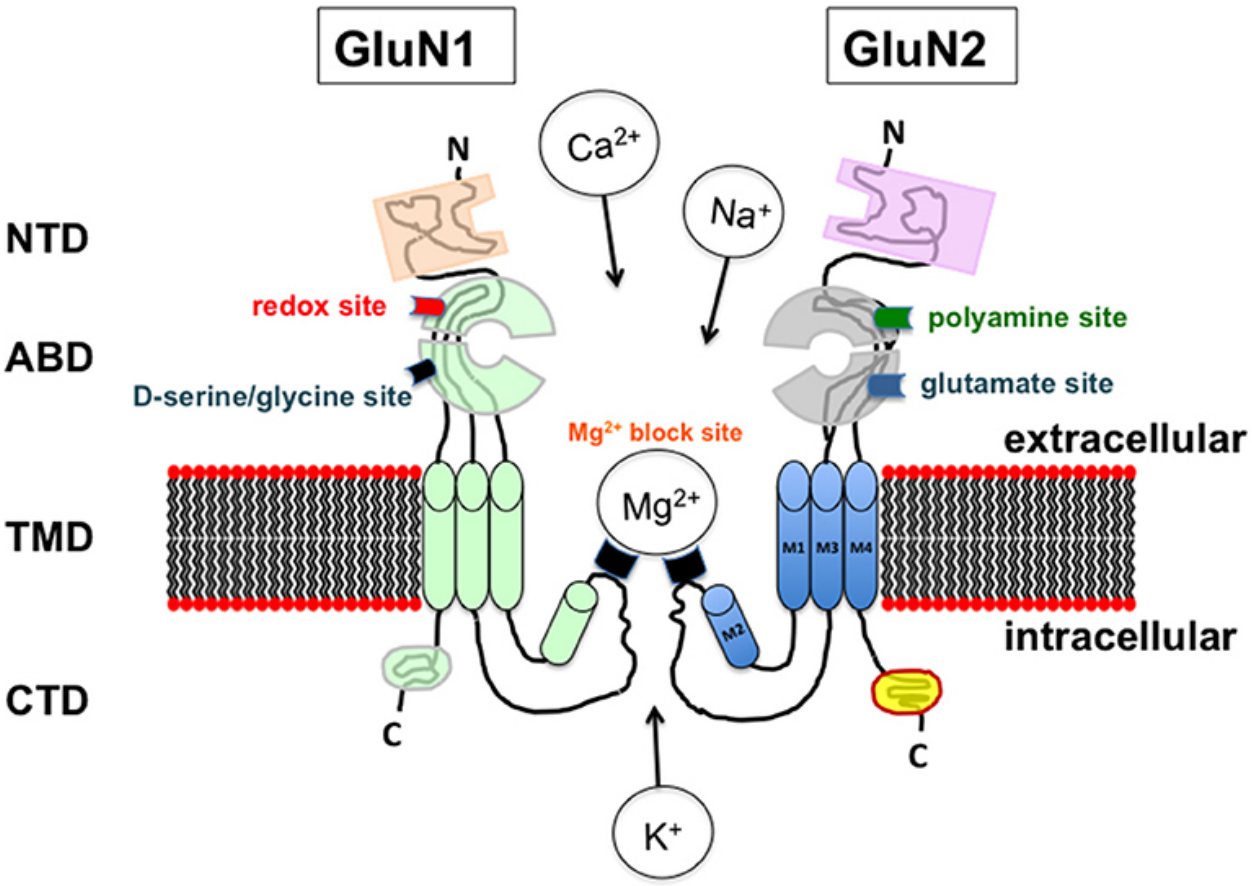


*Figure 1: Structure of NMDARs subtype GluN1 and GluN2 showing the extracellular NTD and ABD domain. Whereas an intracellular CTD domain is shown at the bottom. Two different binding sites are shown for GluN1 and GluN2 agonist binding sites and specific agonists I.e., glycine and glutamate with a pore region going inward at the M2 region. M2 region moving inward and showing the same site for endogenous Mg blocker (Billard, 2018).*

The N-methyl-D-aspartate (NMDA) receptor is composed of several molecular domains that control the unique properties of ion channel opening, deactivation, and intracellular signaling for neuroplasticity. The NMDA receptor has two main domains: the amino-terminal domain (ATD) and the ligand-binding domain (LBD). The ATD is responsible for ion channel opening probability and contains an allosteric modulator site where compounds like zinc, ifenprodil, and polyamines can bind as shown in figure 1. The LBD controls the opening and closing of the ion channel during depolarization, and it is connected to the transmembrane helices through short peptide linkers that link with the M1, M3, and M4 transmembrane domains (Iacobucci et al., 2021; Pabba, Hristova, and Biscaro, 2012).

The permeation properties of the ion channel are mainly controlled by the transmembrane domain, which has four membrane-inserted domains (M1-M4), where M2 forms an inward bend and pore containing asparagine residues at the Q/R/N site (Karakas and Furukawa, 2014). The Q/R/N site on the tip of the M2 loop causes a narrow constriction in the pore where water-containing ions are dehydrated for recognition. The Q/R site is called non-NMDARs due to a change in the mRNA level, while positively charged arginine (R) is found in GluA2, GluK1, and GluK2, rendering the channel $Ca^{2+}$ impermeable. However, the N site, called NMDARs, contains two heteromeric assemblies of NMDARs with two GluN1 and two GluN2 subunits, which have a higher selectivity for $Ca^{2+}$ than non-NMDARs. The Q/R/N site is very significant in determining the channel permeation and blockage by cations (Wollmuth, 2018; Parsons, Stöffler, and Danysz, 2007).

The conformational changes during ion channel opening, agonist-ligand binding, and desensitization are not yet fully understood. The binding of glycine and glutamate to the GluN1 and GluN2A LBD causes a conformational change, while depolarization causes the opening of the cation ion channel in the transmembrane region (Johnson and Kotermanski, 2006). NMDA channels possess two unique properties: they are blocked in a voltage-dependent manner by endogenous $Mg^{2+}$ and they are highly permeable to $Ca^{2+}$. The calcium influx activates a range of intracellular signaling pathways with potentially damaging consequences as shown in figure 2 (Iacobucci et al., 2021).

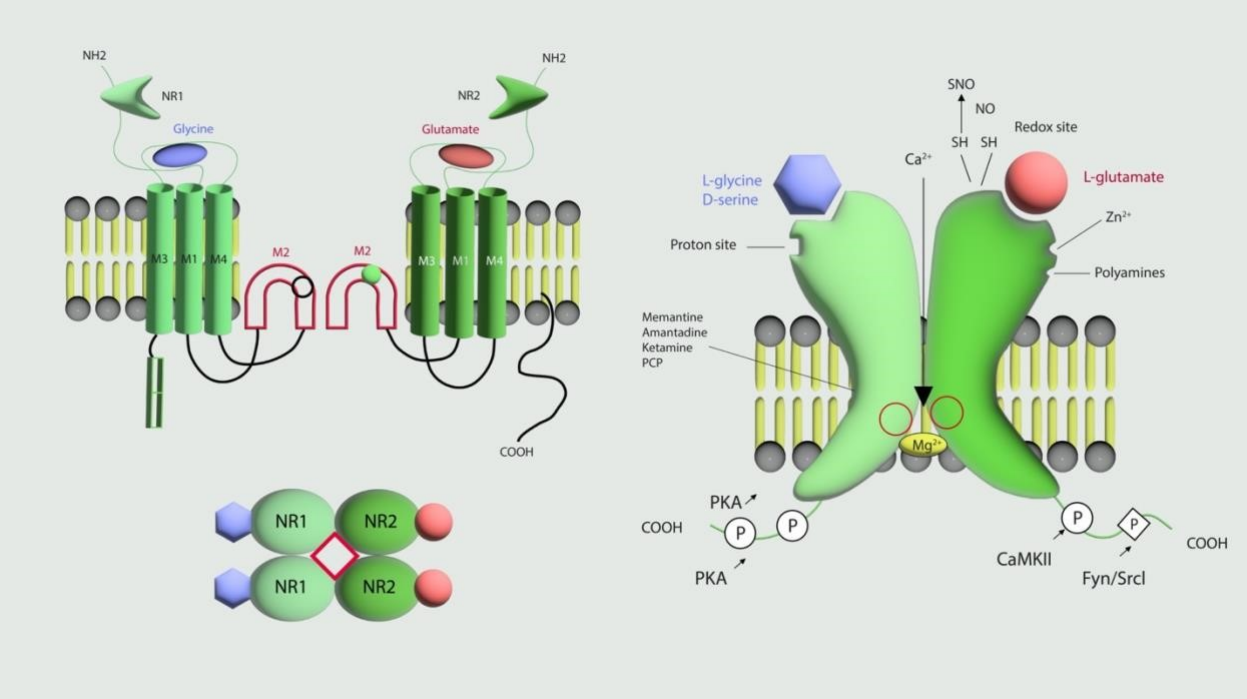


*Fig. 2: Structural and functional dynamics of the NMDA receptors. Showing different subunits and four different molecular domains in each subunit. Four transmembranes are shown with M2 moving inward forming the pore region and the $Mg^{+2}$ blocking site (Johnson and Kotermanski, 2006).*

## 1.4 Diverse pharmacology and Kinetics of NMDA subunits:

The NMDA receptor subunits, GluN2A and GluN2B share about 70% of their genetic code and amino acid sequence. However, they play distinct roles in learning and memory, as well as in neurodegenerative diseases. The conductance and permeation properties of the channel vary between the different subunits. GluN1A/2A and GluN1A/2B have higher channel conductance and calcium influx ability compared to GluN1/GluN2C and GluN2D (Wyllie, Livesey, and Hardingham, 2013).

The sensitivity of each subunit to the magnesium block is determined by the GluN2 subunit. GluN1-2A or GluN1-2B are blocked more strongly than other subunits, reflecting a difference in their voltage dependence (Kuner and Schoepfer, 1996). The affinity of each subunit to the agonist

is regulated by the LBD, with GluN2A exhibiting a different binding mode than other GluN2 subunits (Erreger et al., 2004)

The GluN2 subunit also determines calcium permeability, with specific asparagine residues in M2 responsible for increased efficiency. GluN2A and GluN2B have different channel opening kinetics, with GluN2A/GluN2B varying electrophysiological data. The channel opening probability is 3-5 times higher for GluN1/GluN2A than GluN1/GluN2B (Wyllie, Livesey, and Hardingham, 2013).

Furthermore, NMDARs containing GluN2B subunits have slower kinetics and deactivate more slowly than those containing GluN2A (Erreger et al., 2004). GluN2B-containing NMDARs exhibit slower decay responses than GluN2A-containing receptors. Studies using MK-801 have shown a decreased reduction in open channel probability in GluN2A than GluN2B subunit (Erreger et al., 2005; Erreger et al., 2004). The difference in both subunits' opening probability is not dependent on the receptor surface expression.

### 1.5 NMDA Antagonists and Mechanism of Action:

NMDA antagonists work by blocking the overstimulation and current flow through the channels of NMDA receptors. There are different drugs targeting various sites of NMDA receptors due to their structure. Competitive antagonists target the glutamate or glycine site of action and prevent further excitotoxicity in the brain regions. Whereas some non-competitive inhibitors may involve ion channel blockage and prevent calcium influx (Gonzales and Grotta, 2016). The antagonists bind to specific subunit sites of NMDA receptors According to Ogden and Traynelis (2011) some noncompetitive antagonists may bind to the transmembrane domain blocking the ion channels. The uncompetitive antagonists are open-channel blockers that bind in the pore/transmembrane region with the least impact on synaptic transmission (Olivares et al., 2012). Two examples of uncompetitive antagonists include ketamine and memantine (Cottone et al., 2013). The competitive inhibitor interaction at the glutamate site in the NMDARs is dependent on

the amino and two carboxylic moieties of glutamate (Lodge and Mercier, 2015). Two competitive antagonists at the GluN2 LBD are D-(−)-2-Amino-5-phosphonopentanoic acid (dAP5) and 1-(Phenanthrene-2-carbonyl) piperazine-2,3-dicarboxylic acid (PPDA) (Jespersen et al., 2014).

Memantine is a noncompetitive and uncompetitive NMDA inhibitor blocking the channels when they are excessively open (Cottone et al., 2013). Some noncompetitive inhibitors enter the open channels and bind to the blocking site located in the pores. Other blockers with slower kinetics can remain bound to the channels for a longer period. Memantine inhibition is concentration dependent, and the rate of fast block increases by increasing the concentration of memantine. The unblocking of memantine remains constant with concentration. Memantine can remain trapped after the removal of the agonist thus blocking the ion channel if it is reopened (Gilling et al., 2009). It has been found that the tendency of memantine to be trapped inside the channel is lower as compared to ketamine, phencyclidine, and MK801 due to its fast binding and unbinding kinetics (Blanpied et al., 1997, Sobolevsky and Koshelev, 1998, Johnson and Kotermanski, 2006).

### 1.6 Memantine:

Memantine blocks the NMDA receptor in a very specific way with double exponential kinetics. It binds to the ion channel only in the presence of the agonist. Memantine is used clinically, and its effective nature can be witnessed by its moderate affinity $IC_{50}$ value of 1µM, at –70mV, its fast blocking/unblocking kinetics, and its voltage dependency (Kotermanski, 2006). Therefore, it has a greater ability to leave the ion channel upon depolarization of the neuron. Memantine acts in a voltage-dependent manner with stronger inhibition at a more negative holding potential. According to Bresink et al (1996), memantine antagonized the application of 0.3-30µM L-glutamate in a concentration-dependent manner. The $IC_{50}$ values for GluN1/Glu2A and GluN1/GluN2B had $IC_{50}$ values at -70mV as shown in table 1. However, shifting the holding potential towards +60mV resulted in an increased $IC_{50}$ value of memantine.

| IC50 of GluN2A/GluN2B for Memantine at -70mV | |
|---|---|
| GluN1/2A | GluN1/2B |
| 0.93-1μM | 0.8-0.90μM |

*Table 1: $IC_{50}$ of GluN1/GluN2A and GluN1/GluN2B for Memantine at -70mV (Bresink et al., 1996)*

Memantine, unlike phencyclidine, ketamine, and MK801, has a lower affinity, shorter dwelling time on receptors, and is well tolerated clinically. It acts in a very similar way to Magnesium, closing the channels during pathological over-activation of NMDA receptors, while still allowing the physiological signals essential for synaptic transmission. Moreover, it's the only approved drug till now acting as an antagonist of NMDARs (Liu et al., 2019). Memantine is a low-affinity drug avoiding long-term receptor blockage to avoid negative impacts on learning and memory. It only targets the channel under pathological activation because of increased glutamate in the synaptic cleft (Folch et al., 2018). It provides a balance between normal physiological activity and excessive extrasynaptic activity (Cheng, Lin, and Lane, 2021).

Memantine being an open channel blocker works only in the presence of an agonist and it has the mutual site of action as magnesium block. Thus, the evidence suggests that N-site residues of asparagine in M2 of subunits GluN1 and GluN2 affects the memantine block (Johnson and Kotermanski, 2006).

According to Buisson and Bertrand (1998), the effectivity of memantine was tested against α4β2-nAChR expressed in human embryonic kidney (HEK-293) cells. The whole cell current showed to be effective (14μM) for the ion channel block as well. Furthermore, memantine has been

effective in α9/α10 heteromeric nAChRs in Xenopus oocytes with $IC_{50}$ as shown in table 2 (Oliver et al., 2001). Also, Memantine is effective against serotonin and dopamine uptake at high concentrations as shown in table 2. Moreover, it also targets nicotinic acetylcholine receptors and sodium channels as well. However, electrophysiological recordings and behavioral studies showed a lack of anticholinergic effect in Alzheimer's. Thus, memantine through targets the nicotinic acetylcholine receptors but not at a therapeutic concentration (Maskell et al., 2003).

| $IC_{50}$ of memantine in nAChRs and serotonin and dopamine | |
|---|---|
| α4β2-nAChR (Memantine) | 14μM |
| α9/α10 (Memantine) | 1μM |
| serotonin and dopamine | 10-500μM |

Table 2: $IC_{50}$ of memantine in nAChRs and serotonin and dopamine (Oliver et al., 2001; Maskell et al., 2003)

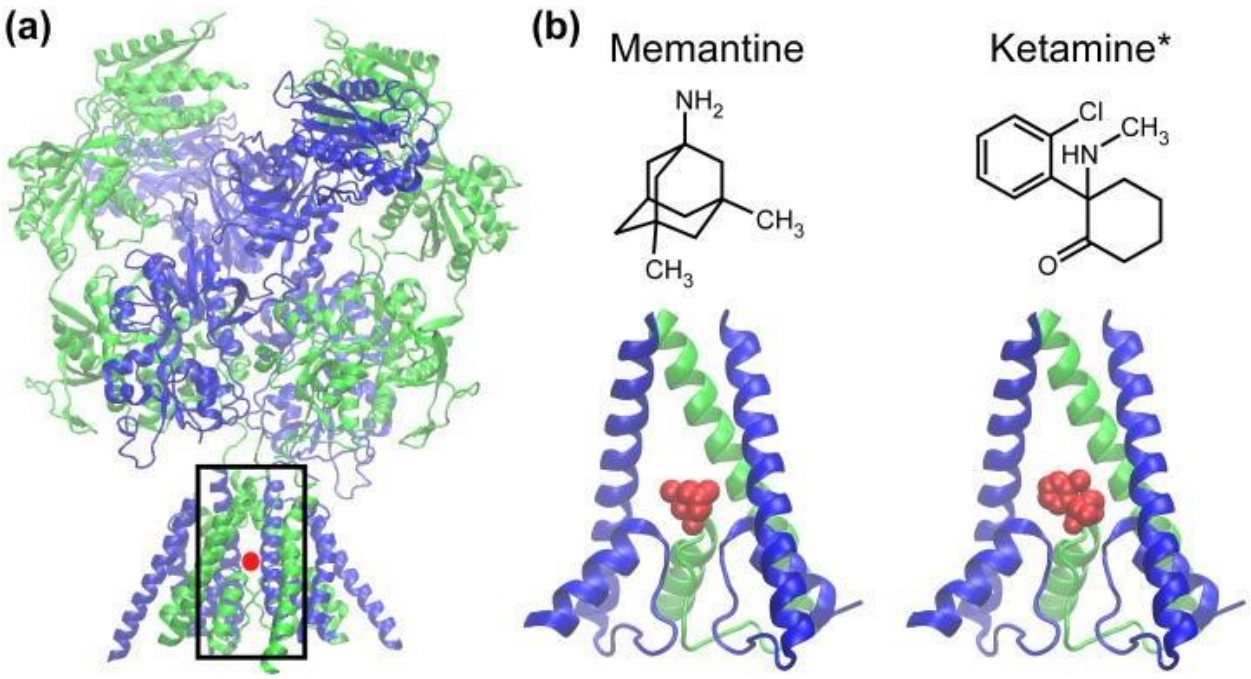


*Fig. 3: X-ray crystal structure of NMDA subunits GluN1 and GluN2B with binding site shown as a red point. (b) is the three-ring structure of memantine with a bridgehead amine (NH2). Ketamine is shown at the right with two enantiomers. GluN1 and GluN2A at the bottom can be seen with the binding site of ketamine and memantine (Johnson, Glasgow, and Povysheva, 2015).*

### 1.7 NMDA antagonists used in the experimentation of AD patients:

NMDA antagonists that have been proposed for use in AD therapy target the high calcium influx that can lead to neuronal cell death. NMDAR antagonists like phencyclidine, ketamine, MK-801, and memantine all target glutamate-mediated excitotoxicity and cell death (Liu et al., 2019). Ketamine is a noncompetitive NMDA inhibitor targeting the ion channel. However, it does not bind the closed channels but rather in an open state (MacDonald, Miljkovic, and Pennefather, 1987). The patch-clamp study in mouse hippocampal neurons showed that ketamine blocks the excitatory currents in a highly voltage-dependent manner. However, the concentration changes of ketamine had less effect on the outward current response, whereas, it had a huge impact on the inward current response at hyperpolarized potential (MacDonald, Miljkovic, and Pennefather, 1987).

A study showed that the HEK 293 cells transfected with GluN1/GluN2A and GluN1/GluN2B at a holding potential of -65mV had an $IC_{50}$ for memantine as shown in Table 2. Whereas the $IC_{50}$ for ketamine at -65mV was slightly lower as shown in table 2. The subunit GluN1/2B had a different $IC_{50}$ at -65mV. This may be due to GluN2B appearing to be critical for LTP (Zhang and Luo, 2013). Recent studies have reported that the D4 dopamine receptor may regulate LTP through the modification of GluN2B (Herwerth et al., 2012). Also, the C-terminal signaling sequence of GluN2B contributes to hippocampal LTP regulation however, the C-terminus of GluN2A has little relevance to hippocampal LTP (Foster et al., 2010). The $IC_{50}$ for memantine and ketamine for GluN2B were different as compared to GluN2A (Erreger et al., 2005). Ketamine is an open-channel blocker like memantine. Therefore, stable inhibition of responses requires the use of a protocol with multiple applications of agonists and antagonists (Gray et al., 2011; Tovar et al., 2013). Also, the inhibition by ketamine and memantine can differ during long-term glutamate application and this also depends on the NMDAR subunits (Glasgow and Johnson, 2014).

| $IC_{50}$ of Memantine and Ketamine at -65mV | |
|---|---|
| GluN1/GluN2A (Memantine) | 1.89µM |
| GluN1/GluN2A (Ketamine) | 0.89µM |
| GluN1/GluN2B (Memantine) | 0.68µM |
| GluN1/GluN2B (Ketamine) | 0.43µM |

Table 3: $IC_{50}$ of Memantine and Ketamine at -65mV for GluN1/GluN2A and GluN1/GluN2B (Zhang and Luo, 2013; Erreger et al., 2005).

Ketamine is less potent than phencyclidine and other NMDA antagonists like MK-801 due to a faster rate of dissociation from the channels. It binds to a site deep into the ion channel pore and

stops the flow of ions. This property helps the block of the ion channel for a shorter period and is relieved upon channel opening (MacDonald and Nowak, 1990). Ketamine inhibits the NMDARs by less than 50% at lower micromolar concentrations and leaves the rest of the NMDARs unblocked. The $IC_{50}$ of ketamine via NMDA channel blockage on the hippocampus was 0.43± 0.10μM at -100 mV with continuous NMDA (500μM) with a potency of 43.3. Studies on NMDARs expressed in Xenopus oocytes have shown that ketamine is selective for and more potent for GluN2B than GluN2A, 2C, and 2D in the absence of magnesium (Dravid et al., 2007).

Phencyclidine is more selective and 10 times more potent than ketamine. A study shows that Phencyclidine has a potency of 0.5μM while Ketamine has a potency of 5μM in vivo on chick embryo retina against 200μM racemic NMDA. Phencyclidine is also longer lasting after local or systemic administration 0.2-0.5mg·$kg^{-1}$ iv reduced the NMDA currents for several hours (Lodge and Mercier, 2015). The inhibition of NMDA by phencyclidine was found to be agonist-dependent (Berry et al., 1984b; Lodge and Anis, 1984; Lodge and Berry, 1984; Lodge et al., 1984). Other NMDA antagonists, including alpha cyclazocine and SKF10047, are known to be selective NMDA antagonists. Cyclazocine is twice as potent as SKF10047 (Lodge et al., 1984). The (−) enantiomer of cyclazocine along with (+) enantiomer of SKF10 047 was more potent than their other configurations (Lodge et al., 1984). MK801 is the most potent NMDA antagonist among all these compounds. In earlier studies, MK-801 was found to be more potent in NMDAR subunits GluN2A and GluN2B. The NMDA antagonists other than memantine can be ranked in the following order as neuroprotectants in-vitro: MK-801 > phencyclidine > ketamine > (-) cyclazocine > (+)SKF10 047 = > pentazocine (Olney et al., 1986, Lodge et al., 1984). However, it was found that MK-801, phencyclidine, and ketamine when administrated in-vivo at higher doses cause cell death in the rat cerebral cortex (Olney et al., 1986).

MK-801 has slower unblocking kinetics than Magnesium, lower voltage dependency and is unable to leave the channel within the functional time. Moreover, MK-801 block the normal physiological and pathological activation of NMDARs (Parsons, Danysz, and Quack, 1999) The kinetics of MK-801 and phencyclidine are slow that makes it unable to leave the channel upon

depolarization (Parsons et al., 1995). A recent study by Chou et al (2022) found the resolutions around the binding site of ketamine, memantine, and phencyclidine. The research was based on single particle electron cry microscopy, molecular dynamics simulations, and electrophysiology to analyze the different kinetics of phencyclidine, ketamine, and memantine on NMDARs subunit GluN1a and GluN2B. A short pulse (5s) of glutamate was applied to patch clamped cells. They found that phencyclidine had the lowest speed and the fastest dissociating compound out of ketamine and phencyclidine. Also, memantine had the least psychomimetic effects (Chou et al., 2022).

A boomerang-shaped density was found for the phencyclidine channel blocker bound to the GluN1a/GluN2A channel pore. This boomerang-shaped density was surrounded by M2 loops and M3 helices and located at the center of the pore with the elbow of the boomerang towards threonine residing on M3. The arms of the density were found to be surrounded by hydrophobic interactions sitting on top of the M2 loop along with an asparagine ring. These residues and asparagine ring were located at the center of the selectivity filter blocking the channel pore as shown in figure 4 (Chou et al., 2022).

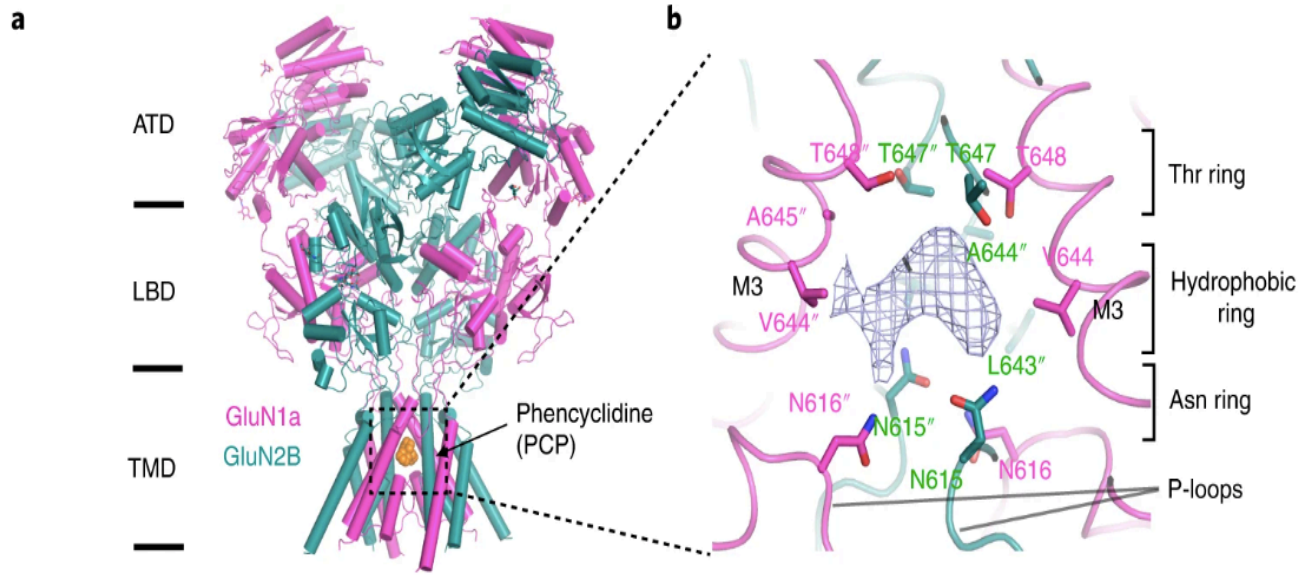


*Fig.4: Structure of GluN1A-GluN2B NMDARs shown bound to phencyclidine at the TMD. (b) The structure shows the phencyclidine molecule surrounded by the hydrophobic ring, threonine, and asparagine ring* (Chou et al., 2022).

The methodology used to assess the specific binding sites of the GluN1a-2B NMDAR in complex with ketamine, like phencyclidine, was molecular dynamic simulation which was used on the cryo-EM structures to better visualize and determine distinct features regarding the transmembrane binding domain. Ketamine was bound with the agonist-activated NMDAR complex in specific binding patterns that the researchers labeled as “poses” as shown in Figure 5. Pose 1 was distinct from the others as the chlorine group did not adhere to the density while in poses 2, 3, and 4 it did adhere to the density. Moreover, poses 1, 2, and 3 have hydrophobic interactions, and pose 4 resembles PCP regarding the cyclohexane ring facing the threonine ring also creating a hydrophobic interaction. As for the binding stability, poses 2, 3, and 4 have more stable binding sites as opposed to posing 1 as shown in figure 5.

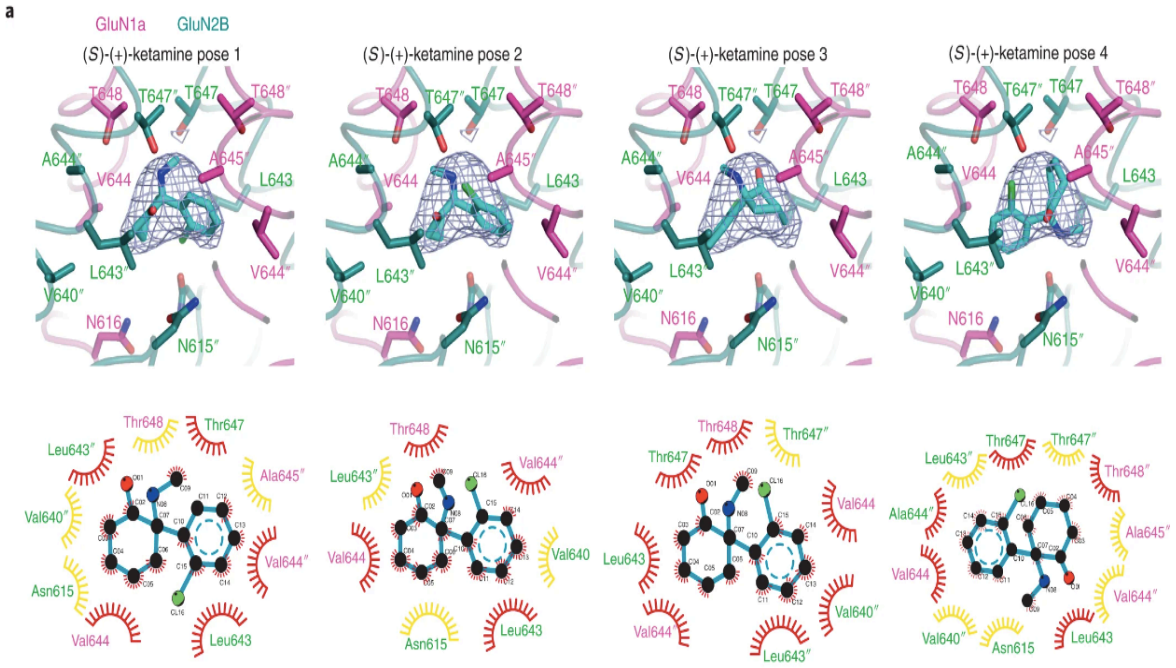


*Fig.5: Four binding poses of ketamine as shown by the Cyro-EM, each poses colored differently. The colored eyelashes represent the hydrophobic interactions* (Limapichat et al., 2013).

Regarding memantine, not only does it have one "pose" when bound to the NMDAR complex, but it has a unique pseudo-tetrahedral density. One of the 'arms' of this density involves an interaction between the amine group of memantine and an Asn ring (Limapichat et al., 2013). The two methyl groups interact with GluN1/GluN2B forming hydrophobic interaction. Also, for binding stability, memantine displayed a stable z-axis position like poses 2, 3, and 4 of ketamine. To study the effects of voltage dependence of NMDAR blocks, voltages of -70mV, 0mV, and +70mV were tested. The chemical change that produced a pronounced effect was the hydrogen bond. This hydrogen bond decreased as the voltage got more positive between the GluN2B Asn ring found in the pseudo-tetrahedral complex. This is because hydrogen bonds are formed specifically by GluN2b-Asn and memantine interaction. However, this was not found for GluN1A-Asn and memantine interactions (Chou et al., 2022).

The study conducted by Chou et al (2022) found that inducing a mutation of a threonine ring which is normally found in the structure of both GluN1a and GluN2B affected the activity of all three channel blockers through changes in the hydrogen bonding along with altering the hydrophobic interactions. Another method used alongside the mutations to measure the on and

off rates of each channel blocker coming was using patch–clamp electrophysiology and two-electrode voltage-clamp. Both the mutated form of the Thr ring and GluN2B-Leu643Ala had decreased hydrophobic interactions and lower potency with a faster coming-off speed for all three channel blockers.

However, the mutated GluN1a-Val644Ala only had a fast off-speed change with ketamine but not phencyclidine or memantine. GluN2B-Asn615Gln has a side chain that interferes with hydrogen bonding, and this affected both memantine and Phencyclidine binding by decreasing potency and increasing the binding off rate, but this was not found for ketamine.

Another aspect of testing found that the Asn ring mutation to Gln caused a significant change to the $Mg^{2+}$ block and lowered potency. Therefore, the Asn ring is more uniquely attributable to channel blockage involving $Mg^{2+}$ as opposed to the three-channel blockers that were tested (Chou et al., 2022).

### 1.8 Clinical Trials of Memantine and its effectivity:

Memantine has been evaluated for different stages of Alzheimer's patients. Three randomized, double-blind, and placebo-controlled studies were conducted and submitted to FDA for approval. The first study submitted to FDA involved using memantine in a long-term care setting in AD patients. The patient's severity was an assessment by the global deterioration scale (stage 5-7) and the mini-mental state examination (<10 points). As the endpoint, the clinicians rated the clinical global impression of change (CGI-C). To further strengthen the assessment, the nursing staff used the behavioral rating scale for geriatric patients i.e., sub-score care dependence (Winblad and Poritis, 1999). It involved 166 patients between 60-80 years of age, with moderate to severe stages of the disease, and who met the criteria for dementia. At the end of 12 weeks, 82 of the patients received memantine 10 mg of per day and 84 received a placebo. According to the CT scan, 49% of those patients had dementia and 51% had vascular dementia. The change in clinical global impression was observed in 73% in favor of the memantine group, and the behavioral rating score was 3.1 points in patients treated with memantine and 1.1 points under

placebo. This clinical trial supported the hypothesis of memantine in the treatment of functional cognitive improvement and reducing care dependence as well (Thomas and Grossberg, 2009).

The second study and the experimental data submitted to the FDA on memantine were carried out in an outpatient setting. The criteria used for this study by Reisberg et al (2003) were similar in selection to that submitted by Thomas and Gorssberg (2009). This study involved 252 patients that were administered 10 mg of memantine twice daily for 28 weeks at 32 US centers. Out of these 252, 181 (72%) finally completed the assessment over the 28-week period. The assessment criteria used afterward were severe impairment battery, the clinician's cognition, and global measurements as primary efficacy variables. Moreover, the secondary variables used were Alzheimer's disease cooperative activities of daily living inventory modified for severe dementia and the neuropsychiatric inventory to measure the impact on behavior. The patients administrated with memantine showed improvement in better cognitive outcomes over the placebo over the 28-week trial (Reisberg et al., 2003).

The third study submitted to the FDA was more promising, covering the multi-targeted pathological activations in Alzheimer's disease patients. It involved the administration of memantine with the cholinesterase inhibitor, donepezil. This study involved 404 patients suffering from moderate to severe AD and mini-mental state examination scores of 5-13 and was conducted at 37 US sites between a time of 2001 and 2002. However, only 80% of the patients completed the trial. The participants received 5mg of memantine per day initially and later increased to 20mg per day. This final study had an inclusion of a behavioral rating scale for geriatric patients in addition to the criteria discussed previously by Reisberg et al (2003). The patients who received memantine and donepezil showed better outcomes than the placebo. The results showed improvement in cognition, activities of daily living, global outcomes, and behavior. These results along with previous studies showed that memantine can be a promising treatment for patients suffering from moderate to severe AD (Tariot et al., 2004). Finally, a fourth study carried out by Schneider et al (2011) tried to assess the efficacy of memantine in mild Alzheimer's disease patients. The patients who were diagnosed had a mini-mental state

examination score of < 20. The data extraction and study selection used in this trial were taken from manufacturer-sponsored meta-analyses, registries, presentations, and publications from clinical trials of memantine in mild to moderate AD. The three trials used for this involved 431 patients with mild AD and no significant difference was found between memantine and placebo in patients with mild AD. Despite its frequent use, there was no evidence seen of using memantine in mild AD patients.

### 1.9 Choline Esterase Inhibitors and Alzheimer's Disease:

AD causes the deterioration of the cholinergic neurons and, therefore, the decline of acetylcholine release in the brain (Bartus et al., 1982). One of the main causes of AD along with the NMDAR-mediated excitotoxicity is the reduction in the synthesis of acetylcholine. Choline Esterase Inhibitors amplify the weakened cholinergic signals by delaying the ACh breakdown (Parsons, Stöffler, and Danysz, 2007). So, targeting the acetylcholine breakdown is one of the therapeutic strategies in the treatment of AD and increasing the acetylcholine levels. Acetylcholine Esterase is the enzyme involved in the hydrolysis of acetylcholine to generate choline and acetate ions (Silman and Sussman, 2008). Cholinesterase inhibitors can be divided into different categories depending on their clinical efficacy. This includes reversible inhibitors such as donepezil and galantamine and pseudo-reversible inhibitors such as eptastigmine, physostigmine, and rivastigmine (Enz et al., 1993).

Donepezil and galantamine only selectively inhibit the acetylcholine esterase. The clinical trials of the 6 months showed that these drugs improved the cognitive function in AD patients. However, the different Choline Esterase Inhibitors show the difference in the dose-response relationship (Antuono, 1995). The IC50 of donepezil in rat brain tissue was found to be 0.68nmol/L. Whereas Rivastigmine had 42000nmol/L and galantamine had 3900 nM/L (Giacobini, 1997). Donepezil was first approved for the treatment of mild AD in 1996 inhibiting the choline esterase (Jacobson and Sabbagh, 2008). In addition to this, Rivastigmine was first approved for the treatment of mild AD in 2000. Although its exact mode of action remains

unclear, it targets Choline Esterase Inhibitors and increases cholinergic function (Bar-On et al., 2002).

The preclinical data have shown that memantine does not block nicotinic acetylcholine receptors at a therapeutically relevant concentration (Enz and Gentsch 2004; Gupta and Dekundy 2005; Wenk et al., 2000) and so can be used in combination therapy. Studies in transgenic mice showed that memantine and donepezil together improved spatial memory (acquisition and retention), however, donepezil on its own only improved retention.

## 2.0 Natural/Toxins NMDA Antagonists:

Several NMDA antagonists have been so far discovered from natural sources, and some block the receptors in a voltage-dependent manner. Though many of them are not clinically effective they still can block the NMDARs. Some of them are natural NMDA toxins that antagonize the receptors.

A type of natural compound that can inhibit NMDA receptors is CGX-1007 or Conantokin G, which is a peptide isolated from the cone snail, *Conus geographus* (Alex et al., 2011). CGX-1007 can antagonize receptors containing GluN2B, which is an NMDA receptor that mediates excitotoxicity in young neurons (Jakob et al., 2007). To test the antagonist effects of CGX-1007, hippocampal slice cultures from Sprague Dawley rat pups were exposed to NMDA to induce excitotoxicity. The methodology used to view the excitotoxic neurodegeneration involved the use of propidium iodide (PI) uptake, which is a non-toxic fluorescent dye. When CGX-1007 was added with NMDA on the hippocampal slice cultures, it caused the preservation of the neural cells. However, ifenprodil, which is a GluN2B selective antagonist of NMDA receptors, failed to protect against neural cell damage. To test the effects of CGX-1007 on NMDA receptors, human embryonic kidney (HEK) 293 cells were used with either GluN1/GluN2A or GluN1/GluN2B NMDA receptors (Alex et al., 2011). CGX-1007 caused inhibition of NMDA-evoked currents in cells expressing both GluN2A and GluN2B containing receptors but with more affinity for those containing GluN2B.

Two other closely related plant-based natural antagonists of NMDA are Rhynchophylline and Isorhynchophylline, which are oxindole alkaloid derived from *Uncaria* species (Tai-Hyun et al., 2002). A previous study discovered that these two alkaloids protected against glutamate-induced neuronal death in cerebellar granule cells (Shimada et al., 1999). Thus, this paper postulated that these plant-derived alkaloids can non-competitively inhibit NMDA receptors. The study used *Xenopus* oocytes that were injected with RNA from rat cortices (Tai-Hyun et al., 2002). The results of the study showed that the two natural alkaloids by themselves were unable to elicit a current response but both rhynchophylline and isorhynchophylline reduced the current responses to 100μM NMDA and 5μM glycine in a concentration-dependent manner. Also, both alkaloids were able to reduce the maximal current responses evoked by NMDA and glycine but had no effect on the NMDA and glycine $EC_{50}$. They also had no interaction with specific binding sites on the NMDA receptor such as the polyamine binding site, the $Zn^{2+}$ site, the proton site, or the redox modulatory site thus demonstrating noncompetitive antagonism of NMDA receptors (Tai-Hyun et al., 2002).

A plant-based alkaloid, Huperzine A, derived from the herb Huperzia serrata was shown to inhibit NMDA receptors by non-competitive inhibition (Shimada et al., 1999). Patch-clamp recording of CA1 pyramidal neurons dissected from Sprague–Dawley rat hippocampus was used, and Huperzine A was applied before and during NMDA application. The result of the experiment showed that the addition of 100μM Huperzine A decreased the NMDA concentration by more than 50%. Also, a concentration–response curve for NMDA was created with and without the presence of Huperzine A and this showed a non-parallel shift confirming its noncompetitive antagonistic nature (Mallozzi et al., 2018). This study also tested the inhibition of Huperzine A on the NMDA receptors at three different membrane potentials, which determined that the inhibition of the NMDA receptors was voltage-independent. Additionally, the addition of spermine, a positive modulator of NMDA receptors, increased the maximal inhibitory concentration of Huperzine A, thus, suggesting that Huperzine A competes with spermine as a competitive antagonist at the polyamine binding sites on the NMDA receptor (Tai-Hyun et al., 2002; Zhang and Hu et al., 2011), unlike the two oxindole alkaloids (Zhang and Hu et al., 2011).

Argiotoxin-636 is polyamine isolated from the spider venom of Argiope lobata and Argiope aurantia. They are very potent NMDARs antagonist blocking the ion channel at a lower concentration. Argiotoxin-636 are open channel blockers and inhibited the NMDARs activity by half at 3mM concentration in a voltage-dependent manner in the rat cortical neurons (Albensi, Alasti, and Mueller, 2000). Argiotoxin-636 is considered to have selective affinity for NMDAR subunits GluN1/2A and GluN1/2B. This makes it a significant toxin for the neuropharmacological study of the NMDARs subtypes (Pałasz and Krzystanek, 2022). It is 20 times more selective for GluN1/2A and GluN1/2B than GluN1/2C and GluN1/2D NMDAR subtypes. Moreover, the rate of channel block is dependent on the ArgTX-636 concentration. Whereas the rate of channel unblocking is independent of the ArgTX-636 concentration (Poulsen et al., 2015). In addition to this, Agatoxin-489 are neuroactive polyamines and natural toxins used as NMDA blockers. They are isolated from the desert grass spider Agelenopsis aperta. Agatoxin-489 is found to be a very potent NMDARs-dependent calcium currents blocker in rat cerebellar granule cells and hippocampal neurons (Monge-Fuentes et al., 2015).

Philanthotoxin-343 are natural toxin isolated from the Egyptian digger wasp. They are polyamine neuroactive toxins playing a significant role in nAChR, NMDA, kainite, and AMPA receptors. They are noncompetitive NMDA, AMPA, and kainite receptor inhibitors. The multiple charges on the PhTX-343 are very crucial for the potency of glutamate receptors (Mellor et al., 2003). According to Fedorov, Screbitsky, and Reymann (1992), in vitro experiments showed 2µM PhTX-343 inhibited the NMDA-induced calcium currents in the hippocampal pyramidal neurons. PhTX-343 showed NMDA inhibition in a voltage-dependent manner. They had an $IC_{50}$ at holding potential of -60, -80, and -100mV as shown in table 4 (Mellor et al., 2003).

| $IC_{50}$ of PhTX-343 | |
|---|---|
| -60mV | 13.2µM |
| -80mV | 2.01µM |
| -100mV | 0.98µM |

*Table 4:* $IC_{50}$ of *PhTX-343 at different holding potentials i.e. -60mV, -80mV, and -100mV (*Mellor et al., 2003).

## 2.1 Harlequin ladybird - Harmonia axyridis:

The Harlequin ladybird, Harmonia axyridis, was initially used as a biological control for aphids in different areas of the world and is native to Asia. The first established population was recorded in 1988 in the US even though it was first taken into the US in 1916. it was first introduced in Europe in 1982 and the first established population was found in 2000-2001. In addition to this, they are now found in different continents including South America, North America, and Africa (Raak-van den Berg et al., 2017). Harmonia axyridis falls under the tribe Coccinellini of the family Coccinellidae. The adults are 4.9-8.2mm in length and 4.0-6.6mm in width. They are convex shaped and oval with 4/5 wide as long. The heads of these ladybirds can either be black, yellow, or with a different variation. The central region is orange to red with black marks in the center. These black spots form an M shape looking from the top (Koch, 2003).

Female H. axyridis lay eggs near the period of infestations of prey. As the larva hatches from the egg, it changes its skin. During the initial larval stage, the larva is dark grey with dark spines-like extensions, black legs, and a head, whereas, during the second larval stage, the color changes to white-yellowish color on the upper side. During the final stages, the colors become more

prominent and strongly yellow with lateral white line (Harlequin ladybird - Harmonia axyridis, 2016). H. axyridis ladybirds release defensive chemicals like harmonine, first found to be a significant defense compound of H. axyridis. Upon attack, ladybirds secrete droplets of their hemolymph from the tibiofemoral joints of the legs (Alam et al., 2002). The ladybirds defend themselves by secreting the chemical and by coating the laid eggs with the defensive fluid. This helps to protect them from predators and other insects. The defensive chemicals also cause toxicity to the animals ingesting them. The alkaloids that are produced within these ladybirds are a component of the secretions and are synthesized in their bodies (Santi and Maini, 2006; Laurent et al., 2002; Haulotte et al., 2012).

Despite the chemical defense in the alkaloids of the ladybirds, they are still attacked, and predation is common. H. Axyridis larvae are more aggressive in consuming prey and non-prey food items. It was also found that H. axyridis larvae are stronger in their ability to ingest defense chemicals compared to other ladybirds. The quantification of alkaloids in H. axyridis eggs showed a difference in females and the egg size was positively correlated with the number of alkaloids (Kajita et al., 2010). More than 50 different kinds of alkaloids have been identified, isolated, and categorized from the ladybeetles. This includes perhydroazaphenalenes, homotropanes, piperidines, pyrrolidines, aza macrolides, linear amines, and others (Kajita et al., 2010). Harmonine was one of the alkaloids found in H. axyridis It was first identified and isolated by acetylation and fractionation of extract from *Harmonia leis conformis* (Braconnier et al., 1985). High-resolution mass spectrometry showed the detailed structure of harmonine possessing a secondary amine.

H.axyridis like other ladybirds of the coccinellids family is protected by defensive alkaloids. The alkaloids of H. axyridis are long-chain diamine harmonine [(17R, 9Z)-1,17-diaminooctadec9-ene] and (S)-3-hydroxypiperidin-2-one (Alam et al., 2002). In addition to this, there are other compounds like 2,5-dimethyl-3-methoxypyrazine, 2-isopropyl-3-methoxypyrazine, 2-sec-butyl3-methoxypyrazine, and 2-isobutyl-3-methoxypyrazine that provide H. axyridis with foul warning

smell (Cudjoe et al., 2005; Cai et al., 2007). It has also been previously proposed by Bezzerides et al (2007) that the color indication of H. axyridis depicts the alkaloid content within them. Moreover, it was also found that the orange-colored elytra in females were correlated with harmonine concentration in H. axyridis. The melanic ladybirds were supposed to have a lower content of chemical defense as compared to the non-melanic as found in the north American Harmonia axyridis (Sloggett, Haynes, Davis, 2010).

## 2.2 Role of Harmonia axyridis Extracts on Nicotinic Acetyl Choline Receptors:

Patel et al (2020) conducted electrophysiological studies to analyze the impact of HAE (which is 90% harmonine) on nAChRS using voltage clamp and patch clamp studies. The experimental study involved human-α7, rat-α4β2, rat-α3β4 and hybrid Drosophila-α2/chick-β2 (Dα2/β2)-nAChRs at -75mV. They showed that HAE inhibited the acetylcholine response in mammalian neuronal nAChRs expressed in Xenopus oocytes. The $IC_{50}$ (µg/mL) of different receptor subtypes α7, α4β2, α3β4, and Dα2/β2 was 2.30, 3.24, 1.47, and 0.440. However, the study found that HAE inhibition on human-α7 and rat-α3β4 was voltage-independent. Whereas the HAE inhibition for rat-α4β2 was voltage-dependent (Patel et al., 2020). Similarly, a study by Maskell et al (2003) found that memantine blocks human α7 in a voltage-independent and in non-competitive manner.

However, its inhibition on α4β2 and α9/α10 is in a voltage-dependent manner. The $IC_{50}$ of memantine on humanα7 was found to be 5µM (Maskell et al., 2003). Rohit et al (2020) found that Dα2/β2 IC50 was 3.34 times lower than the mammalian nAChRS.

Moreover, HAE was shown to inhibit the human muscle type nAChR expressed in the TE671 cells and insect neuronal type nAChR in locust neurons. The application of HAE inhibited the inward currents for the nAChRs in the TE671 cells and locust neurons. The extracted HAE alkaloids had two fractions (A and B) and showed different $IC_{50}$ values for insect neuronal type nAChR in locust neurons and TE671 cells for the human muscle type. HAE fraction A had $IC_{50}$ of 4.77µg/mL and fraction B had 1.68µg/mL in TE671 cells expressing human muscle type nAChR. In addition to this,

fractions A and B had $IC_{50}$ of 3.23 and 0.072µg/mL in insect neuronal type nAChR. HAE (90% harmonine) was also examined on rat NMDAR subtypes GluN1/GluN2A and GluN2B. It was found that HAE inhibited NMDARs in a voltage-dependent manner. It had an $IC_{50}$ of 2.65, 1.11, and 1.72µg/mL at -50mV, -75mV, and -100mV in GluN1/GluN2A subunits. However, it had an $IC_{50}$ of 14.6, 5.87, and 1.51µg/mL in GluN1/GluN2B subunits (Kaur, 2022).

## Aims and Objectives:

This research consisted of two distinct components. The first component involved studying the efficacy of memantine as an NMDAR inhibitor, while the second component involved investigating the effectiveness of Harmonia axyridis alkaloids, specifically Harmonine, as an NMDAR inhibitor, using memantine as a reference compound. Both components of the study utilized human NMDAR clones, which is a novel experimental approach compared to previous research that used rat NMDAR clones.

In the first component, the research team focused on evaluating the inhibition of human NMDAR clones by memantine. The effectiveness of memantine was tested using a two-electrode voltage clamp (TEVC) on GluN1A-GluN2A NMDARs expressed in Xenopus oocytes. This is a significant step forward in the research, as most of the previous studies used rat NMDAR clones.

The second component of the study involved investigating the effectiveness of Harmonine as an NMDAR inhibitor. The team used TEVC to test the effectiveness of Harmonine on human NMDAR clones, which was also performed for the first time. Overall, this research provides novel insights into the inhibition of NMDARs and represents a significant step forward in the understanding of how compounds like memantine and Harmonine can be used to modulate the activity of NMDARs.

# 3. Materials and Methods

The entire experimental approach was carried out on *Xenopus* oocytes provided by Ecocyte Biosciences.

## 3.1 Materials and Solutions:

D-Glucose anhydrous was provided by Scientific Fischer. Calcium Chloride Solution 1L and Potassium Chloride used were provided by Honeywell Fluka. HEPES was provided by SIGMA. Magnesium Chloride was provided by BDH chemicals Ltd Poole England. Yeast Extract was provided by SIGMA Life Science. Theophylline anhydrous was provided by SIGMA Life Science. Sodium Chloride 99.5% analytical reagent grade was provided by Fischer Scientific. Agarose, Molecular Grade was provided by Bioline. Gentamicin Solution was provided by SIGMA ALDRICH. Sodium Pyruvate powder (Stored at 2-8°C) was provided by SIGMA Life Science. Collagenase from Clostridium histolyticum was provided by SIGMA. Tryptone enzymatic digest from casein was provided by Fluka Analytical. AGAR granulated (Solidification point 32-38°C) was provided by Melford Laboratories Ltd. 1µL (10 units) Restriction enzyme, 5µL NE Buffer, $ddH_2O$, 2.5µL of EDTA solution, 5µL ammonium acetate, 5µL nuclease-free water were provided by Thermo Fisher Scientific.

XL-10 Ultracompetent cells were provided by Agilent Technologies (stored at -80°C). GenElute™ Plasmid Miniprep Kit was provided by SIGMA. The mMESSAGE mMACHINE® Kit High Yield was provided by ThermoFischer. Human NMDA clones were provided by GenScript Biotech (UK) Limited in pcDNA3.1+/C-(K)-DYK vector (stored at -20°C).

*Table 5. Solutions for Molecular Biology and Electrophysiological Analysis*

| **GTP Calcium Solution** | | | | | | |
|---|---|---|---|---|---|---|
| | **NaCl** | **KCl** | **$CaCl_2$** | **HEPES** | **Sodium Pyruvate** | **Theophylline** |
| **g/L** | 5.61 | 0.15 | 1.8 | 1.19 | 0.275 | 0.09 |
| **mM** | 95 | 2 | 1 | 5 | 2.5 | 0.5 |
| **Note: pH 7.5 with NaOH and 5 ml/L gentamycin solution (50 mg/L) added after autoclaving. Calcium-free GTP was prepared in the same way but omitting $CaCl_2$** | | | | | | |
| **Xenopus Ringer Solution** | | | | | | |
| | **NaCl** | **KCl** | **$CaCl_2$** | **HEPES** | | |
| **g/1L** | 5.60 | 0.15 | 2.0 | 3.57 | | |
| **mM** | 95 | 2 | 2 | 5 | | |
| **Note: pH 7.5 with NaOH and stored in the incubator at 37°C** | | | | | | |
| **Luria Broth and LB Agar Solution** | | | | | | |
| | **NaCl** | **Tryptone** | **Yeast Extract** | **Agar** | | |
| **g/1L** | 10 | 10 | 5 | 17g | | |
| pH 7.0, autoclaved and stored at 4°C. Antibiotic added to LB agar after autoclave. Agar was only added to the LB agar solution. | | | | | | |

## 3.2 Alkaloid Extraction from Harmonia Axidris beetles:

The alkaloid extraction from Harlequin ladybirds (Harmonia axyridis) was carried out by Charlotte Taylor (University of Nottingham) and Dr. Michael Birkett (Roth Amsted Research) as follows using the method employed by Patel et al (2020). Ladybirds were collected from the grounds of University Park (Nottingham) and Roth Amsted Research (Harpenden, Hertfordshire). They were

stored at -20°C until the extraction. To obtain the whole alkaloid extract from the ladybirds (187 g), they were first frozen in liquid nitrogen and crushed with a pestle and mortar. The crushed ladybirds were placed in methanol (250mL) for 24h at room temperature with stirring. The methanol was collected, and the process was repeated. A grade 4, Whatman filter paper was used to filter the extracts in the methanol solution and dried using the rotary evaporator (BUCHI, Switzerland). The extracts after this procedure weighed around 8g and were subject to acid-base extraction at room temperature to separate out the alkaloid material. This was done using 1M HCL (50mL) and diethyl ether (3× 20mL) and keeping the aqueous phase each time. This was adjusted to pH 10-12 using 2M NaOH and extracted with dichloromethane (3× 20mL). The organic layers from the extractions were washed with NaCl solution, dried with $MgSO_4$, and evaporated later to obtain a residue weighing 450mg. To confirm the presence of alkaloids, Dragendorff's reagent was used. The residue was redissolved in dichloromethane and aliquoted into 1 mg samples followed by evaporation of dichloromethane for storage under nitrogen in sealed glass ampoules (Patel et al., 2020).

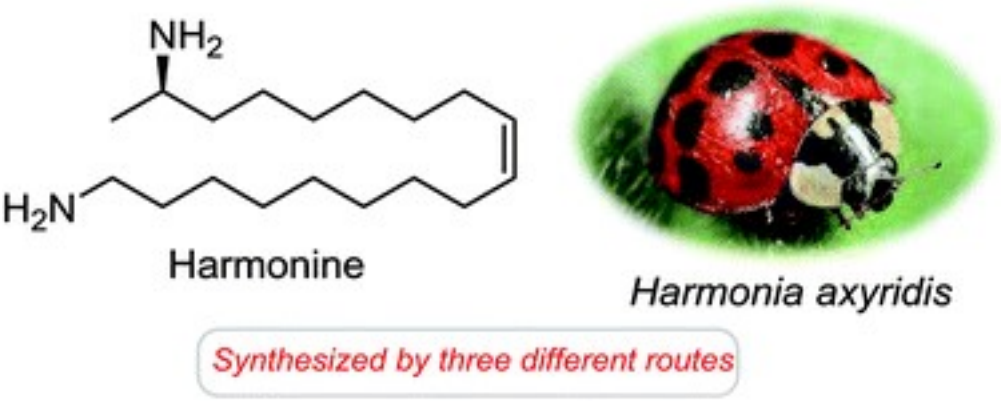


*Fig 6. The chemical structure of harmonine obtained from the Harmonia axyridis ladybeetle.*

### 3.2 DNA Transformation and Isolation:

GenEZ ORF clone was delivered as 10µg of lyophilized plasmid DNA in a vial. To amplify each of the DNA samples, XL10-Gold Super competent E. coli were used with the heat shock method. These were stored at -80°C and on removal from the freezer were thawed on ice. 2µL of

βmercaptoethanol was added to the Eppendorf tube along with 200µL of XL10-Gold Super competent E. coli. The tube was gently mixed and then incubated on ice for 10 minutes and it was mixed after every 2 minutes. Then, 1µL of DNA plasmid solution was added to the tube containing the E. coli and incubated on ice for 30 minutes mixing it after every 10 minutes. The tube containing DNA, super competent cells, and β-mercaptoethanol was then heated in a water bath at 42°C for precisely 45 seconds and then returned to the ice for 2 minutes to cool down. 950µL of

Super optimal catabolite medium (SOC) was added to the tube. The prepared SOC solution was heated to 42°C before adding to the tube. The tube was incubated in a shaking incubator at 37°C for 1 hour at 250rpm. Following this, 250µL of the mixture was added to a Luria Broth (LB) agar plate and it was spread using a sterilized glass spreader all over the LB agar plate. The LB agar plate was labeled and kept in an incubator at 37°C for 24 hours for bacterial replication of the DNA.

The next day, a colony was picked from the LB agar plate using a pipette tip and dropped into a 5mL LB broth solution with 100µg/mL ampicillin in a 14mL Falcon tube. The pipette tip was left in the tube containing the LB broth solution. The tube was placed in a shaking incubator at 37°C for 24 hours at 250 rpm. The next day, the tube was removed from the incubator for isolation of the bacterially replicated plasmid DNA using a GenElute™ Plasmid Miniprep Kit (SIGMA). The kit had the following contents. The next day, three 10mL falcon tubes were taken from the incubator. The bacterially replicated plasmid DNA of each subunit was isolated using GenElute™ Plasmid Miniprep Kit (SIGMA). The kit had the following solutions.

*Table 6. Solutions for Plasmid Preparation and DNA Isolation*

| Reagents Provided | Catalog No. | PLN10 10 Preps |
|---|---|---|
| **Resuspension Solution** | R1149 | 2.5mL |
| **RNase A Solution** | R6148 | 0.25mL |
| **Lysis Solution** | L1912 | 2.5mL |
| **Neutralization Solution** | N5158 | 4mL |
| **Column Preparation Solution** | C2112 | 7mL |
| **Wash Solution** | W4011 | 5.5mL |
| **Elusion Solution** | E5650 | 1.5mL |
| **Binding Columns** | G6415 | 10 each |
| **2mL Collection Tubes** | T5449 | 20 each |

13µL of RNase A solution was added to all the resuspension solutions before starting the isolation step. 10mL of 95-100% ethanol was added to the entire wash solution to dilute it. Three times 1.5mL of the bacterial solution from the previous step was collected into three different Eppendorf tubes. The Eppendorf tubes were centrifuged at 14000rpm (Eppendorf 5417R centrifuge) for 1 minute to harvest the cells. After taking out of the centrifuge, the LB broth solution was poured out to leave the cell pellet.

This step was performed until all the bacterial solution in the Falcon tube was finished. 200µL of the resuspension solution was added into each Eppendorf and was pipetted up and down until the pellet was resuspended. 200µL of the lysis solution was added into each Eppendorf for 4 minutes and inverted 6-8 times. The timer was set to avoid exceeding 4 minutes because longer lysis can denature the plasmid DNA. After 4 minutes, 350µL of the neutralization solution was added and inverted 4-6 times. The solution was placed into the centrifuge (Eppendorf 5417R) for 10 minutes at 14000rpm. This step separated the cell debris, proteins, lipids, and chromosomal DNA from the clear solution containing the plasmid DNA. A GenElute miniprep binding column filter was added to the collection tube.

500µL of column prep solution was added into the miniprep binding filter and centrifuged (Eppendorf 5417R) at 14000rpm for 1 minute. Once centrifuged, the flow-through liquid was

discarded and the clear lysate solution from the neutralization step was added to the binding column. It was again centrifuged (Eppendorf 5417R) at 14000rpm for 1 minute. The flow-through liquid was again discarded and 750µL of the wash solution was added into the column and centrifuged (Eppendorf 5417R) at 14000rpm for 1 minute. The flow-through liquid was again discarded and now the tubes were centrifuged again for 2 minutes without adding any additional wash solution. This was done to remove any excess ethanol and improve cDNA purity level. To elute cDNA, the binding column was placed in a new collection tube and 50µL of the elution solution was added and centrifuged (Eppendorf 5417R) at 14000rpm for 1 minute. At this stage, the binding column was removed leaving the cDNA solution in the collection tube. The cDNA concentration was measured using a Nanodrop (Implen, Nanophotometer NP80) spectrophotometer. The cDNA was stored at -20°C.

### 3.3 DNA Linearization:

The cDNA was in circular form and to linearize restriction enzymes were needed for the proper restriction digest. The restriction enzymes specific to each subunit can be found in the table above. The mMESSAGE mMACHINE® Kit High Yield Capped RNA Transcription Kit was used for cDNA linearization and mRNA transcription consisting of SP6 and T7 kits.

The pcDNA was in circular form but it was necessary to linearize it for later RNA transcription. This was done by digestion using restriction enzymes. The restriction enzyme specific to each subunit was NotI.

1µL of the restriction enzyme was added into an Eppendorf tube. 3. 5µL of 10x NE Buffer and 2µg of the plasmid DNA was added. The total volume was made up to 50µL with nuclease-free water. The digestion reaction mixture in the Eppendorf tube was incubated in a water bath at 37°C for 2 hours to allow the linearization to happen. 2.5µL of the 0.5M EDTA, 5µL 5M ammonium acetate, and 150µL ice-cold 100% ethanol were added into the Eppendorf tube to terminate the reaction after 2 hours.

The mixture was centrifuged at 4°C for 15 minutes at 14000rpm. After this, the supernatant was carefully removed with a pipette and discarded. To avoid any pellet loss, the last traces of supernatant was also taken out using a small piece of tissue paper. This took the maximum amount of ethanol without losing DNA. The tubes were placed on a heat block at 50°C for 5 minutes to dry the DNA pellet. Once it was dried, the pellet was resuspended with 10µL of nuclease-free water. After that, the tubes were closed and kept in the water bath at 50°C for 5 minutes. The Eppendorf tube was spun in the centrifuge at maximum speed for 5 minutes. Now, the DNA was linearized, and the concentration was determined using the Nanodrop spectrophotometer.

### 3.4 Electrophoresis Gel:

To prepare the electrophoresis gel, Tris/Borate/EDTA (TBE) buffer was prepared. It was prepared in 1L distilled water by adding 54g of Tri's base, 27.5g of boric acid, and 20mL of 0.5M EDTA and adjusted to pH 8.0. The electrophoresis was run by preparing 1% agarose gel. 1g of agarose gel was weighed out and transferred to a 100mL clean bottle. 100mL of 1× TBE buffer was added into that bottle and mixed. 1× TBE was prepared by adding 100mL of 5× TBE and 400mL of distilled water. The lid of the bottle was loosened, and it was microwaved until the agarose had completely dissolved. Once dissolved, it was placed under cold water with a closed lid. Once it was cool enough to hold in the hand, 1µL of ethidium bromide (1mg/mL was added. The gel tray was cleaned, and a comb was attached to the tray. The ends of the tray were sealed using masking tape and agarose was poured into the tray.

To prepare the samples for loading, 1µL of linearized DNA was added to 4µL of nuclease-free water and 1µL of 6× dye. The 1kb DNA ladder was prepared by adding 2µL of 6× dye and 10µL of the ladder. Finally, the masking tape and comb were removed, and the gel was placed in the electrophoresis tank and topped up with 1×TBE buffer. The first lane was loaded with the 1kb

ladder and samples in the later lanes were linearized and non-linearized DNA. The electrophoresis gel was run at 100V for 60 minutes.

## 3.5 RNA Transcription:

The T7 mMESSAGE mMACHINE® High Yield Capped RNA Transcription Kit was used for mRNA transcription kits. T7 promotor was used for GluN1, GluN2A, and GluN2B.

To proceed with the transcription step, 1µg of the linearized DNA, 10µL NTP/CAP 2x, 2µL of reaction buffer 10x, and 2µL of enzyme mix were added into an Eppendorf tube. The total volume was made up to 20µL with nuclease-free water. The reaction mixture was incubated at 37°C in a water bath for 2 hours. RNA was recovered by adding 30 µL of lithium chloride solution and 30µL nuclease-free water. Now, the mixture was frozen overnight at -20°C to completely terminate the reaction. The following day the recovered RNA was centrifuged at 24000rpm for 30 minutes at 4°C.

The resultant supernatant was carefully taken out with a pipette. The RNA pellet was resuspended with 10µL of 70% ethanol and spun at 14000rpm for 30 minutes. The supernatant was again taken out with the help of small pieces of tissue and spun for 30 seconds. The Eppendorf tube was then placed in the heat block at 50°C for 5 minutes to make sure that the pellet dried. The pellet was resuspended with 15µL of nuclease-free water. After that, the RNA concentration was measured using the Nanodrop. Afterward, the RNA solution was aliquoted into 3µL volumes and stored at -80°C. The gel was visualized using the iBright 750 (Invitrogen by Thermo Fisher Scientific) comparing the linearized and non-linearized cDNA.

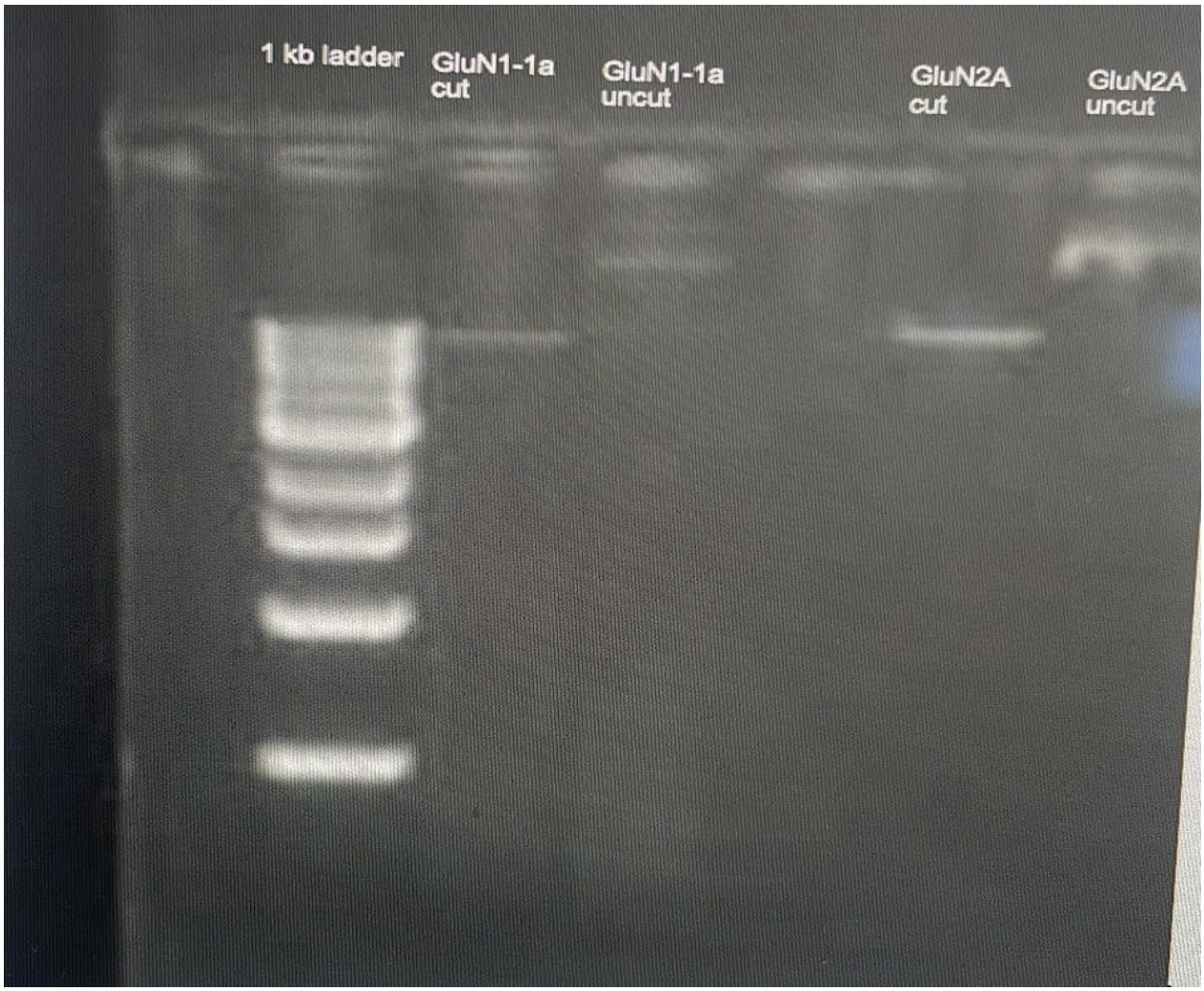


*Fig 7: Gel image from iBright 750 Invitrogen by Thermo Fisher Scientific showing the linearized and non-linearized cDNA. On left, a 1kb DNA ladder follows linearized GluN1, non-linearized GluN1A, linearized GluN2A, and non-linearized GluN2A. The gaps in between not labeled were not properly ejected into the Gel.*

## 3.6 Oocytes Preparation:

Xenopus Leavis oocytes were obtained from the European Xenopus Resource Centre, University of Portsmouth, UK. The oocytes were delivered to the laboratory in a box filled with ice in a 14mL falcon tube containing GTP solution as ovary tissue. after taking them out of the ice box, the oocytes were left to acclimatize for some time. They were placed in a new petri dish along with the solution in the falcon tube and placed in the incubator at 18 °C. As they were in large clumps, to get the individual oocytes, they were placed in a new 14mL falcon tube by cutting off smaller

clumps with help of forceps and scissors. The tube was filled with calcium-free GTP solution containing 2.5mg/mL of collagenase enzyme. Collagenase treatment was used to break the clumps and release the individual oocytes. Calcium-free GTP was used for this process because the enzyme activity with calcium is higher and had a risk of damaging the oocytes. After adding the enzyme and the GTP calcium-free solution to the tube. The falcon tube was placed on a roller for 1 hour.

After 1 hour the oocytes were washed thoroughly with the calcium-free GTP solution multiple times until the solution became clear (usually 6-7 washes). Oocytes were placed into a 90 mm petri dish filled with normal GTP solution. The normal GTP solution was used from here on for the oocyte's maintenance. Separated oocytes were put under the microscope to select healthy cells and any remaining follicular layer was removed using fine forceps. This was taken off to avoid any obstruction during injection and recording. The oocytes, after peeling the follicular layer, were placed in GTP solution in the incubator at 20°C.

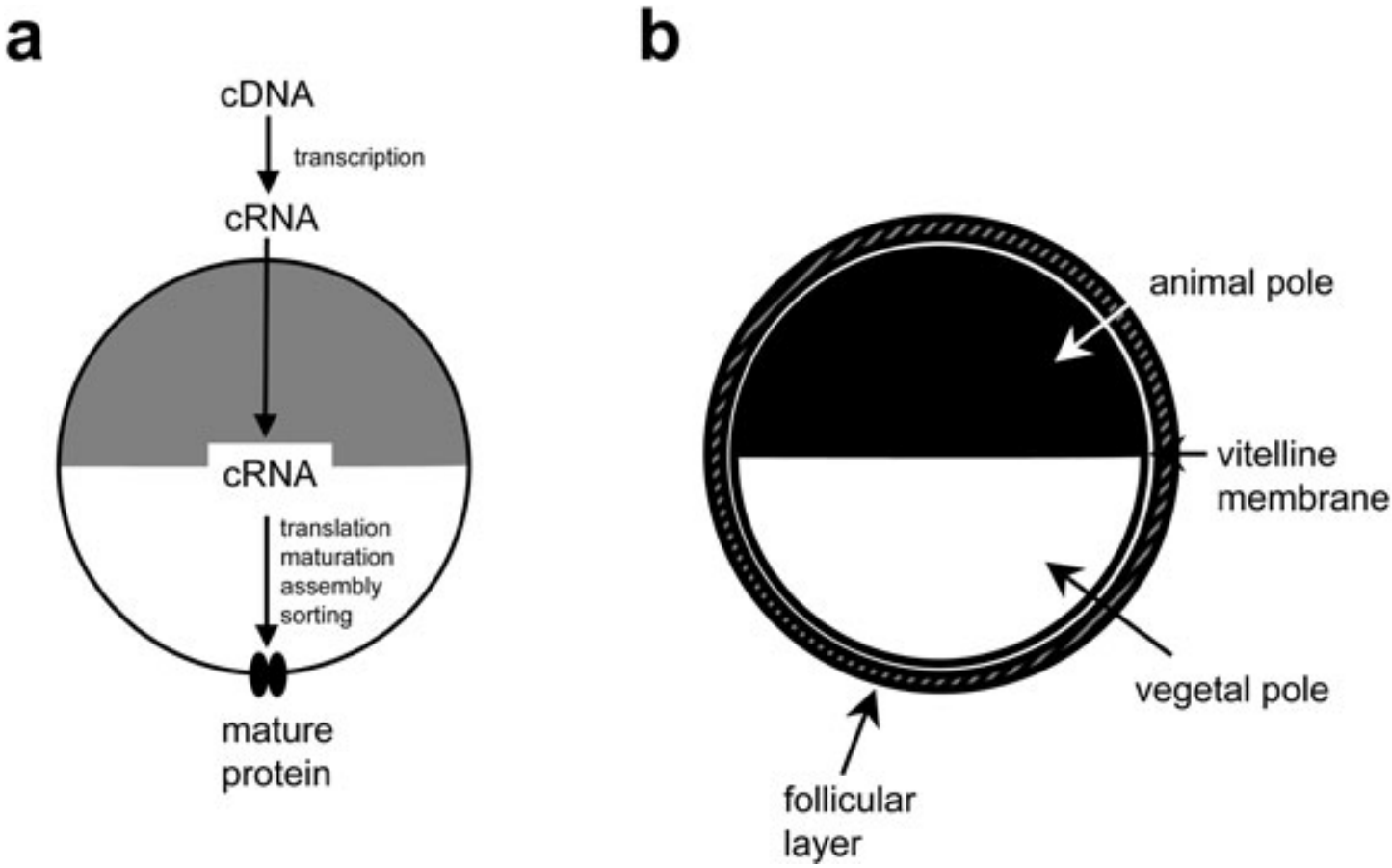


*Fig 8. Fig shows the microinjection of cDNA and cRNA into Xenopus oocytes and the process of expression of proteins. Fig b shows the structure of Xenopus oocytes with a darker animal pole and a vegetal pole surrounded by a follicular layer. cDNA was injected into an animal pole with a nucleus for the expression of proteins, whereas cRNA was injected regardless of the animal/vegetal pole (Bianchi & Driscoll, 2006).*

### 3.7 Injection of cRNA into Xenopus Oocytes:

Using a clean plastic 3mL Pasteur pipette, the separated and defolliculated cells were placed in a petri dish with custom-designed grooved plastic to keep the cells in place while being injected. The petri-dish was filled with GTP solution. Small aliquots (3µL) of cRNA encoding GluN1 and GluN2A was removed from the -80°C freezer and thawed on ice. The Nanoliter injector 2010 (World Precision Instruments 504126) was used to inject the cRNA into the oocytes. The nanoliter injector was connected to a foot switch to make it convenient to inject the cells.

Borosilicate glass capillaries (30-0066, GC150TF-10 World Precision Instruments, US) were used to inject the oocytes. The injecting pipettes were pulled using a programmable Sutter puller (P97, Sutter Instruments Co.). The tip of the glass capillary was broken to a diameter of about 25µm such that it did not rupture the membrane of the oocytes but allowed a good flow of cRNA through the tip. Before charging the capillary with the cRNA, it was filled with paraffin oil to keep the pressure for the cRNA injection. The paraffin oil was added by backfilling using a hypodermic needle in a way that no bubbles were retained within the capillary. After mounting the paraffin-filled capillary onto the plunger of the Nanoliter Injector, 1µL of GluN1 and GluN2A subunit cRNA (100-200ng/µL) was slowly drawn up into the glass capillary from a drop placed on a clean surface, ensuring no air was taken up. The oocytes were then injected with 50nL of cRNA solution each. The injected oocytes were then transferred to 24 well plates filled with GTP solution to keep them healthy. Afterward, they were kept in the incubator at 18°C for 3-5 days to allow for protein expression. The GTP solution was changed daily and the oocytes that died were removed.

### 3.8 Two Electrode Voltage Clamp and Electrophysiological Readings:

The electrophysiological recording of membrane currents was performed using an Axoclamp-2A voltage clamp amplifier (Axon Instruments Inc, USA) consisting of the main control interface connected to the two remote head stages mounted on micromanipulators. Both head stages had microelectrode holders (Harvard Apparatus) connected to them. One of the electrodes was used for the current injection into the cells, while the other monitored the membrane potential. Microelectrodes were made from glass capillaries (Harvard Apparatus GC150TF-10). They were pulled using the Sutter Puller-Model P-97 flaming brown micropipette puller (Sutter Instruments Co). The microelectrodes were ~⅔ filled with 3M KCl solution and were inserted back into the holders making sure the silver/silver chloride wires connected properly. The resistance of the microelectrodes needed to be 0.5-2MΩ.

The reference electrode was the silver/silver chloride electrode that was placed in the bath (extracellularly) and was connected to the amplifier signal ground via one of the head stages. This is assumed to be 0mV and the bath was not actively clamped to 0mV. In fact, it was made sure that the bath voltage was 0mV and that it was stable before the oocytes were impaled. This was referred to it as the bath electrode. Series resistance is the resistance between the recording electrode input at the head stage and the internal face of the oocyte membrane. The main contribution was from the glass microelectrodes that were made sure to have resistances of less than 2 megaohms (checked this before every oocyte). In that case, it was not necessary to compensate the series resistance for relatively small and slowly changing currents that were measured. If the series resistance is too high and not compensated, then it could lose voltage control and the holding potential that was set tends toward zero. This was monitored and made sure it didn't drop by more than an mV or two, it could be said that the clamping efficiency was always >95% and usually very close to 100%.

Oocytes were placed in a perfusion bath that was connected to an MPS-2 Multichannel perfusion system (World Precision Instrument). One of the perfusion tubes supplied frog Ringer solution to provide oocytes with a maintained resting environment. The oocytes were impaled by each of the two microelectrodes, indicated by the recorded (in bridge mode) membrane potential deflecting from 0mV in the bathing solution to a negative value once through the oocyte membrane. The oocytes were then voltage-clamped in two-electrode voltage clamp mode and the holding potential ($V_h$) was set to the desired value. The currents were recorded to a PC via an analogue to digital interface (National Instruments USB-6211) using WinEDR software (John Dempster, Institute of Pharmacy & Biomedical Sciences, University of Strathclyde, UK).

All other tubes of the perfusion system were used to apply the agonist and antagonist solutions at different concentrations. The agonist was $10^{-4}$M NMDA and $10^{-5}$M glycine. The antagonist (memantine) solutions were made using serial dilutions starting from $10^{-4}$M NMDA and $10^{-8}$M glycine in 10-fold steps. To test the expression of GluN1-2A NMDA subunits, the agonist was

applied using the perfusion system at different holding potentials -50, -75, -100mV. Once expression was established, memantine was co-applied with the agonist at varying concentrations of $10^{-8}$ – $10^{-4}$M. Firstly, an agonist was applied until a stable current response was obtained about 10s, then memantine was added at the lowest concentration until a new plateau was obtained, working up to the highest concentration, each time establishing a new plateau current. This was repeated at different holding potentials as mentioned above. HAE inhibition was tested in a similar way with the alkaloid solution being applied at varying concentrations from 0.003µg/mL up to 30µg/mL and these concentrations were again tested at different holding potentials as mentioned for memantine.

### 3.9 Data Analysis:

The NMDA current traces were measured at each plateau phase following the addition of the agonist (control current) or antagonist using WinEDR software (John Dempster, Institute of Pharmacy & Biomedical Sciences, University of Strathclyde, UK) to normalize the data. The data were normalized using GraphPad Prism 8. The normalized data were plotted against the Log of memantine or HAE concentration at each holding potential -50mV, -75mV, and -100mV using GraphPad Prism 9. The plots were fitted using the "log inhibitor vs normalized response variable slope" non-linear regression equation built into GraphPad Prism:

$$\% \text{ Control response} = 100/(1+(IC_{50}/B)S)$$

In this equation, B was the concentration of the NMDA blocker (memantine or HAE) and S was the Hill slope. This equation was used to get an estimate of $IC_{50}$ values of memantine and HAE. $IC_{50}$ is the half maximal value of the drug that inhibits biological functioning by half. The voltage

dependence inhibition of memantine and HAE can be calculated by using the Woodhull equation (Woodhull, 1973):

$IC_{50}(VH) = IC_{50}(0)e(z\delta VFRT)$

## 4. Results:

150-200 *Xenopus* oocytes were injected with human NMDAR subunit GluN1-GluN2A within intervals. But on average 50-70 *Xenopus* oocytes showed expression of the NMDARs subunit GluN1-GluN2A. Xenopus Oocytes showed NMDAR expression within 3-5 days of injecting cRNA.

### Electrophysiological Recordings at Varying Membrane Potentials:

Xenopus oocytes were injected with RNA for the NMDAR GluN1-GluN2A subunit combination to analyze the expression of NMDARs in the oocytes. To confirm the NMDAR expression, a solution of NMDA $10^{-4}$M + glycine $10^{-5}$ M was applied to oocytes via the perfusion system with resultant responses measured using the TEVC technique. To investigate the current-voltage relationship of the expressed NMDA receptors was conducted at a range of holding potentials. Figure (a, b, and c) below shows TEVC recordings in response to the agonist at several holding potentials.

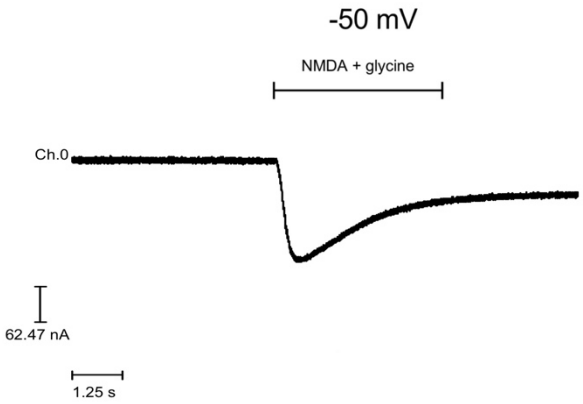
-50 mV
NMDA + glycine
Ch.0
62.47 nA
1.25 s

(a)

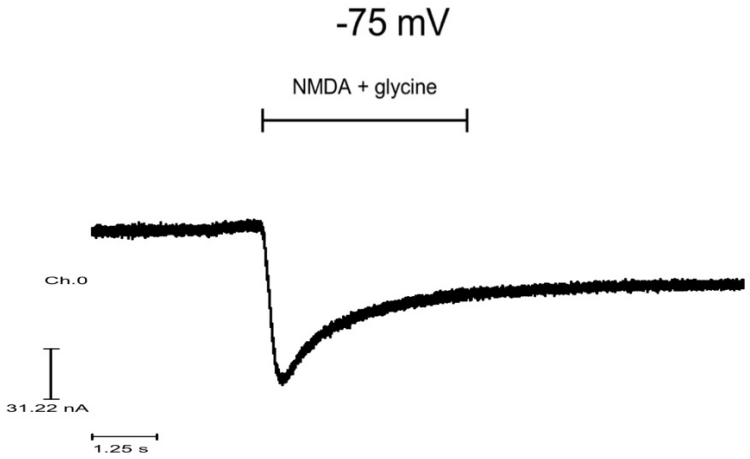
-75 mV
NMDA + glycine
Ch.0
31.22 nA
1.25 s

(b)

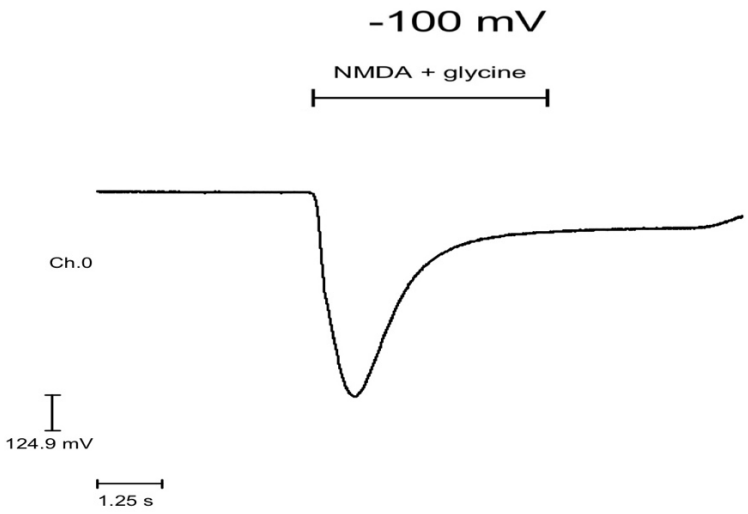
-100 mV
NMDA + glycine
Ch.0
124.9 mV
1.25 s

(c)

*Fig 9 shows responses to the application of NMDA* $10^{-4}M$ *and glycine* $10^{-5}M$ *solution for NMDAR subunits GluN1/GluN2A expressed in Xenopus oocytes. The traces above show WinEDR readings at -50mV, -75mV, and -100mV for the GluN1-GluN2A subunits combination. The readings above were obtained from a single oocyte using the agonists mentioned above.*

The study involved applying the agonist on NMDAR subunits GluN1/GluN2A $10^{-4}M$ +glycine $10^{-5}$M and measuring the resulting currents at different holding potentials -50mV, 75mV, and -100mV. The results showed that the current varied depending on the membrane potential, with the smallest current observed at -50mV and a larger response obtained at more negative potentials at -100mV. These findings were further supported by the current-voltage relationship shown in a, b, and c which demonstrated an increase in NMDA current as the membrane potential became more negative.

## Inhibition of human GluN1-1a/GluN2A NMDARs by memantine

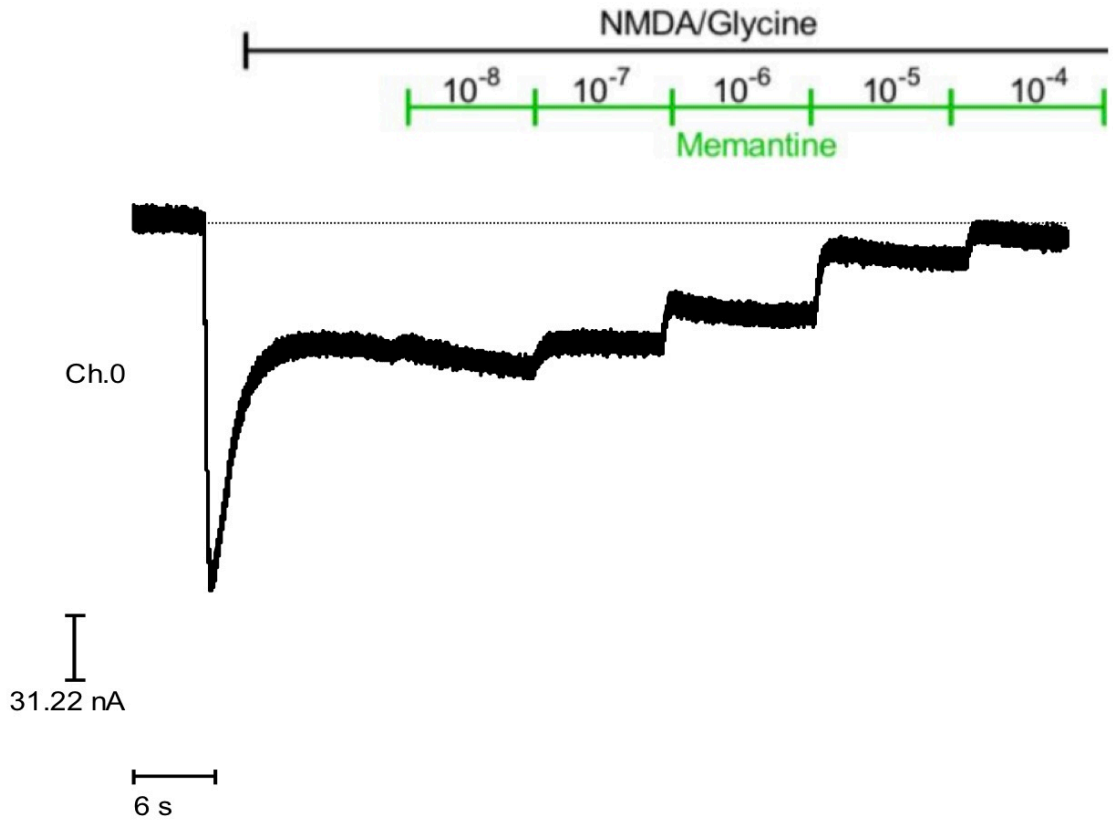


(a)

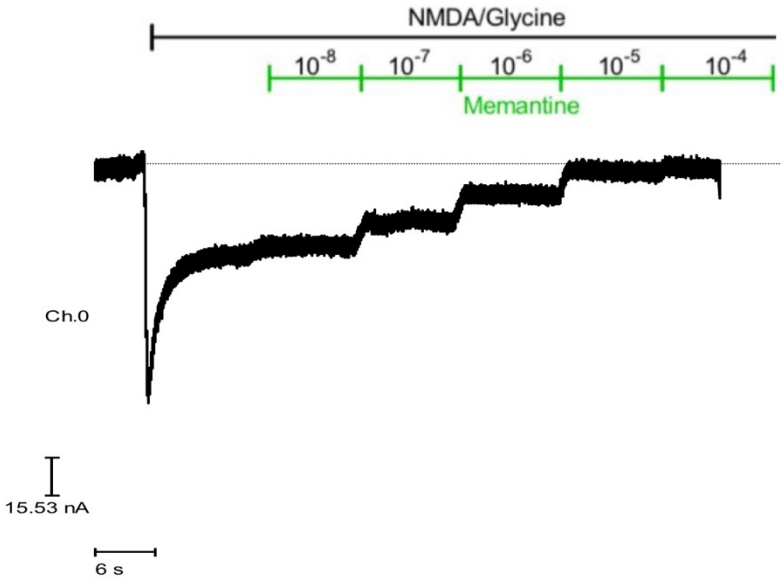


(b)

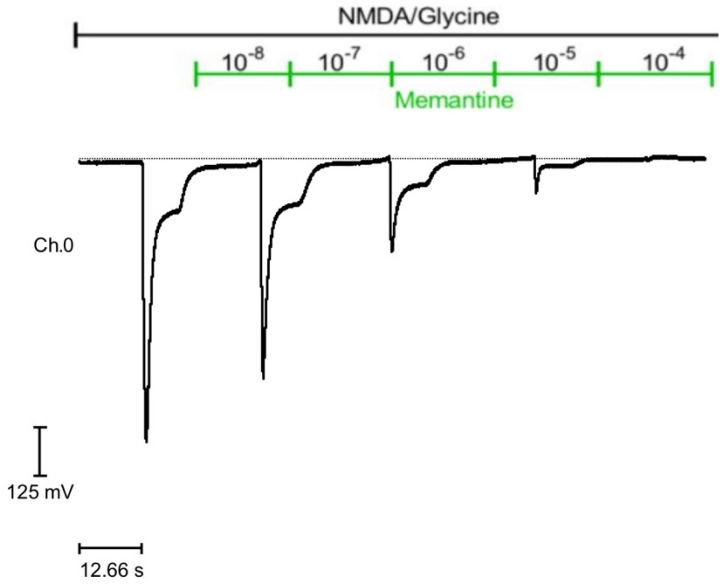


(c)

*Fig (10): Electrophysiological responses of NMDARs subunits GluN1-GluN2A with the application of NMDA* $10^{-4}M$ *+ glycine* $10^{-5}$ *M solution with co-application of memantine at different concentrations ranging from* $10^{-8}M$ *to* $10^{-4}M$ *at varying membrane*

*potentials -50mV, -75mV, and -100mV. The trace reading at -100mV were recorded using the application of an agonist followed by the NMDA Inhibitor memantine with intervals at different concentrations. However, due to uncertainty in NMDARs expression, it was unable to obtain the reading using the method as applied in Vh -50mV (Fig a) and -75mV (fig b) for -100mV (Fig c).*

The data presented in Fig 10 demonstrates the effect of memantine on the inhibition of NMDA-evoked currents. The recordings were obtained after co-applying memantine at different concentrations, starting from the lowest to the highest. It was observed that at a concentration of $10^{-8}$M, the memantine inhibition after applying the agonist was negligible. However, as the concentration increased, there was a marked increase in the inhibition of NMDA-evoked currents. The NMDA currents were almost completely inhibited at a concentration of $10^{-4}$M, which was the highest concentration tested. These results suggest that memantine causes concentration-dependent inhibition of NMDA-evoked currents.

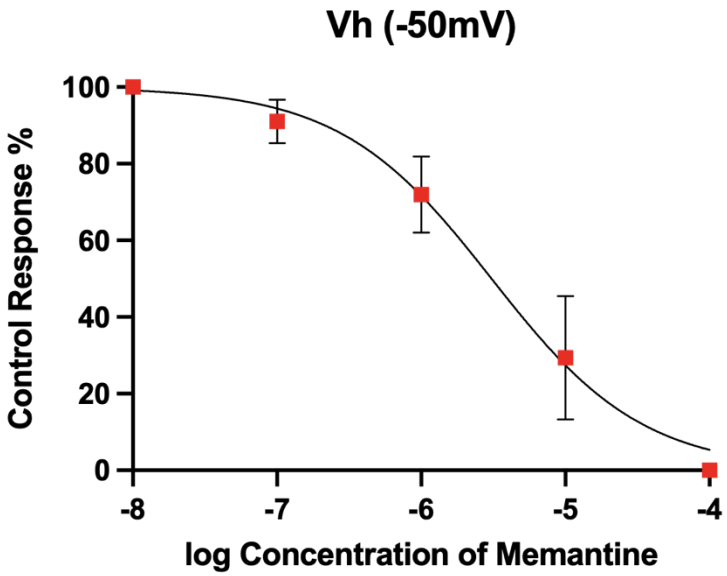

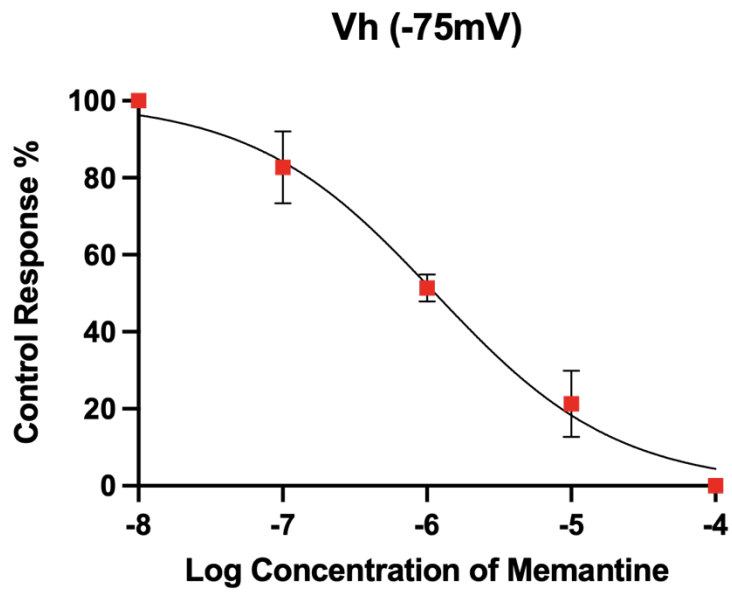


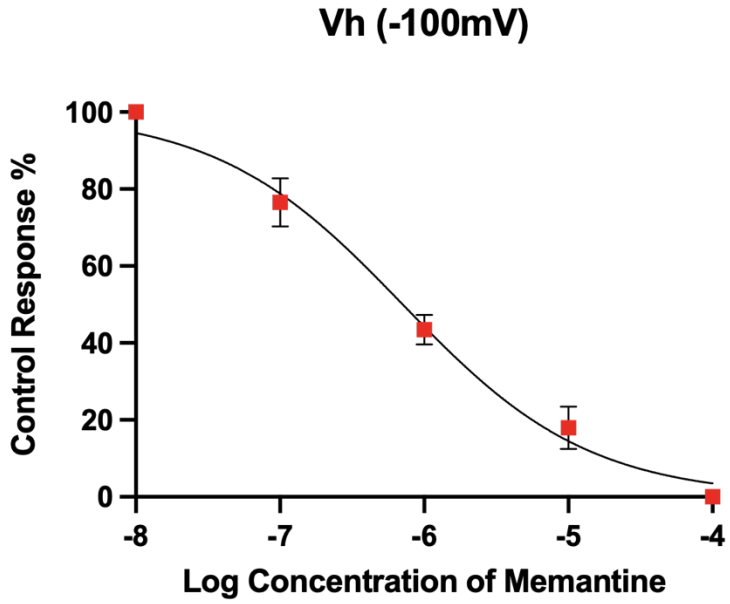


*Fig. (11): Log memantine concentration vs Normalized response showing the concentration-dependent effect of memantine on NMDARs expressed in the Xenopus Oocytes. The recordings were taken at different membrane potentials -50mV, -75mV, and -100mV. The responses were examined after applying memantine at different concentrations. The GraphPad Prism plot shows the*

*mean % control response ±SEM of 6 replicates per VH. Curves were obtained using the fitting equation as stated in methods in the GraphPad Prism.*

*Table 7:* $IC_{50}$ *values of the NMDARs subunits GluN1-GluN2A inhibition by memantine at varying holding potentials. Values were obtained from GraphPad Prism through curve fitting.*

| $IC_{50}$ values of Memantine in GluN1/GluN2A | | | | |
|---|---|---|---|---|
| | $IC_{50}$ | Hill Slope Value | Goodness of Fit | Sum of Squares |
| GluN1/GluN2A (-50mV) | 3.0µM | -1.046 to 0.6595 | 23 | 1790 |
| GluN1/GluN2A (-75mV) | 1.13µM | -0.792 to 0.6008 | 28 | 1138 |
| GluN1/GluN2A (-100mV) | 0.7µM | -0.761 to -0.593 | 23 | 632.3 |

The data presented in figure 11 suggest that memantine exhibits voltage-dependent inhibition of NMDARs. As depicted in the concentration-inhibition curves, the curves shift leftward as the Vh becomes more negative. The $IC_{50}$ values for memantine extracted from the curve fitting show that the values decrease as the membrane potential becomes more negative. The lowest $IC_{50}$ value of 0.77µM was found at -100mV membrane potential for GluN1-GluN2A, which was 3 times higher ($P < 0.05$) at -50mV. The optimal $IC_{50}$ value of 1.13µM was found at -75mV membrane potential. These results suggest that memantine inhibits NMDARs subunits in a voltage-dependent manner.

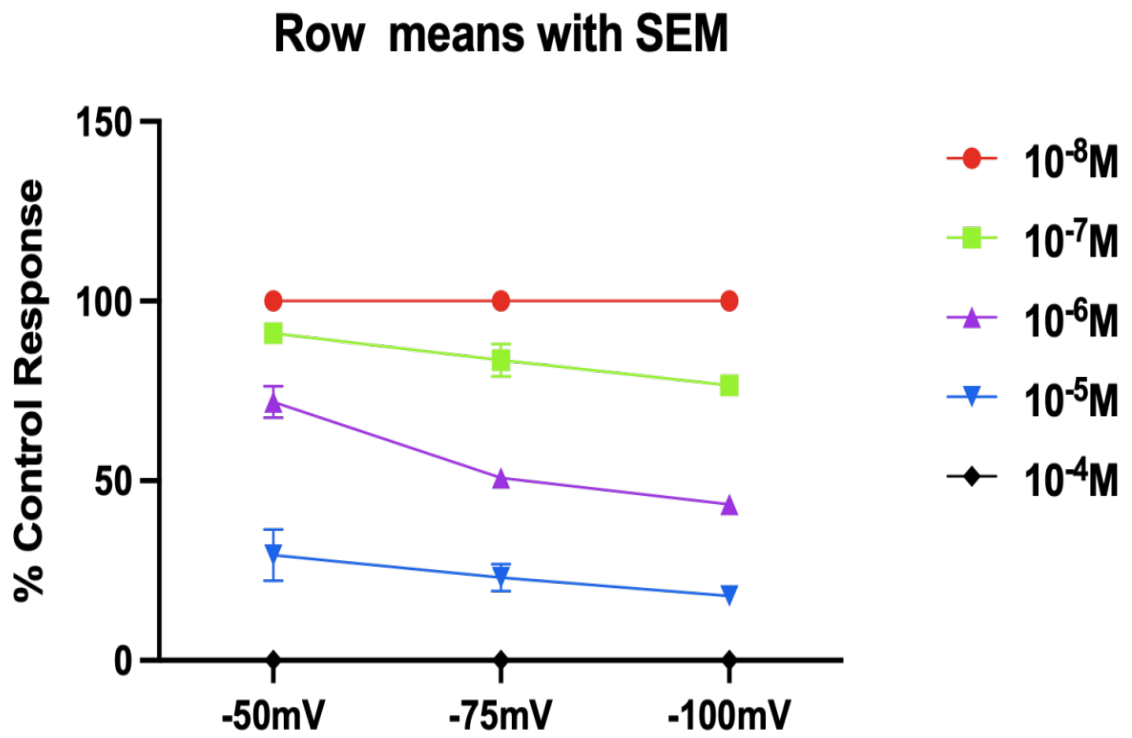


*Figure (12): Linear representation of the mean ±SEM of 5-6 replicates and the percentages response of the concentration-dependent inhibition of memantine on NMDAR subunits GluN1GluN2A expressed in Xenopus Oocytes. The y-axis shows the percentage of the concentration-response of memantine. The x-axis shows varying membrane potentials at -50mV, -75mV, and 100mV with different concentrations color-coded from $10^{-4}$M depicted in black, $10^{-5}$M in blue, $10^{-6}$M in purple, $10^{-7}$M in green, and $10^{-8}$M in red.*

| Statistical analysis of Memantine using Woodhull Equation | |
|---|---|
| zDELTA | 0.8728 |
| $IC_{50}$zero | 16.35 |
| 95% CI Values | |
| $IC_{50}$zero | 15.67 to 16.97 |
| zDELTA | 0.6365 to 0.9983 |
| Goodness of Fit | |
| Degrees of Freedom | 1 |
| R squared | 0.9849 |
| Sum of Squares | 0.04511 |

*Table 8:* Statistical analysis of Woodhull Equation from GraphPad Prism

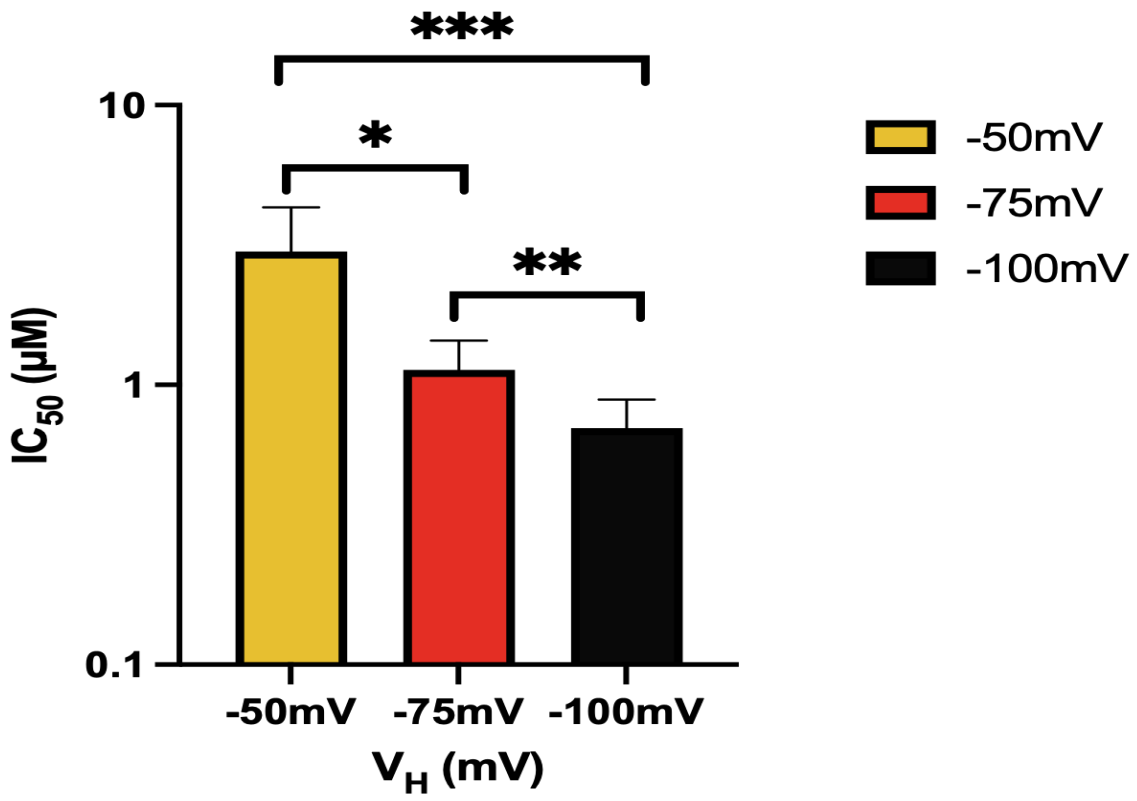


*Fig (13) Bar graph depicting the mean normalized response of the $IC_{50}$ values of the NMDARs subunits GluN1-GluN2A inhibition by memantine vs voltage holding potentials $V_h$ (mV). The x-axis of this bar graph depicts $V_h$ (mV) of varying voltage holding potentials that are color-coded at 50mV in yellow, -75mV in orange, and -100mV in black. The y-axis depicts the mean values of $IC_{50}$ (µmol). The error bars are 95% CI.* ***Asterisk*** ** Shows the p-value* ***<0.0001****, ** shows the p-value* ***<0.0054****, and *** shows the p-value as* ***<0.0001****. The comparison of different holding potential and $IC_{50}$* values were obtained using the extra sum-of-square F test using the PRISM.

In Figure 14, the $IC_{50}$ values for inhibition of NMDAR subunits GluN1-GluN2A by memantine at different voltages are shown. At -100mV, a significant decline in the $IC_{50}$ values compared to -50mV and -75mV is observed, indicating that as the voltage becomes more negative, the $IC_{50}$ decreases, reaching a value of 0.77µmol. At -75mV, the $IC_{50}$ value of 1.13µmol is reached, which corresponds to the resting membrane potential. On the other hand, at -50mV, which is closer to the reversible membrane potential, the highest $IC_{50}$ value of 3.0µmol is observed, compared to the other voltages. This suggests that there is a significant increase in the $IC_{50}$ at the less negative membrane potential of -50mV. Therefore, the evidence presented in this study supports the

conclusion that memantine's inhibition of NMDARs subunits GluN1-GluN2A is voltage-dependent.

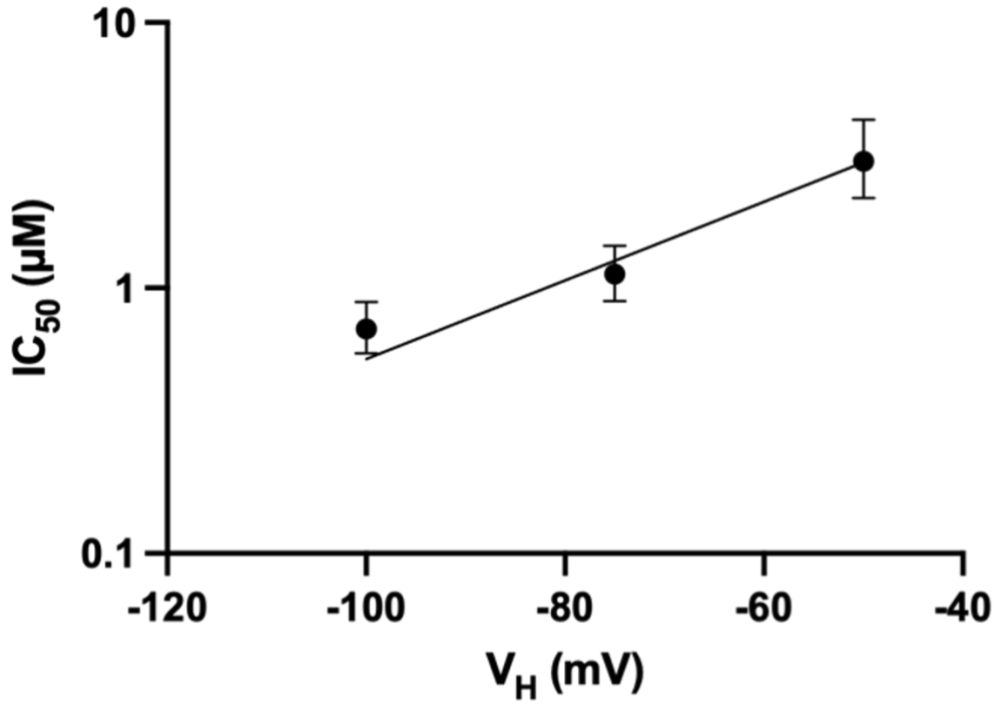


*Fig (14). Linear representation of the Woodhull equation from GraphPad Prism depicting the mean $IC_{50}$ (μmol) values of the NMDARs subunits GluN1-GluN2A inhibition by memantine vs voltage holding potential $V_h$ (mV). The y-axis depicts 95% CI highest and lowest the $IC_{50}$ (μmol) values of the NMDARs subunits GluN1-GluN2A inhibition by memantine. The x-axis depicts various voltage-holding potentials $V_h$ (mV) at -50mV, -75mV, and -100mv. The error bars are 95% CI*

Figure 14 analyzes the voltage dependence inhibition of memantine using GraphPad Prism software and the Woodhull equation, which is explained in the methods section.

The Woodhull equation describes the electric field ($\delta$) sensed by the blocker and the charge (z) on the blocker. Since memantine has a charge of 1, the z$\delta$ value of memantine is 0.8728. This indicates that 87% of memantine binds and reaches the inner side of the channel by crossing the two transmembrane pore regions.

Thus, the Woodhull equation provides an explanation for the binding affinity through the pore region and the voltage dependency of memantine. The information presented in figure 14 supports the understanding of the mechanism of action of memantine as a blocker of the NMDA receptor.

## 4.3 Recordings of NMDARs Subunits inhibition by H.axyridis Extract in Xenopus Oocytes:

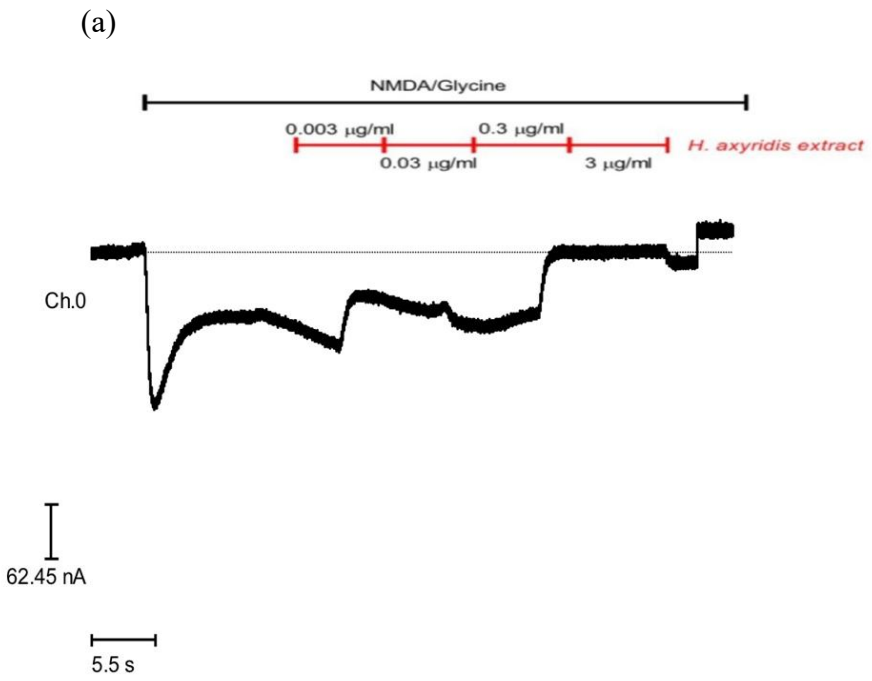

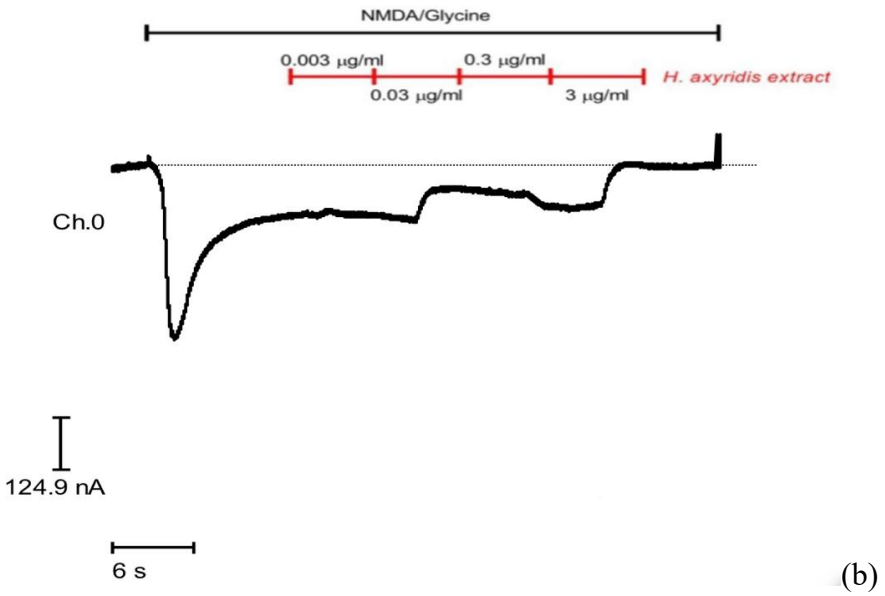


*Fig (15): Electrophysiological traces of NMDA currents in response to the application of agonist NMDA* $10^{-4}$ *M and Glycine* $10^{-5}$ *M using TEVC. Application of HAE at different concentrations ranging from* $10^{-7}$*M to* $10^{-4}$*M can be seen at varying membrane potential. The trace recording file at -100mV crashed due to an error in winEDR software and was not able to retrieve from the PC. Fig a, at -50mV and fig b at -75mV for HAE.*

Figure 15 illustrates the electrophysiological traces of NMDAR currents, which were examined using NMDA $10^{-4}$M and Glycine $10^{-5}$M agonists at various membrane potentials. The response to NMDA was observed to change at different membrane potentials.

Subsequently, HAE was applied at different concentrations ranging from $10^{-7}$M to $10^{-4}$M, which corresponded to 0.003µg/mL to 3µg/mL, respectively. The lowest concentration of HAE 0.003µg/mL had the least inhibitory effect on NMDA currents, as shown in Figure 15. Similarly, the inhibitory effect did not change significantly at 0.03µg/mL.

However, a slight change in HAE response was observed at 0.3µg/mL, and the maximum inhibitory effect was observed at 3µg/mL. It is worth noting that even at the highest concentration of HAE (3µg/mL), the NMDA currents were not entirely inhibited, and the inhibitory effect was only partial.

Overall, these results suggest that HAE has a dose-dependent inhibitory effect on NMDAR currents, with a maximum effect at 3µg/mL. The information provided in Figure 15 offers insights into the potential therapeutic applications of HAE in NMDAR-mediated disorders.

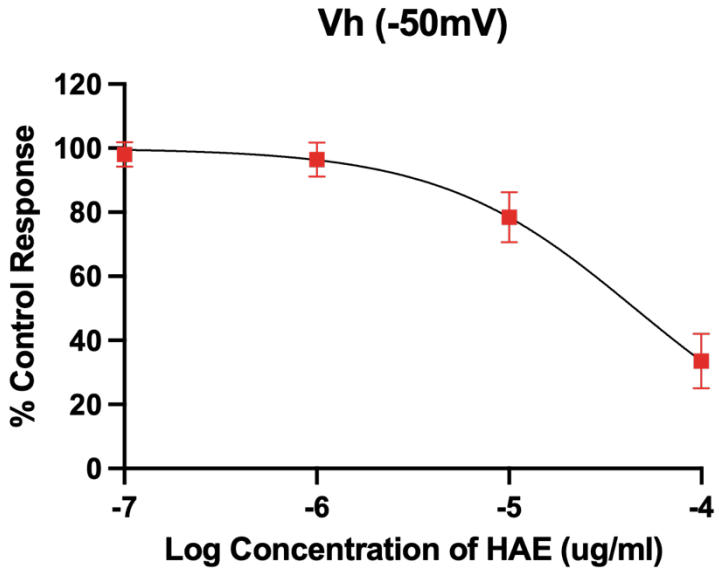


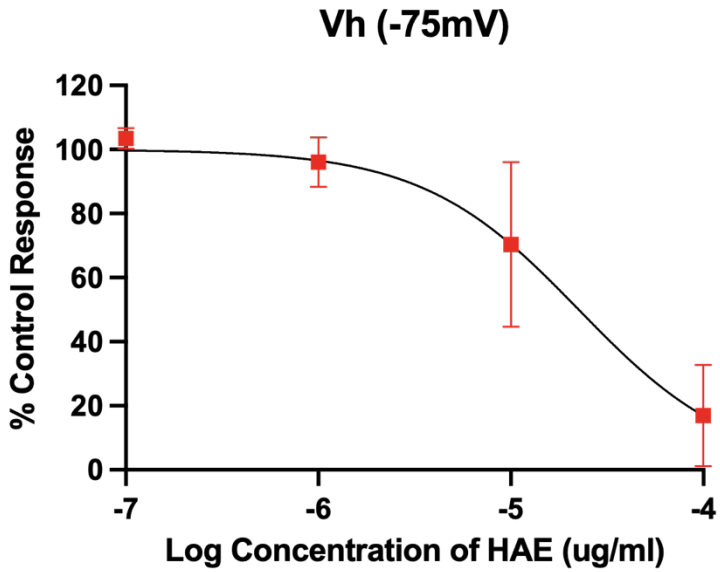

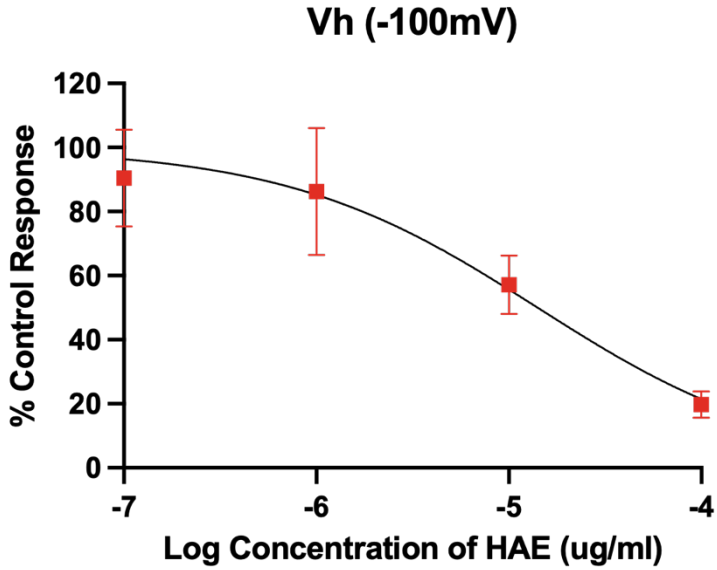


*Fig (16): Concentration-dependent inhibition of HAE at -50mV, -75mV, and -100mV membrane potential at different concentrations ranging from* $10^{-7}M$ *and* $10^{-4}M$*. The curve fitting shows the effect of HAE on NMDAR subunits GluN1-GluN2A expressed in Xenopus Oocytes. The plots show the mean ±SEM of 5-6 replicates and the percentages response and the concentration of the HAE. Curves were obtained using the GraphPad Prism.*

In Fig 16, the concentration-dependent inhibition graph and the readings taken from traces of WinEDR readings are shown. The graphs were constructed for curve fitting and generating the IC50 values at different membrane potentials -50mV, -75mV, and -100mV.

The -50mV graph shows the least inhibition at $10^{-7}$M and $10^{-6}$M concentrations of HAE, which can be examined from the curve fitting in the graph. The curve shows negligible difference at -50 mV, -75mV, and -100mV at the concentration of $10^{-7}M$ for HAE. However, there was a slight change in the curve found at $10^{-6}$ M and $10^{-5}M$ at -50mV and -75mV respectively.

The inhibition effect of HAE at $10^{-5}M$ concentration for -100mV increased as compared to -50mV and -75mV. Similarly, the dose inhibition curve for -50mV and -75 at $10^{-4}M$ (3µg/mL) had no clear difference. But a difference was again seen for -100mV membrane potential at maximum concentration. It is important to note that the maximum concentration at $10^{-4}M$ (3µg/mL) of HAE

did not completely inhibit the NMDA currents at -50mV, -75mV, and -100mV membrane potential.

Table 9*:* $IC_{50}$ *values of the NMDARs subunits GluN1-GluN2A inhibition by HAE at varying holding potentials. Values were obtained from GraphPad Prism through curve fitting as in fig above.*

| $IC_{50}$ values of HAE in GluN1/GluN2A | | | | |
|---|---|---|---|---|
| | $IC_{50}$ | Hill Slope Value | Goodness of Fit | Sum of Squares |
| GluN1/GluN2A (-50mV) | 8.80µM (2.502.50µg/mL) | -1.036 to -0.543 | 18 | 1916 |
| GluN1/GluN2A (-75mV) | 5.16µM (1.46µg/mL) | -1.082 to -0.423 | 10 | 2089 |
| GluN1/GluN2A (-100mV) | 3.04µM (0.86µg/mL) | -0.9413 to 0.505 | 6 | 252.8 |

Table 9 shows the $IC_{50}$ values of HAE at different membrane potentials. The $IC_{50}$ values were obtained after plotting the curve fit graph on GraphPad Prism, and they demonstrated voltage-dependent inhibition for HAE. Specifically, the $IC_{50}$ value at -50mV was higher than at -75mV and -100mV, indicating that the voltage-dependent inhibition increased as the membrane potential became more negative. In fact, the $IC_{50}$ of HAE was lowest at -100mV, and it inhibited the NMDA currents at a higher rate than at membrane potentials closer to a positive value.

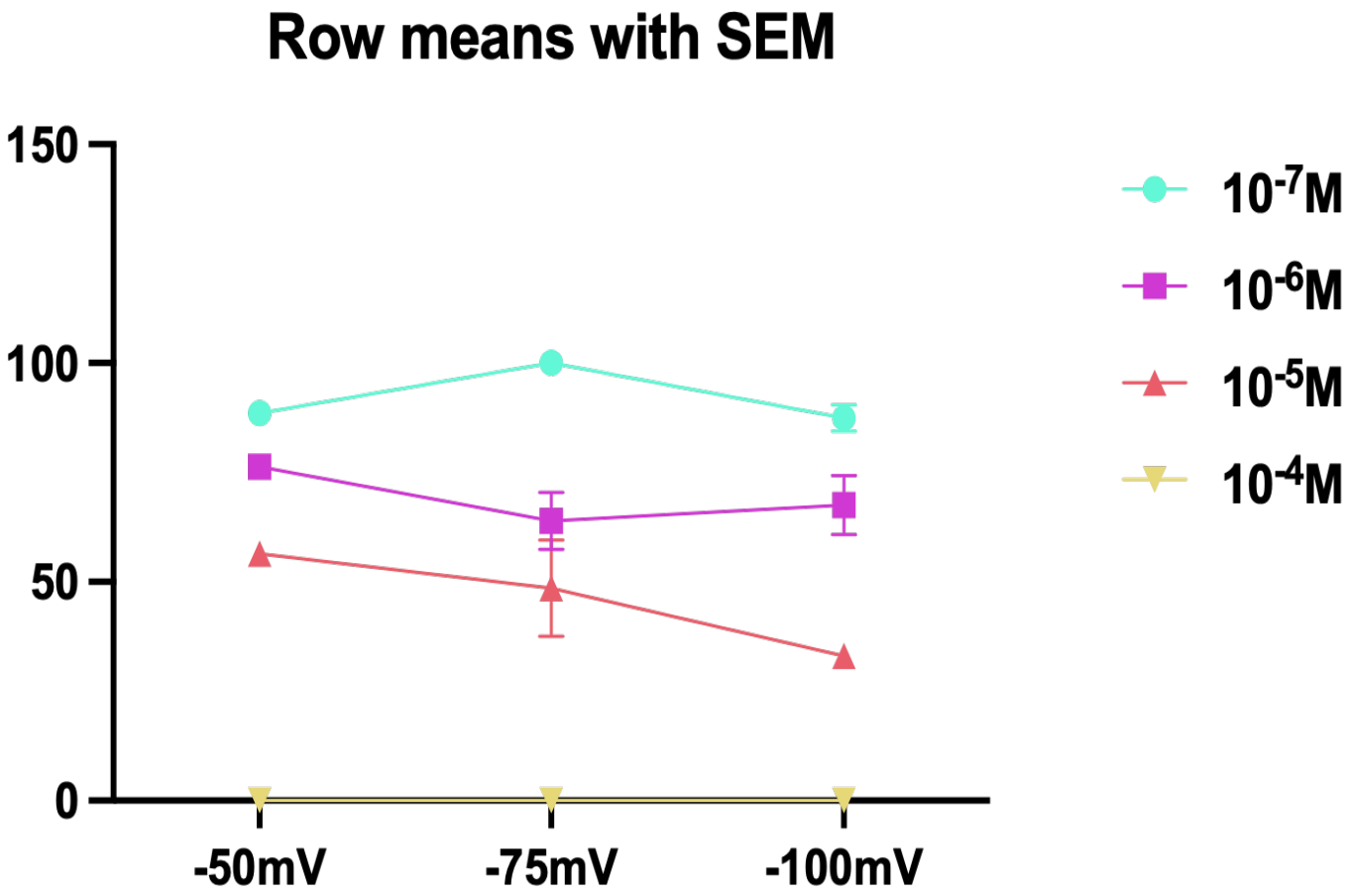


*Figure (17): Linear representation of the mean ±SEM of 5-6 replicates and the percentages response of the concentration-dependent inhibition of HAE on NMDAR subunits GluN1-GluN2A expressed in Xenopus Oocytes. The y-axis shows the percentage of the concentration-response of HAE. The x-axis shows varying membrane potentials at -50mV, -75mV, and -100mV with different concentrations color-coded from* $10^{-4}$ *M depicted in yellow,* $10^{-5}$*M in red,* $10^{-6}$*M in purple, and* $10^{-7}$*M in teal. The error bars are 95% CI*

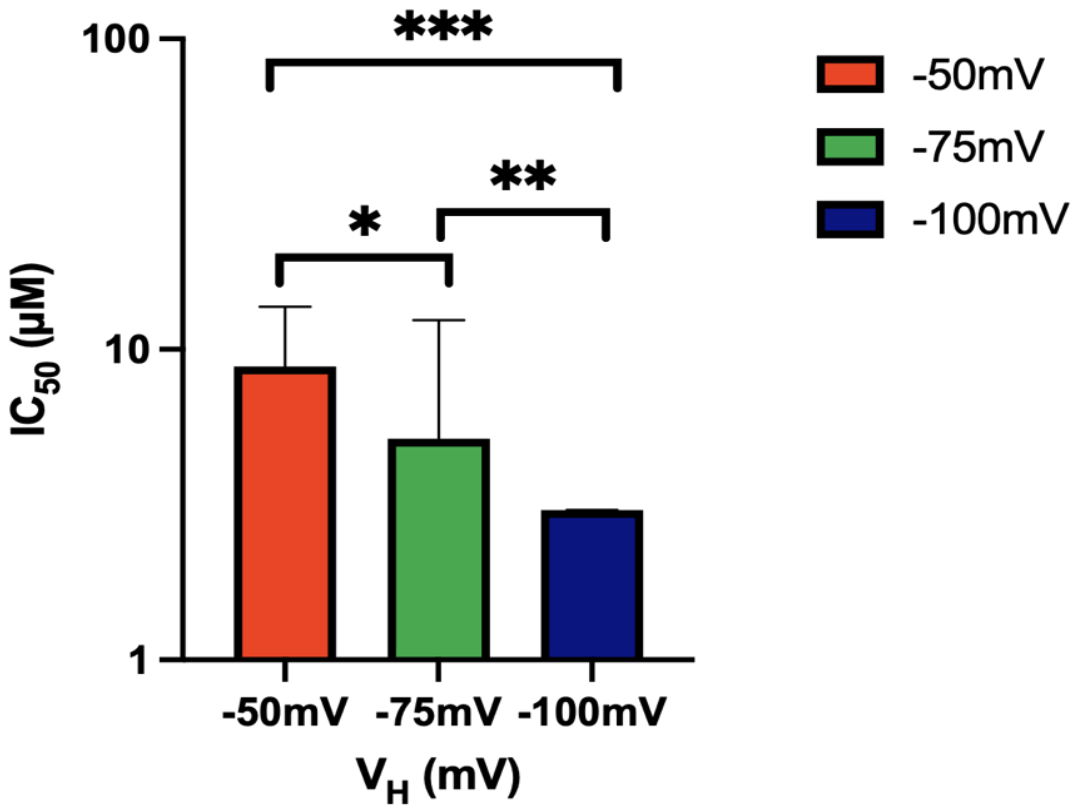


*Fig (18) Bar graph depicting the mean normalized response of the $IC_{50}$(µmol) values of the NMDARs subunits GluN1-GluN2A inhibition by HAE vs voltage holding potentials $V_h$ (mV). The x-axis of this bar graph depicts $V_h$ (mV) of varying voltage holding potentials that are color coded with -50mV in red, -75mV in green, and -100mV in blue. The y-axis depicts the mean values of $IC_{50}$ (µmol). The error bars are 95% CI.* ***Asterisk*** ** Shows the p-value* ***<0.0003***, *** shows the p-value* ***<0.0001***, *and *** shows the p-value as* ***<0.00045***. *The comparison of different holding potential and $IC_{50}$* values were obtained using the extra sum-of-square F test using the PRISM.

In Figure 18, the $IC_{50}$ values for the inhibition of NMDAR subunits GluN1-GluN2A by HAE at different membrane potentials are depicted. The results indicate that as the membrane potential becomes more negative, the $IC_{50}$ value decreases significantly. At -100mV, the $IC_{50}$ value of 3.04µmol is the lowest observed. At -75mV, the $IC_{50}$ value of 5.16µmol is consistent with the resting membrane potential. The $IC_{50}$ value of 8.80µmol observed at -50mV, which is closer to the reversible membrane potential, is the highest observed among the different membrane potentials. Therefore, the evidence suggests that HAE may be voltage-dependent, like memantine. These findings further strengthen the hypothesis that HAE could be a potential

therapeutic agent for the treatment of neurological disorders associated with NMDAR dysfunction.

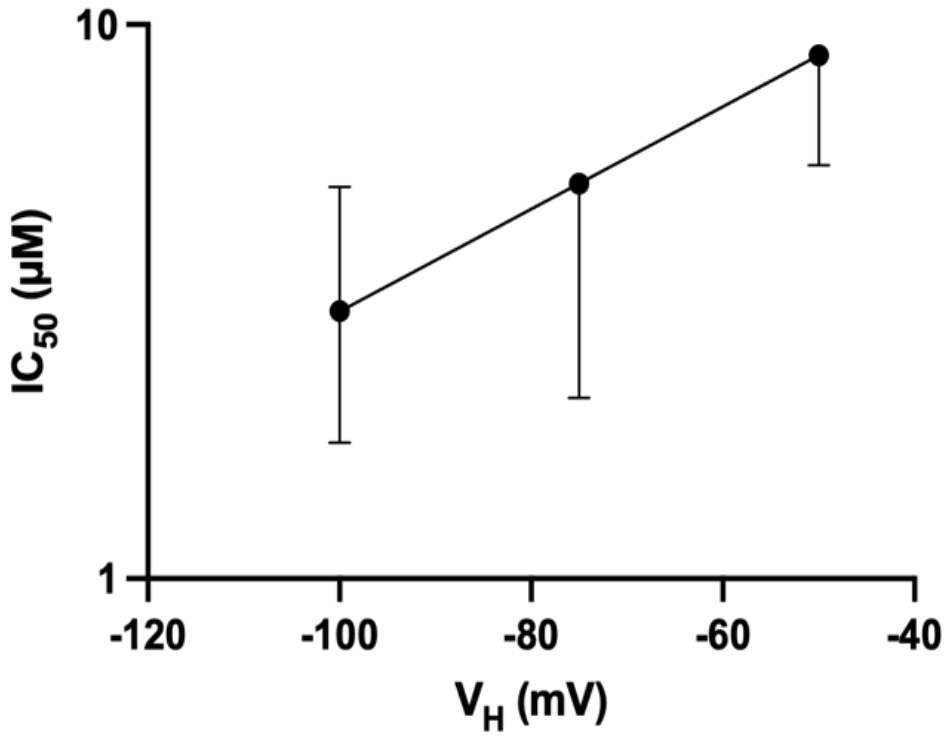


*Fig (19) Linear representation of the Woodhull equation from GraphPad Prism depicting the mean $IC_{50}$ (µmol) values of the NMDARs subunits GluN1-GluN2A inhibition by HAE vs voltage holding potential $V_h$ (mV). The y-axis depicts 95% CI highest and lowest the $IC_{50}$ (µmol) values of the NMDARs subunits GluN1-GluN2A inhibition by HAE. The x-axis depicts various voltage holding potentials $V_h$ (mV) at -50mV, -75mV, and -100mV. The error bars are 95% CI.*

| Statistical analysis of Harmonine using Woodhull Equation | |
|---|---|
| zDELTA | 0.5449 |
| $IC_{50}$zero | 25.51 |
| 95% CI Values | |
| $IC_{50}$zero | 24.45 to 26.62 |
| zDELTA | 0.5275 to 0.5625 |
| Goodness of Fit | |
| Degrees of Freedom | 1 |
| R squared | 1.000 |
| Sum of Squares | 8.266e-005 |

*Table 10:* Statistical analysis of Woodhull Equation from GraphPad Prism

The voltage dependence inhibition of HAE was analyzed in figure 19 using the Woodhull equation, which was previously mentioned in the methods section. The electric field sensed by the blocker is denoted by Delta ($\delta$), and the charge on the blocker is denoted by z. For HAE, the z charge was 2. The $IC_{50}$ values were plotted against the membrane holding potential of -50mV, -75mV, and -100mV. This provided a z$\delta$ value for HAE of 0.5449. Due to the charge of +2 on HAE, the value was divided by 2, giving a $\delta$ value of 0.272. This value shows that HAE crossed 27% of the transmembrane pore region on binding. However, it is hard to be precise in the case of HAE since it is about 90% harmonine on which the charge is based. In the case of multi-charged molecules like harmonine, one amine could bind to the outer region, whereas the other could bind deeper into the pore region. Nevertheless, this analysis confirms the voltage dependency of HAE action on NMDARs, which was also observed in the earlier results from their $IC_{50}$ values. Memantine and HAE were found to be voltage-dependent.

## 5. Discussion:

This study consisted of two main components. The first component focused on examining the effect of memantine on human NMDA clones (GluN1-GluN2A) and comparing it with previous research performed on rat NMDA clones. The second component involved examining the inhibition of H. axyridis Extract (HAE) on NMDARs (GluN1-GluN2A) and comparing it with previous research on rat NMDA clones. It is important to note that HAE, a new drug, had never been tested before on human NMDA clones. Therefore, this study was significant in determining the efficacy of HAE (which contains 90% harmonine) for the potential treatment of Alzheimer's disease. Additionally, although memantine has been approved by the FDA, it has been minimally tested on human NMDA clones. This study further strengthened the clinical efficacy of memantine and its frequent use for Alzheimer's disease. Prior experimental studies primarily focused on rat NMDA clones. The second component of the research was the first to examine the efficacy of HAE inhibition on human NMDA clones, making it a novel contribution to the field.

NMDARs play a very significant role in synaptic transmission, plasticity, learning, and memory. The pathological activation of these receptors, and increased calcium influx cause synaptic dysfunction and gradual neuronal cell death. The toxicity in the NMDARs is mostly mediated through the calcium influx. GluN2A and GluN2B are the most significant NMDA subunit playing an integral part in the synaptic function (Danysz and Parsons, 2003; Wenk, 2006; Wang and Reddy, 2017; Monyer et al., 1994; Takai et al., 2003). Therefore, targeting these subunits would be the prime target in AD treatment. This study found memantine and HAE to inhibit the NMDA subunits in both human and rat NMDA clones.

This study involved two components. Firstly, it focused on the effect of memantine on the human recombinant GluN1-GluN2A NMDARs subtype and compared it to the earlier research performed almost entirely on rat NMDARs. Secondly, the same experimental study was performed to examine the inhibition of NMDARs (GluN1-GluN2A) by HAE and compare with limited previous research performed on rat NMDARs. It should be noted that HAE being a newly

studied compound was never tested before on Human NMDARs. So, this study was very significant in examining the efficacy of HAE (90% harmonine) for the potential treatment of AD disease. In addition to this, memantine, although approved by FDA, has been least tested on human NMDARs. This further strengthened our knowledge of memantine and its impact on human NMDARs. This study on human NMDARs is likely to be more relevant to the clinical efficacy of memantine and its frequent use for AD.

NMDARs play a very significant role in synaptic transmission, plasticity, learning, and memory. The pathological activation of these receptors increases calcium influx, causes synaptic dysfunction, and gradual neuronal cell death. The toxicity in the NMDARs is mostly mediated through the calcium influx. NMDARs containing GluN2A and GluN2B are the most significant types playing an integral part in the synaptic function along with being the most $Ca^{2+}$ permeable (Danysz and Parsons, 2003; Wenk, 2006; Wang and Reddy, 2017; Monyer et al., 1994; Takai et al., 2003). Therefore, targeting these subunits would be ideal in AD treatment. This study found memantine and HAE to inhibit the NMDA subunits in both human and rat NMDA clones.

This study found that memantine inhibited the NMDARs in a concentration and voltage-dependent manner fig 11 as might be expected from previous data. At a Vh close to normal resting membrane potential -75mV, memantine had an IC50 value of 1.13µM. The previous research findings by Kaur 2022, of memantine on rat NMDA clones, support the $IC_{50}$ values of this study. The study showed that at a Vh of -75mV, the IC50 value of the memantine inhibition of rat clones NMDARs GluN1/GluN2A was 1.45µM compared to our value of 1.13µM. Also, the study showed at a Vh of -50mV and -100mV $IC_{50}$ values of memantine being 4.19µM and 1.84µM respectively while our $IC_{50}$ values of memantine at a Vh of -50mV and -100mV $IC_{50}$ values of 3.0µM and 0.77µM respectively (Kaur 2022). Another study by McClymont et al (2012) displayed $IC_{50}$ values of the memantine inhibition of rat clones NMDARs GluN1/GluN2A at a Vh of -50mV, -75mV, and -100mV to be 3.94µM, 2.48µM, and 0.80µM respectively (McClymont et al 2012). Thus, the present study closely aligns with the data reported from the $IC_{50}$ values of the memantine inhibition on rat clones NMDARs GluN1/GluN2A mentioned in the two previous

studies which support our findings in human NMDAR's GluN1/GluN2A.Therefore, this suggests that the mechanism of action for AD disease is a voltage-dependent open channel blocker of NMDARs which can be confirmed for both rat and human NMDARs.

Research by Kotermanski et al (2009), transfected the HEK293T cells with GluN1-GluN2A subunits. They found the $IC_{50}$ for memantine was 1.25µM at -75mV. The moderate affinity of memantine at resting membrane potential in numerous other studies were also demonstrated at around 1µM (Rogawski, 1993, Parsons et al., 1993, Parsons et al., 1999, Johnson and Kotermanski, 2006; Parsons et al., 1995, Parsons et al., 1996, Parsons et al., 1998, Bresink et al., 1996, Chen and Lipton, 1997, Blanpied et al., 1997, Sobolevsky and Koshelev, 1998, Sobolevsky et al., 1998, Losi et al., 2006). These findings also confirmed the functional properties of memantine. The studies were mostly carried out on the primary culture of rat hippocampal, cortical neurons, and rat NMDARs expressed in HEK-293 cells. The moderate affinity of memantine in previous research supports our findings in this study. A recent study performed by Kaur (2022) on rat NMDA clones found the $IC_{50}$ for memantine as 1.45µM at -75mV. This again strengthens our findings and results of memantine at resting membrane potential. As mentioned previously, there had been few studies on human NMDARs and the effect of memantine.

Until now, only one other study found the $IC_{50}$ of memantine for Human NMDARs (GluN1GluN2A) at resting membrane potential of -70mV, being in the range 0.79-1.3µM, to be very close to that obtained in this study (Ferrer-Montiel et al., 1998). They used human GluN1GluN2A NMDARs subunit and expressed them in the human cell line (HEK-293 cells) and detected changes in the intracellular calcium using the FLIPR device. Additionally, the study used the patch clamp technique to have a faster perfusion system for better measurement of blocking kinetics (Gilling et al., 2009). This was the first study that support our findings of memantine in Human NMDARs (GluN1-GluN2A). according to Gilling et al (2009), the only other data on memantine on Human NMDARs (GluN1-GluN2A) was presented by Ferrer-Montiel et al (1998). Ferrer-Montiel et al (1998) showed the $IC_{50}$ of memantine for Human NMDARs GluN1-GluN2A as 0.22µM at resting

membrane potential. This was clearly in contrast to the previous findings in rat NMDA clones in all experimental studies. The study by Ferrer-Montiel et al (1998) also showed memantine to be voltage independent in Human NMDARs. This is also in contrast to all the data we have for memantine in human NMDA clones. All the previous experimental findings had shown memantine to be voltage-dependent in the rat NMDA clones (Gilling et al., 2009). Therefore, this present study was novel research showing memantine to be voltage-dependent in Human NMDARs as well. And this study observed the $IC_{50}$ values of memantine in (human NMDARs) to be like the rat NMDA clones.

Memantine was tested at varying holding potentials in our study. The $IC_{50}$ values of memantine changed at different holding potentials. It was found to have higher $IC_{50}$ at less negative membrane potential, whereas, decreasing the membrane holding potential to 100mV, decreased the $IC_{50}$. We propose that decreasing the holding potential to a more negative value causes the membrane to have a stronger electrical gradient such that it causes the externally applied positively charged memantine to move inside the receptor pores more effectively. Thus, memantine blocks the NMDARs at -100mV more strongly as compared to 50mV. This causes the $IC_{50}$ of memantine at -100mV to be lower. According to Johnson and Kotermanski (2006), memantine being an open-channel blocker works in the presence of an agonist and binds at the same site as magnesium. Moreover, magnesium blockade decreases the inhibition of memantine by competition. According to Chiu and Carter (2022), the NMDA component in the postsynaptic neurons is negligible due to voltage-dependent Mg block. However, this is observed only at resting membrane potential.

The first part of our study compared the inhibition effects of both memantine and HAE on the human NMDARs containing GluN1-GluN2A subunits by comparing the $IC_{50}$ values of both against varying voltage holding potentials Vh. As previously stated above, the $IC_{50}$ values of memantine inhibition for varying voltages of -50mV, -75mV, and -100mV are 3.0µM, 1.13µM, and 0.77µM,

respectively. The trend seen regarding Vh and $IC_{50}$ values depicts that at the more positive membrane potential of -50mV, the $IC_{50}$ value is the highest while at the most negative membrane potential of -100mV, the $IC_{50}$ value is the lowest. A similar trend was observed with HAE inhibition of human NMDARs containing GluN1-GluN2A subunits for HAE, an $IC_{50}$ value of 2.50µg/mL is seen at a Vh of -50mV. Also, Vh at -100mV had the lowest $IC_{50}$ values for HAE which was at 0.86µg/mL. At a Vh of -0.75mV near resting membrane potential, HAE had an $IC_{50}$ value of 1.46µg/mL. Thus, both memantine and HAE had the lowest $IC_{50}$ at -100mV which shows that they may both block the NMDARs at -100mV more than at -50mV.Therefore, the similar trends found in the $IC_{50}$ values of both NMDAR subunits GluN1-GluN2A blockers memantine and HAE were found to be dependent on the voltage holding potential.

The second part of the study focused on the effect of HAE on the human NMDARs containing GluN1-GluN2A subunits. It was found that HAE acted in a similar way to memantine. As seen in the results, HAE inhibited the NMDARs in a concentration-dependent manner. The comparative analysis of this study showed that memantine unlike HAE completely inhibited the NMDARs at the highest concentration of $10^{-4}$M. However, as mentioned in the results the highest concentration of HAE (3µg/mL) was about 10-fold lower than the highest concentration of memantine $10^{-4}$M, based on the conversion using the harmonine (90% of HAE) molecular weight of 283. This implies that 3µg/mL was equivalent to around 10µM. Moreover, HAE also inhibited the NMDARs in a voltage-dependent way like memantine. This shows the binding mechanism of memantine and HAE to the pores in the NMDARs as similar.

The $IC_{50}$ values for memantine and HAE had quite a difference in human NMDA. Whereas the comparison of rat NMDA clones for HAE showed similarity in the $IC_{50}$ values. This was demonstrated by (Kaur, 2022) in her study of rat NMDA clones that HAE had $IC_{50}$ of 2.65µg/mL, 1.11µg/mL, and 1.72µg/mL at -50mV, -75mV, and -100mV. However, the present experimental study found the $IC_{50}$ of HAE in human NMDARs to be 2.50µg/mL, 1.46µg/mL, and 0.86µg/mL at -50mV, -75mV, and -100mV. As this was the first study in human NMDARs, this was novel research

showing the efficacy of HAE in human NMDA clones. In addition to this, this study showed the $IC_{50}$ values of HAE in a voltage-dependent manner for the first time in Human NMDARs.

HAE inhibited the NMDAR subunits GluN1-GluN2A in a voltage-dependent manner. This voltage dependence was like memantine. Decreasing the membrane potential to more negative values decreased the $IC_{50}$ value. Whereas the holding potential closer to the reversal potential, e.g. -50mV, resulted in a higher $IC_{50}$. This implies the impact of HAE as an open channel blocker like memantine. This strongly supports HAE as an NMDAR blocker and a potential treatment for Alzheimer's. Future work could also involve the use of higher concentrations of HAE for better results.

As mentioned previously, the Woodhull equation was used to further analyze the voltage dependency and the binding affinity of both memantine and HAE through the transmembrane pore region. As shown in the results, through the Woodhull equation the z charge for memantine was 1. The $\delta$ value of memantine was 87% which shows the crossing of the transmembrane pore region thus reaching the inside of the channel. However, in HAE the z charge was 2. Thus, the $\delta$ value for HAE was 27%, meaning that only 27% may have crossed the transmembrane pore region on the binding site but it is difficult to determine exactly since HAE is about 90% harmonine. Also, due to the multiple charges found on HAE, a functional group such as an amine could bind to the outer region or into the pore region. Thus, both memantine and HAE are voltage-dependent and have varying binding affinities of the pore regions as found through the Woodhull equation in the results.

Moreover, aside from HAE inhibiting the NMDAR's subunit GluN1/GluN2A seen in this study as well as from previous studies mentioned above, HAE has also been shown to inhibit AChE. For example, as previously stated above, HAE can inhibit nAChRs expressed in Xenopus oocytes with $IC_{50}$ values µg/mL) of (of different receptor subtypes α7, α4β2, α3β4, and Dα2/β2 at a voltage of -75mV were 2.30µg/mL, 3.24µg/mL, 1.47µg/mL, and 0.440µg/mL, respectively. Thus, the study

found the HAE inhibition of nAChRs was found on rat α4β2 which was voltage-dependent at -75mV. (Patel et al., 2020). Another study displaying HAE's ability to inhibit nAChR, from Kiran 2022, compared the human nAChR in the TE671 cells and insect nAChR in locust neurons. The application of HAE inhibited the inward currents for the nAChRs in the TE671 cells and locust neurons. The extracted HAE alkaloids had two fractions (A and B) and showed different $IC_{50}$ values for insect nAChR and human TE671 cells. In the human TE671 cells, HAE fraction A had $IC_{50}$ of 4.77μg/mL and fraction B had 1.68μg/mL. In the insect nAChR, fractions A and B had $IC_{50}$ of 3.23 and 0.072μg/ml respectively. Thus, it can be stated that HAE is a multitarget-directed ligand (MTDL) (Simoni et al., 2017).

Other MTDLs have also been known to target AChE along with other important ligands. For example, in an experiment by Rosini et al (2008), a compound tetrahydro acridine pharmacophore (6-9) can block NMDAR GluN1/GluN2A subunit. Thus, (6-9) was coapplied with NMDA (100μM +10μM glycine) on *Xenopus* oocytes by voltage clamping at -100mV, which showed an NMDAR uncompetitive antagonistic effect like memantine. Carbacrine, (6) had an $IC_{50}$ value of 0.74μM while memantine had an $IC_{50}$ value of 9.52μM. Thus, the lower IC50 value of 6 showed a higher level of antagonism than memantine. Carbacrine was tested at more positive holding potentials which displayed voltage-dependent like memantine. Furthermore, 6 was able to inhibit human AChE activity with an $IC_{50}$ value of the concentration of the inhibition at 2.15nM. Furthermore, Carbacrine was also able to block in vitro Aβ peptide self-aggregation, and Aβ peptide aggregation by AChE, and reduce oxidative stress. Another example of an MTDL, conducted by Simoni et al 2017, includes the compound {6-[4-(2-Methoxy-benzyl)-piperazin-1yl]-hexyloxy}-*9H*-carbazole (4). 4 was also able to inhibit AChE activity with an $IC_{50}$ value of the concentration of the inhibition of 0.773μM. In addition, 4 stimulated nAChRs subtype α4β2 showed a slight activation between 15-20% at 100μM on a membrane current at -80mV. However, 4 had no response seen with the nAChR subtype α7. Lastly, 4 is also able to block in vitro (1-42) peptide self-aggregation mediated by AChE (Rosini et al., 2008).

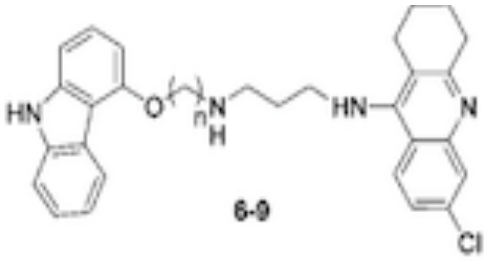


*Fig 20: Structure of compound 6-9* MTDLs

Furthermore, HAE extract contains several other alkaloids present in it. Therefore, it is hard to compare the potency of both compounds. So, future work should isolate the harmonine completely from other alkaloids present within HAE. As the $IC_{50}$ values of HAE were shown in the table above, they apparently seem higher than the $IC_{50}$ of memantine. The natural extracts from the insects could be a more useful and therapeutic treatment for Alzheimer's and neuropsychiatric disorders. Due to the minimal side effects like memantine or any other drugs in trial.

## Future Work:

Ladybirds have a lot more other alkaloids present in the hemolymph. There is a further need to know the functional and inhibitory ability of each alkaloid. 4 analogues of harmonine were provided to us for testing the inhibitory effect on NMDARs. But due to a shortage of time and uncertainty of NMDAR expression in Xenopus oocytes, they were not tested. The 4 analogues were ACB-6-82 (MW:284.48g), ACB-6-84(282.52g), ACB-6-89 (MW: 284.48g), and ACB-6-90 (MW: 282.52). Testing these analogues in studies ahead would provide a more diverse nature of harmonine and its analogs. Harmonine was tested on Human GluN1-GluN2A, there is a need to test it on another subtype GluN1-GluN2B to see its impact. HAE did not inhibit the NMDARs subtype GluN1-GluN2A fully, so maybe using a higher concentration could inhibit the NMDARS like memantine. There are different analogues of HAE and possibly testing them to see if they

could completely inhibit the NMDARS like memantine would be good progress. Moreover, testing harmonine and finding the onset time for the NMDA traces. And finding the binding affinity of different HAE analogs and calculating their $\delta$ value would be great progress.

## Conclusion:

The present study investigated the efficacy of memantine and harmonine, a compound found in Harmonia axyridis alkaloids, on human NMDAR clones of subtype GluN1-GluN2A using a two-electrode voltage clamp (TEVC) technique. The results revealed that memantine and harmonine are concentration and voltage-dependent inhibitors of GluN1-GluN2A NMDARs, like previous findings in rat NMDAR clones. The similarity in results between human and animal clones creates a potential for harmonine as a treatment for Alzheimer's disease, as well as a multi-ligand-like memantine that targets both NMDARs and nAChRs and acts as an acetylcholine esterase inhibitor.

However, the expression of GluN2B subtype NMDARs was uncertain, and recordings were not performed using TEVC. Initially, cDNA was used for NMDARs injection, but the expression was not achieved as expected. Later, cRNA was injected after RNA transcription using cDNA for easier expression. Although the expression was not as frequent as expected, it was more frequent when oocytes were obtained without the follicular layer and peeled to have proper NMDAR expression. Additionally, four analogues (ACB-6-82, ACB-6-84, ACB-6-89, and ACB-6-90) were expected to be tested against NMDAR subtypes, but due to the uncertainty in oocyte expression, it was difficult to test these analogues.

The study also overcame the issue faced by previous research by properly comparing the HAE $IC_{50}$ values with memantine by converting the units of µg/mL into millimolar for equivalent $IC_{50}$ values with memantine. Overall, the study highlights the potential of harmonine as a treatment for Alzheimer's disease and the importance of proper expression and comparison methods in NMDAR research.

## Reference List:


*Abramov, A. Y., Canevari, L. and Duchen, M. R. (2004) "Calcium signals induced by amyloid beta peptide and their consequences in neurons and astrocytes in culture," Biochimica et biophysica acta, 1742(1–3), pp. 81–87. doi: 10.1016/j.bbamcr.2004.09.006.*

*Agarwala BK, Dixon AFG (1992) Laboratory study of cannibalism and interspecific prédation in ladybirds.*

*Alam, N. et al. (no date) A New Alkaloid from Two Coccinellid Beetles Harmonia axyridis and Aiolocaria hexaspilota, Koreascience.or.kr. Available at: https://www.koreascience.or.kr/article/JAKO200202727203946.pdf (Accessed: May 29, 2022).*

*Albensi, B. C., Alasti, N. and Mueller, A. L. (2000) "Long-term potentiation in the presence of NMDA receptor antagonist arylalkylamine spider toxins," Journal of neuroscience research, 62(2), pp. 177–185. doi: 10.1002/1097-4547(20001015)62:2<177:AIDJNR3>3.0.CO;2-D.*

*Alex, A. B., Saunders, G. W., Dalpé-Charron, A., Reilly, C. A., & Wilcox, K. S. (2011). CGX1007 prevents excitotoxic cell death via actions at multiple types of NMDA receptors. Neurotoxicology, 32(4), 392–399.*

*Allan Butterfield, D. (2002) "Amyloid β-peptide (1-42)-induced Oxidative Stress and Neurotoxicity: Implications for Neurodegeneration in Alzheimer's Disease Brain. A Review," Free radical research, 36(12), pp. 1307–1313. doi: 10.1080/1071576021000049890.*

*Andorfer, C. et al. (2003) "Hyperphosphorylation and aggregation of tau in mice expressing normal human tau isoforms: Pathology of non-mutant tau in transgenic mice," Journal of neurochemistry, 86(3), pp. 582–590. doi: 10.1046/j.14714159.2003.01879. x.*

*Antuono, P. G. (1995) "Effectiveness and safety of quinacrine for the treatment of Alzheimer's disease. A double-blind, placebo-controlled study. Mentane Study Group," Archives of internal medicine, 155(16), pp. 1766–1772. doi: 10.1001/archinte.155.16.1766.*

*Arispe, N., Rojas, E. and Pollard, H. B. (1993) "Alzheimer disease amyloid beta protein forms calcium channels in bilayer membranes: blockade by tromethamine and aluminum," Proceedings of the National Academy of Sciences of the United States of America, 90(2), pp. 567–571. doi: 10.1073/pnas.90.2.567.*

*Bar-On, P. et al. (2002) "Kinetic and structural studies on the interaction of cholinesterases with the anti-Alzheimer drug rivastigmine," Biochemistry, 41(11), pp. 3555–3564. doi: 10.1021/bi020016x.*

*Bartus, R. T. et al. (1982) "The cholinergic hypothesis of geriatric memory dysfunction," Science (New York, N.Y.), 217(4558), pp. 408–414. doi: 10.1126/science.7046051.*

*Bekris, L. M. et al. (2010) "Genetics of Alzheimer's disease," Journal of geriatric psychiatry and neurology, 23(4), pp. 213–227. doi: 10.1177/0891988710383571.*

*Benarroch, E. E. (2011) "NMDA receptors: recent insights and clinical correlations," Neurology, 76(20), pp. 1750–1757. doi: 10.1212/WNL.0b013e31821b7cc9.*

*Berberich, S. et al. (2007) "The role of NMDAR subtypes and charge transfer during hippocampal LTP induction," Neuropharmacology, 52(1), pp. 77–86. doi: 10.1016/j.neuropharm.2006.07.016.*

*Blanke, M. L. and VanDongen, A. M. J. (2009) Activation mechanisms of the NMDA receptor. CRC Press/Taylor & Francis.*

*Blanpied, T. A. et al. (1997) "Trapping channel block of NMDA-activated responses by amantadine and memantine," Journal of neurophysiology, 77(1), pp. 309–323. doi: 10.1152/jn.1997.77.1.309.*

*Boyle, K. A. et al. (2019) "Defining a spinal microcircuit that gates myelinated afferent input: Implications for tactile allodynia," Cell reports, 28(2), pp. 526-540.e6. doi: 10.1016/j.celrep.2019.06.040.*

*Braconnier, M. F. et al. (1985) "(Z)-1,17-diaminooctadec-9-ene, a novel aliphatic diamine from Coccinellidae," Experientia, 41(4), pp. 519–520. doi 10.1007/bf01966179.*

*Bresink, I. et al. (1996) "Effects of memantine on recombinant rat NMDA receptors expressed in HEK 293 cells," British journal of pharmacology, 119(2), pp. 195–204. doi 10.1111/j.1476-5381. 1996.tb15971.x.*

*Buisson, B. and Bertrand, D. (1998) "Open-channel blockers at the human alpha4beta2 neuronal nicotinic acetylcholine receptor," Molecular pharmacology, 53(3), pp. 555–563. doi 10.1124/mol.53.3.555.*

*Burnashev, N. et al. (1992) "Control by asparagine residues of calcium permeability and magnesium blockade in the NMDA receptor," Science (New York, N.Y.), 257(5075), pp. 1415–1419. doi 10.1126/science.1382314.*

*Cai L, Koziel JA, O'Neal ME (2007) Determination of characteristic odorants from Harmonia axyridis beetles using in vivo solid-phase microextraction and multidimensional gas chromatography–mass spectrometry–olfactometry. J Chromatogr A 1147:66–78*

*Chen, G.-F. et al. (2017) "Amyloid beta: structure, biology, and structure-based therapeutic development," Acta pharmacological Sinica, 38(9), pp. 1205–1235. doi: 10.1038/aps.2017.28.*

*Chen, H. S. and Lipton, S. A. (1997) "Mechanism of memantine block of NMDA-activated channels in rat retinal ganglion cells: uncompetitive antagonism," The journal of physiology, 499 (Pt 1), pp. 27–46. doi: 10.1113/Physiol. 1997.sp021909.*

*Chen, N., Luo, T. and Raymond, L. A. (1999) "Subtype-dependence of NMDA receptor channel open probability," The Journal of neuroscience: the official journal of the Society for Neuroscience, 19(16), pp. 6844–6854. doi: 10.1523/jneurosci.19-16-06844.1999.*

*Cheng, Y.-J., Lin, C.-H. and Lane, H.-Y. (2021) "Involvement of cholinergic, adrenergic, and glutamatergic network modulation with cognitive dysfunction in Alzheimer's disease," International journal of molecular sciences, 22(5), p. 2283. doi: 10.3390/ijms22052283.*

*Chiu, D. N. and Carter, B. C. (2022) "Synaptic NMDA receptor activity at resting membrane potentials," Frontiers in cellular neuroscience, 16, p. 916626. doi 10.3389/fncel.2022.916626.*

*Chou, T.-H. et al. (2022) "Structural insights into binding of therapeutic channel blockers in NMDA receptors," Nature structural & molecular biology, 29(6), pp. 507–518. doi 10.1038/s41594-022-00772-0.*

*Citron, M. (2010) "Alzheimer's disease: strategies for disease modification," Nature reviews. Drug discovery, 9(5), pp. 387–398. doi 10.1038/nrd2896.*

*Collingridge, G. L. and Singer, W. (1990) "Excitatory amino acid receptors and synaptic plasticity," Trends in pharmacological sciences, 11(7), pp. 290–296. doi: 10.1016/01656147(90)90011-v.*

*Cotman, C. W., Monaghan, D. T. and Ganong, A. H. (1988) "Excitatory amino acid neurotransmission: NMDA receptors and Hebb-type synaptic plasticity," Annual review of neuroscience, 11(1), pp. 61–80. doi: 10.1146/annurev.ne.11.030188.000425.*

*Cottone, P. et al. (2013) "The uncompetitive NMDA receptor antagonist's ketamine and memantine preferentially increase the choice for a small, immediate reward in low impulsive rats," Psychopharmacology, 226(1), pp. 127–138. doi 10.1007/s00213-0122898-3.*

*Cudjoe E, Wiederkehr TB, Brindle ID (2005) Headspace gas chromatography-mass spectrometry: a fast approach to the identification and determination of 2-alkyl-3methoxypyrazine pheromones in ladybugs. Analyst 130:152–155*

*Cunningham, E. L. et al. (2015) "Dementia," The Ulster medical journal, 84(2), pp. 79–87. Available at: https://www.ncbi.nlm.nih.gov/labs/pmc/articles/PMC4488926/ (Accessed: March 15, 2022).*

*Danysz, W. and Parsons, C. G. (2012) "Alzheimer's disease, β-amyloid, glutamate, NMDA receptors, and memantine--searching for the connections: Alzheimer's disease, βamyloid, glutamate, NMDA receptors and memantine," British journal of pharmacology, 167(2), pp. 324–352. doi: 10.1111/j.1476-5381.2012.02057. x.*

*Danysz, W. et al. (2000) "Neuroprotective and symptomatological action of memantine relevant for Alzheimer's disease--a unified glutamatergic hypothesis on the mechanism of action," Neurotoxicity Research, 2(2–3), pp. 85–97. doi 10.1007/bf03033787.*

*De Felice, F. G. et al. (2007) "Abeta oligomers induce neuronal oxidative stress through an N-methyl-D-aspartate receptor-dependent mechanism that is blocked by the Alzheimer drug memantine," The Journal of biological chemistry, 282(15), pp. 11590– 11601. doi: 10.1074/jbc.M607483200.*

*Demuro, A. et al. (2005) "Calcium dysregulation and membrane disruption as a ubiquitous neurotoxic mechanism of soluble amyloid oligomers," The Journal of biological chemistry, 280(17), pp. 17294–17300. doi 10.1074/jbc.M500997200.*

*Dong, X.-X., Wang, Y., and Qin, Z.-H. (2009) "Molecular mechanisms of excitotoxicity and their relevance to the pathogenesis of neurodegenerative diseases," Acta pharmacological Sinica, 30(4), pp. 379–387. doi 10.1038/aps.2009.24.*

*Dravid, S. M. et al. (2007) "Subunit-specific mechanisms and proton sensitivity of NMDA receptor channel block: Proton sensitivity of NMDA receptor channel blockers," The journal of physiology, 581(Pt 1), pp. 107–128. doi 10.1113/jphysiol.2006.124958.*

*Enz, A. et al. (1993) "Brain selective inhibition of acetylcholinesterase: a novel approach to therapy for Alzheimer's disease," Progress in brain research, 98, pp. 431–438. doi: 10.1016/s0079-6123(08)62429-2.*

*Erreger, K. et al. (2005) "Subunit-specific gating controls rat NR1/NR2A and NR1/NR2B NMDA channel kinetics and synaptic signaling profiles: NMDA receptor gating," The journal of physiology, 563(Pt 2), pp. 345–358. doi: 10.1113/jphysiol.2004.080028.*

*Erreger, K. et al. (2007) "Subunit-specific agonist activity at NR2A-, NR2B-, NR2C-, and NR2D-containing N-methyl-D-aspartate glutamate receptors," Molecular pharmacology, 72(4), pp. 907–920. doi: 10.1124/mol.107.037333.*

*Esposito, Z. et al. (2013) "Amyloid ß, glutamate, excitotoxicity in Alzheimer's disease: are we on the right track?," CNS neuroscience & therapeutics, 19(8), pp. 549–555. doi: 10.1111/cns.12095.*

*Fedorov, N. B., Screbitsky, V. G. and Reymann, K. G. (1992) "Effects of philanthotoxin-343 on CA1 pyramidal neurons of rat hippocampus in vitro," European journal of pharmacology, 228(4), pp. 201–206. doi 10.1016/0926-6917(92)90030-g.*

*Feldmeyer, D. et al. (2002) "Synaptic connections between layer 4 spiny neuron-layer 2/3 pyramidal cell pairs in juvenile rat barrel cortex: physiology and anatomy of interlaminar signaling within a cortical column," The journal of physiology, 538(Pt 3), pp. 803–822. doi 10.1113/jphysiol.2001.012959.*

*Ferreira-Vieira, T. H. et al. (2016) "Alzheimer's disease: Targeting the cholinergic system," Current neuropharmacology, 14(1), pp. 101–115. doi 10.2174/1570159x13666150716165726.*

*Folch, J. et al. (2018) "Memantine for the treatment of dementia: A review on its current and future applications," Journal of Alzheimer's disease: JAD, 62(3), pp. 1223–1240. doi: 10.3233/JAD-170672.*

*Foster, K. A. et al. (2010) "Distinct roles of NR2A and NR2B cytoplasmic tails in long-term potentiation," The Journal of neuroscience: the official journal of the Society for Neuroscience, 30(7), pp. 2676–2685. doi: 10.1523/JNEUROSCI.4022-09.2010.*

*Giaccone, G. et al. (1989) "Down patients: extracellular amyloid deposits precede neuritic degeneration and senile plaques," Neuroscience letters, 97(1–2), pp. 232–238. doi: 10.1016/0304-3940(89)90169-9.*

*Giacobini, E. (1997) "From molecular structure to Alzheimer therapy," The Japanese Journal of Pharmacology, 74(3), pp. 225–241. doi 10.1254/jjp.74.225.*

*Gilling, K. E. et al. (2009) "Potency, voltage-dependency, agonist concentrationdependency, blocking kinetics and partial untrapping of the uncompetitive N-methyl-Daspartate (NMDA) channel blocker memantine at human NMDA (GluN1/GluN2A) receptors," Neuropharmacology, 56(5), pp. 866–875. doi: 10.1016/j.neuropharm.2009.01.012.*

*Glasgow, N. G. and Johnson, J. W. (2014) "Whole-cell patch-clamp analysis of recombinant NMDA receptor pharmacology using brief glutamate applications," Methods in molecular biology (Clifton, N.J.), 1183, pp. 23–41. doi 10.1007/978-1-4939-1096-0_2.*

*Glenner, G. G. and Wong, C. W. (1984) "Alzheimer's disease: initial report of the purification and characterization of a novel cerebrovascular amyloid protein," Biochemical and biophysical research communications, 120(3), pp. 885–890. doi: 10.1016/s0006-291x(84)80190-4.*

*Goedert, M., Klug, A. and Crowther, R. A. (2006) "Tau protein, the paired helical filament, and Alzheimer's disease," Journal of Alzheimer's disease: JAD, 9(s3), pp. 195–207. doi: 10.3233/jad-2006-9s323.*

*Gong, C.-X. and Iqbal, K. (2008) "Hyperphosphorylation of microtubule-associated protein tau: A promising therapeutic target for Alzheimer's disease," Current medicinal chemistry, 15(23), pp. 2321–2328. doi 10.2174/092986708785909111.*

*Gonzales, N. R. and Grotta, J. C. (2016) "Pharmacologic modification of acute cerebral ischemia," in Stroke. Elsevier, pp. 916-936.e5.*

*Halliwell JV, Plant TD, Robbins J, Standen NB (1994) Voltage clamp techniques. In: Ogden D (ed) Microelectrode techniques: the Plymouth workshop handbook, 2nd ed. Company of Biologists, Cambridge, pp 17–35*

*Hampel, H. et al. (2018) "The cholinergic system in the pathophysiology and treatment of Alzheimer's disease," Brain: a journal of neurology, 141(7), pp. 1917–1933. doi 10.1093/brain/awy132.*

*Hansen, K. B. et al. (2018) "Structure, function, and allosteric modulation of NMDA receptors," The journal of general physiology, 150(8), pp. 1081–1105. doi 10.1085/jgp.201812032.*

*Harlequin ladybird - Harmonia axyridis (no date) Landcareresearch.co.nz. Available at: https://nzacfactsheets.landcareresearch.co.nz/factsheet/InterestingInsects/Harlequinladybird---Harmonia-axyridis.html (Accessed: May 7, 2022).*

*Haulotte, E., Laurent, P. and Braekman, J.-C. (2012) "Biosynthesis of defensive Coccinellidae alkaloids: Incorporation of fatty acids in Adaline, coccinellids, and harmonine," European journal of organic chemistry, 2012(10), pp. 1907–1912. doi: 10.1002/ejoc.201101563.*

*Herwerth, M. et al. (2012) "D4 dopamine receptors modulate NR2B NMDA receptors and LTP in stratum oriens of hippocampal CA1," Cerebral cortex (New York, N.Y.: 1991), 22(8), pp. 1786–1798. doi: 10.1093/cercor/bhr275.*

*Hodgkin AL, Huxley AF, Katz B (1952) Measurement of current–voltage relations in the membrane of the giant axon of Loligo. J Physiol 116:424–488*

*Iacobucci, G. J. et al. (2021) "Cross-subunit interactions that stabilize open states mediate gating in NMDA receptors," Proceedings of the National Academy of Sciences of the United States of America, 118(2), p. e2007511118. doi: 10.1073/pnas.2007511118.*

*Iqbal, K. et al. (2005) "Tau pathology in Alzheimer disease and other tauopathies," Biochimica et biophysica acta, 1739(2–3), pp. 198–210. doi: 10.1016/j.bbadis.2004.09.008.ISSN 0014-2999, https://doi.org/10.1016/S00142999(02)02581-5.*

*Izumi, Y. and Zorumski, C. F. (2014) "Metaplastic effects of subanesthetic ketamine on CA1 hippocampal function," Neuropharmacology, 86, pp. 273–281. doi: 10.1016/j.neuropharm.2014.08.002.*

*Jacobson, S. A. and Sabbagh, M. N. (2008) "Donepezil: potential neuroprotective and disease-modifying effects," Expert opinion on drug metabolism & toxicology, 4(10), pp. 1363–1369. doi 10.1517/17425255.4.10.1363.*

*Jakob von Engelhardt, Irinel Coserea, Verena Pawlak, Elke C. Fuchs, Georg Köhr, Peter H. Seeburg, Hannah Monyer, Excitotoxicity in vitro by NR2A- and NR2B-containing NMDA receptors, Neuropharmacology, Volume 53, Issue 1,2007, Pages 10-17, ISSN 00283908, https://doi.org/10.1016/j.neuropharm.2007.04.015.*

*Jespersen, A. et al. (2014) "Structural insights into competitive antagonism in NMDA receptors," Neuron, 81(2), pp. 366–378. doi: 10.1016/j.neuron.2013.11.033. Johnson, J. W. and Ascher, P. (1990) "Voltage-dependent block by intracellular Mg2+ of N-methyl-D-aspartate-activated channels," Biophysical journal, 57(5), pp. 1085–1090. doi: 10.1016/s0006-3495(90)82626-6.*

*Johnson, J. W. and Kotermanski, S. E. (2006) "Mechanism of action of memantine," Current opinion in pharmacology, 6(1), pp. 61–67. doi: 10.1016/j.coph.2005.09.007.*

*Johnson, J. W., Glasgow, N. G. and Povysheva, N. V. (2015) "Recent insights into the mode of action of memantine and ketamine," Current opinion in pharmacology, 20, pp. 54–63. doi: 10.1016/j.coph.2014.11.006.*

*Kajita, Y., Obrycki, J. J., Sloggett, J. J., & Haynes, K. F. (2010). Intraspecific alkaloid variation in ladybird eggs and its effects on con-and hetero-specific intraguild predators. Oecologia, 163(2), 313–322. http://www.jstor.org/stable/40606589*

*Kampa, B. M. et al. (2004) "Kinetics of Mg2+ unblock of NMDA receptors: implications for spike-timing-dependent synaptic plasticity: Mg2+unblock of NMDA receptors and STDP," The journal of physiology, 556(Pt 2), pp. 337–345. doi: 10.1113/jphysiol.2003.058842.*

*Kang, J. et al. (1987) "The precursor of Alzheimer's disease amyloid A4 protein resembles a cell-surface receptor," Nature, 325(6106), pp. 733–736. doi 10.1038/325733a0.*

*Karakas, E. and Furukawa, H. (2014) "Crystal structure of a heterotetrameric NMDA receptor ion channel," Science (New York, N.Y.), 344(6187), pp. 992–997. doi 10.1126/science.1251915.*

*Karantzoulis, S. and Galvin, J. E. (2011) "Distinguishing Alzheimer's disease from other major forms of dementia," Expert review of neurotherapeutics, 11(11), pp. 1579–1591. doi 10.1586/ern.11.155.*

*Koch, R. L. (2003) "The multicolored Asian lady beetle, Harmonia axyridis: a review of its biology, uses in biological control, and non-target impacts," Journal of insect science, 3(1), p. 32. doi: 10.1093/jis/3.1.32.*

*Kotermanski, S. E., Wood, J. T. and Johnson, J. W. (2009) "Memantine binding to a superficial site on NMDA receptors contributes to partial trapping: Partial trapping of memantine by NMDA receptors," The journal of physiology, 587(Pt 19), pp. 4589–4604.*
*doi: 10.1113/jphysiol.2009.176297.*

*Kushner, T. and Schoepfer, R. (1996) "Multiple structural elements determine subunit specificity of Mg2+ block in NMDA receptor channels," The Journal of neuroscience: the official journal of the Society for Neuroscience, 16(11), pp. 3549–3558. doi: 10.1523/jneurosci.16-11-03549.1996.*

*Lacor, P. N. et al. (2007) "Abeta oligomer-induced aberrations in synapse composition, shape, and density provide a molecular basis for loss of connectivity in Alzheimer's disease," The Journal of neuroscience: the official journal of the Society for Neuroscience, 27(4), pp. 796–807. doi: 10.1523/JNEUROSCI.3501-06.2007.*

*Laurent, P. et al. (2002) "In vitro production of Adaline and coccinellid, two defensive alkaloids from ladybird beetles (Coleoptera: Coccinellidae)," Insect biochemistry and molecular biology, 32(9), pp. 1017–1023. doi: 10.1016/s0965-1748(02)00038-3.*

*Li, C.-T., Yang, K.-C. and Lin, W.-C. (2018) "Glutamatergic dysfunction and glutamatergic compounds for major psychiatric disorders: Evidence from clinical neuroimaging studies," Frontiers in psychiatry, 9, p. 767. doi: 10.3389/fpsyt.2018.00767.*

*Li, V. and Wang, Y. T. (2016) "Molecular mechanisms of NMDA receptor-mediated excitotoxicity: implications for neuroprotective therapeutics for stroke," Neural regeneration research, 11(11), pp. 1752–1753. doi 10.4103/1673-5374.194713.*

*Limapichat, W. et al. (2013) "Key binding interactions for memantine in the NMDA receptor," ACS chemical neuroscience, 4(2), pp. 255–260. doi: 10.1021/cn300180a.*

*Lin, H., Bhatia, R. and Lal, R. (2001) "Amyloid beta protein forms ion channels: implications for Alzheimer's disease pathophysiology," FASEB journal: official publication of the Federation of American Societies for Experimental Biology, 15(13), pp. 2433–2444.*
*doi 10.1096/fj.01-0377com.*

*Liu, J. et al. (2019) "The role of NMDA receptors in Alzheimer's disease," Frontiers in neuroscience, 13, p. 43. doi 10.3389/fnins.2019.00043.*

*Liu, J. P. et al. (1996) "Calcium binds dynamin I and inhibits its GTPase activity," Journal of neurochemistry, 66(5), pp. 2074–2081. doi 10.1046/j.1471-4159.1996.66052074. x.*

*Lodge, D. and Mercier, M. S. (2015) "Ketamine and phencyclidine: the good, the bad and the unexpected: Ketamine and phencyclidine," British journal of pharmacology, 172(17), pp. 4254–4276. doi 10.1111/bph.13222.*

*Losi, G. et al. (2006) "Functional in vitro characterization of CR 3394: a novel voltage-dependent N-methyl-D-aspartate (NMDA) receptor antagonist," Neuropharmacology, 50(3), pp. 277–285. doi 10.1016/j.neuropharm.2005.09.002.*

*MacDonald, J. F. and Nowak, L. M. (1990) "Mechanisms of blockade of excitatory amino acid receptor channels," Trends in pharmacological sciences, 11(4), pp. 167–172. doi 10.1016/0165-6147(90)90070-o.*

*MacDonald, J. F., Miljkovic, Z. and Pennefather, P. (1987) "Use-dependent block of excitatory amino acid currents in cultured neurons by ketamine," Journal of neurophysiology, 58(2), pp. 251–266. doi: 10.1152/jn.1987.58.2.251.*

*Mahley, R. W. and Rall, S. C., Jr (1999) "Is ϵ4 the ancestral human apoE allele?" Neurobiology of Aging, 20(4), pp. 429–430. doi 10.1016/s0197-4580(99)00081-0.*

*Mallozzi, C., Parravano, M., Gaddini, L., Villa, M, Pricci, F., Malchiodi-Albedi F., Matteucci A., Curcumin Modulates the NMDA Receptor Subunit Composition Through a Mechanism Involving CaMKII and Ser/Thr Protein Phosphatases. Cell Mol Neurobiol 38, 1315–1320 (2018).*

*Markram, H. and Segal, M. (1992) "The inositol 1,4,5-trisphosphate pathway mediates cholinergic potentiation of rat hippocampal neuronal responses to NMDA," The journal of physiology, 447(1), pp. 513–533. doi 10.1113/jphysiol. 1992.sp019015.*

*Martins, C. A. R. et al. (2005) "APOE alleles predict the rate of cognitive decline in Alzheimer disease: a nonlinear model," Neurology, 65(12), pp. 1888–1893. doi 10.1212/01.wnl.0000188871.74093.12.*

*Maskell, P. D. et al. (2003) "Inhibition of human alpha 7 nicotinic acetylcholine receptors by open channel blockers of N-methyl-D-aspartate receptors," British journal of pharmacology, 140(7), pp. 1313–1319. doi 10.1038/sj.bjp.0705559.*

*Mayer, M. L., Westbrook, G. L. and Guthrie, P. B. (1984) "Voltage-dependent block by Mg2+ of NMDA responses in spinal cord neurons," Nature, 309(5965), pp. 261–263. doi 10.1038/309261a0.*

*Mellor, I. R. et al. (2003) "Modification of the philanthotoxin-343 polyamine moiety results in different structure-activity profiles at muscle nicotinic ACh, NMDA, and AMPA receptors," Neuropharmacology, 44(1), pp. 70–80. doi 10.1016/s00283908(02)00336-2.*

*Monge-Fuentes, V. et al. (2015) "Neuroactive compounds obtained from arthropod venoms as new therapeutic platforms for the treatment of neurological disorders," The Journal of venomous animals and toxins including tropical diseases, 21(1), p. 31. doi: 10.1186/s40409-015-0031-x.*

*Mucke, L. et al. (2000) "High-Level neuronal expression of β1–42in wild-type human amyloid protein precursor transgenic mice: Synaptotoxicity without plaque formation," The Journal of neuroscience: the official journal of the Society for Neuroscience, 20(11), pp. 4050–4058. doi 10.1523/jneurosci.20-11-04050.2000.*

*Mufson, E. J. et al. (2008) "Cholinergic system during the progression of Alzheimer's disease: therapeutic implications," Expert review of neurotherapeutics, 8(11), pp. 1703–1718. doi 10.1586/14737175.8.11.1703.*

*Murphy, M. P. and LeVine, H., 3rd (2010) "Alzheimer's disease and the amyloid-beta peptide," Journal of Alzheimer's disease: JAD, 19(1), pp. 311–323. doi 10.3233/JAD2010-1221.*

*Nagele, R. G. et al. (2002) "Intracellular accumulation of β-amyloid1–42 in neurons is facilitated by the α7 nicotinic acetylcholine receptor in Alzheimer's disease," Neuroscience, 110(2), pp. 199–211. doi: 10.1016/s0306-4522(01)00460-2.*

*Neher E, Sakmann B, Steinbach JH (1978) The extracellular patch clamp: a method for resolving currents through individual open channels in biological membranes. Pflugers Arch 375:219–228*

*Nichols, E. and Vos, T. (2020) "Estimating the global mortality from Alzheimer's disease and other dementias: A new method and results from the Global Burden of Disease study 2019:*

*Epidemiology / Prevalence, incidence, and outcomes of MCI and dementia," Alzheimer's & dementia: the journal of the Alzheimer's Association, 16(S10). doi 10.1002/alz.042236.*

*Nusser, Z. et al. (1998) "Cell type and pathway dependence of synaptic AMPA receptor number and variability in the hippocampus," Neuron, 21(3), pp. 545–559. doi 10.1016/s0896-6273(00)80565-6.*

*Ogden, K. K. and Traynelis, S. F. (2011) "New advances in NMDA receptor pharmacology," Trends in pharmacological sciences, 32(12), pp. 726–733. doi 10.1016/j.tips.2011.08.003.*

*Oliver, D. et al. (2001) "Memantine inhibits efferent cholinergic transmission in the cochlea by blocking nicotinic acetylcholine receptors of outer hair cells," Molecular pharmacology, 60(1), pp. 183–189. doi 10.1124/mol.60.1.183.*

*Olney, J. W. et al. (1986) "The anti-excitotoxic effects of certain anesthetics, analgesics, and sedative-hypnotics," Neuroscience letters, 68(1), pp. 29–34. doi 10.1016/0304-3940(86)90224-7.*

*Pabba, M., Hristova, E. and Biscaro, D. (2012) "The elusive roles of NMDA receptor amino-terminal domains," The journal of physiology, 590(22), pp. 5561–5562. doi 10.1113/jphysiol.2012.243311.*

*Pałasz, A. and Krzystanek, M. (2022) "Spider neurotoxins as modulators of NMDA receptor signaling," Neuromolecular medicine, 24(3), pp. 250–256. doi 10.1007/s12017021-08692-w.*

*Parsons, C. G. et al. (1993) "Patch clamp studies on the kinetics and selectivity of N-methyl-D-aspartate receptor antagonism by memantine (1-amino-3,5dimethyladamantan)," Neuropharmacology, 32(12), pp. 1337–1350. doi 10.1016/00283908(93)90029-3.*

*Parsons, C. G. et al. (1995) "Comparison of the potency, kinetics and voltage dependency of a series of uncompetitive NMDA receptor antagonists in vitro with anticonvulsive and motor impairment activity in vivo," Neuropharmacology, 34(10), pp. 1239–1258. doi 10.1016/0028-3908(95)00092-k.*

*Parsons, C. G. et al. (1996) "Comparative patch-clamp studies with freshly dissociated rat hippocampal and striatal neurons on the NMDA receptor antagonistic effects of amantadine and memantine," The European journal of neuroscience, 8(3), pp. 446–454. doi 10.1111/j.1460-9568. 1996.tb01228.x.*

*Parsons, C. G. et al. (2013) "Memantine and cholinesterase inhibitors: complementary mechanisms in the treatment of Alzheimer's disease," Neurotoxicity Research, 24(3), pp. 358–369. doi: 10.1007/s12640-013-9398-z. Parsons, C. G., Danysz, W. and Quack, G. (1999) "Memantine is a clinically well tolerated N-methyl-D-aspartate (NMDA) receptor antagonist--a review of preclinical data," Neuropharmacology, 38(6), pp. 735–767. doi 10.1016/s0028-3908(99)00019-2.*

*Parsons, C. G., Stöffler, A., and Danysz, W. (2007) "Memantine: an NMDA receptor antagonist that improves memory by restoration of homeostasis in the glutamatergic system--too little activation is bad, too much is even worse," Neuropharmacology, 53(6), pp. 699–723. doi 10.1016/j.neuropharm.2007.07.013.*

*Pastor, P. et al. (2003) "Apolipoprotein Eepsilon4 modifies Alzheimer's disease onset in an E280A PS1 kindred: Age of Onset Modifiers in Familial AD," Annals of neurology, 54(2), pp. 163–169. doi 10.1002/ana.10636.*

*Patel, R. N. et al. (2020) "Actions on mammalian and insect nicotinic acetylcholine receptors of harmonine-containing alkaloid extracts from the harlequin ladybird Harmonia axyridis," Pesticide biochemistry and physiology, 166(104561), p. 104561. doi 10.1016/j.pestbp.2020.104561.*

*Poulsen, M. H. et al. (2015) "Binding of ArgTX-636 in the NMDA receptor ion channel," Journal of molecular biology, 427(1), pp. 176–189. doi: 10.1016/j.jmb.2014.05.017.*

*Raak-van den Berg, C. L. et al. (2017) "Life history of the harlequin ladybird, Harmonia axyridis: a global meta-analysis," BioControl (Dordrecht, Netherlands), 62(3), pp. 283–296. doi 10.1007/s10526-017-9805-0.*

*Rammes, G., Danysz, W. and Parsons, C. G. (2008) "Pharmacodynamics of memantine: an update," Current neuropharmacology, 6(1), pp. 55–78. doi 10.2174/157015908783769671.*

*Regan, M. C., Romero-Hernandez, A. and Furukawa, H. (2015) "A structural biology perspective on NMDA receptor pharmacology and function," Current opinion in structural biology, 33, pp. 68–75. doi 10.1016/j.sbi.2015.07.012.*

*Reisberg, B. et al. (2003) "Memantine in moderate-to-severe Alzheimer's disease," The New England journal of medicine, 348(14), pp. 1333–1341. doi 10.1056/NEJMoa013128.*

*Reynolds, I. J. (1990) "Modulation of NMDA receptor responsiveness by neurotransmitters, drugs, and chemical modification," Life sciences, 47(20), pp. 1785– 1792. doi 10.1016/0024-3205(90)90280-5.*

*Riedel, G., Platt, B. and Micheau, J. (2003) "Glutamate receptor function in learning and memory," Behavioural brain research, 140(1–2), pp. 1–47. doi 10.1016/s0166-4328(02)00272-3.*

*Romas, S. N. et al. (2002) "Familial Alzheimer's disease among the Caribbean*

*Hispanics: A reexamination of its association with APOE," Archives of neurology, 59(1), p. 87. Doi 10.1001/archneur.59.1.87. Santi, Fabrizio (7005848267); Maini, Stefano (7003914996)*

*Schellenberg, G. D. and Montine, T. J. (2012) "The genetics and neuropathology of Alzheimer's disease," Acta neuropathologica, 124(3), pp. 305–323. doi 10.1007/s00401-012-0996-2.*

*Schneider, L. S. et al. (2011) "Lack of evidence for the efficacy of memantine in mild Alzheimer's disease," Archives of neurology, 68(8), pp. 991–998. doi 10.1001/archneurol.2011.69.*

*Sharma, K. (2019) "Cholinesterase inhibitors as Alzheimer's therapeutics (Review)," Molecular medicine reports, 20(2), pp. 1479–1487. doi 10.3892/mmr.2019.10374.*

*Shen, H. et al. (2010) "Neuroprotection by donepezil against glutamate excitotoxicity involves stimulation of alpha7 nicotinic receptors and internalization of NMDA receptors: Neuroprotection via NMDA receptor internalization," British journal of pharmacology, 161(1), pp. 127–139. doi 10.1111/j.1476-5381.2010.00894.x.*

*Sherman-Gold R (ed) (2008) The axon guide for electrophysiology and biophysics laboratory techniques, 3rd ed. Axon Instruments, Inc., Foster City, CA*

*Shokri-Kojori, E. et al. (2018) "β-Amyloid accumulation in the human brain after one night of sleep deprivation," Proceedings of the National Academy of Sciences of the United States of America, 115(17), pp. 4483–4488. doi: 10.1073/pnas.1721694115.*

*Silman, I. and Sussman, J. L. (2008) "Acetylcholinesterase: how is structure related to function?" Chemico-biological interactions, 175(1–3), pp. 3–10. doi 10.1016/j.cbi.2008.05.035.*

*Simoni, E. et al. (2017) "Multitarget drug design strategy in Alzheimer's disease:*

*focus on cholinergic transmission and amyloid-β aggregation," Future medicinal chemistry, 9(10), pp. 953–963. doi 10.4155/fmc-2017-0039.*

*Sloggett JJ, Haynes KF, Obrycki JJ, Davis AJ (2010) Harmonia axyridis as a model for predator adaptation to chemically defended prey. In: Babendreier D, Kenis M, Aebi A, Roy H (eds) Working group ‘‘Benefits and risks associated with exotic biological control agents’’ at Engelberg (Switzerland), 6–10 September 2009. IOBC/ WPRS Bull 58:105–113*

*Snyder, E. M. et al. (2005) "Regulation of NMDA receptor trafficking by amyloid-beta," Nature Neuroscience, 8(8), pp. 1051–1058. doi 10.1038/nn1503.*

*Sobolevsky, A. and Koshelev, S. (1998) "Two blocking sites of amino-adamantane derivatives in open N-methyl-d-aspartate channels," Biophysical journal, 74(3), pp. 1305–1319. doi: 10.1016/s0006-3495(98)77844-0.*

*Stauffer, W. R. et al. (2016) "Dopamine neuron-specific optogenetic stimulation in Rhesus macaques," Cell, 166(6), pp. 1564-1571.e6. doi 10.1016/j.cell.2016.08.024.*

*Tabet, N. (2006) "Acetylcholinesterase inhibitors for Alzheimer's disease: anti-inflammatories in acetylcholine clothing!" Age and Aging, 35(4), pp. 336–338. doi 10.1093/aging/afl027.*

*Tai-Hyun Kang, Yukihisa Murakami, Kinzo Matsumoto, Hiromitsu Takayama, Mariko Kitajima, Norio Aimi, Hiroshi Watanabe, Rhynchophylline and isorhynchophylline*

*Inhibit NMDA receptors expressed in Xenopus oocytes, European Journal of Pharmacology, Volume 455, Issue 1,2002, Pages 27-34,*

*Talesa, V. N. (2001) "Acetylcholinesterase in Alzheimer's disease," Mechanisms of aging and development, 122(16), pp. 1961–1969. doi 10.1016/s0047-6374(01)00309-8.*

*Tampi, R. R. and van Dyck, C. H. (2007) "Memantine: efficacy and safety in mild-to-severe Alzheimer's disease," Neuropsychiatric disease and treatment, 3(2), pp. 245– 258. doi 10.2147/nedt.2007.3.2.245.*

*Tariot, P. N. et al. (2004) "Memantine treatment in patients with moderate to severe Alzheimer disease already receiving donepezil: a randomized controlled trial: A randomized controlled trial," JAMA: the journal of the American Medical Association, 291(3), pp. 317–324. doi 10.1001/jama.291.3.317.*

*Theuns, J. et al. (2000) "Genetic variability in the regulatory region of presenilin 1 associated with risk for Alzheimer's disease and variable expression," Human molecular genetics, 9(3), pp. 325–331. doi: 10.1093/hmg/9.3.325.*

*Thomas, S. J. and Grossberg, G. T. (2009) "Memantine: a review of studies into its safety and efficacy in treating Alzheimer's disease and other dementias," Clinical interventions in aging, 4, pp. 367–377. doi: 10.2147/cia. s6666.*

*Tsuang, D. et al. (1999) "The utility of apolipoprotein E genotyping in the diagnosis of Alzheimer's disease in a community-based case series," Archives of neurology, 56(12), pp. 1489–1495. doi 10.1001/archneur.56.12.1489.*

*Vance, K. M., Hansen, K. B. and Traynelis, S. F. (2012) "GluN1 splice variant control of GluN1/GluN2D NMDA receptors: GluN1 splice variant control of*
*GluN1/GluN2D NMDA receptors," The journal of physiology, 590(16), pp. 3857–3875. doi 10.1113/jphysiol.2012.234062.*

*Vrajová, M. et al. (2010) "Expression of the hippocampal NMDA receptor GluN1 subunit and its splicing isoforms in schizophrenia: postmortem study," Neurochemical Research, 35(7), pp. 994–1002. doi 10.1007/s11064-010-0145-z.*

*Vyklicky, V. et al. (2021) "Conformational rearrangement of the NMDA receptor amino-terminal domain during activation and allosteric modulation," Nature communications, 12(1), p. 2694. doi 10.1038/s41467-021-23024-z.*

*Walsh, D. M. et al. (2002) "Naturally secreted oligomers of amyloid beta protein potently inhibit hippocampal long-term potentiation in vivo," Nature, 416(6880), pp. 535–539. doi 10.1038/416535a.*

*Wang, R. and Reddy, P. H. (2017) "Role of glutamate and NMDA receptors in Alzheimer's disease," Journal of Alzheimer's disease: JAD, 57(4), pp. 1041–1048. Doi 10.3233/jad-160763.*

*Wijsman, E. M. et al. (2005) "APOE and other loci affect age-at-onset in Alzheimer's disease families with PS2 mutation," American journal of medical genetics. Part B, Neuropsychiatric genetics: the official publication of the International Society of Psychiatric Genetics, 132B(1), pp. 14–20. doi: 10.1002/ajmg.b.30087.*

*Winblad, B. and Poritis, N. (1999) "Memantine in severe dementia: results of the the9M-best study (benefit and efficacy in severely demented patients during treatment with memantine)," International journal of geriatric psychiatry, 14(2), pp. 135–146. Doi 10.1002/(sici)1099-1166(199902)14:2<135: aid-gps906>3.0.co;2-0.*

*Wollmuth, L. P. (2018) "Ion permeation in ionotropic glutamate receptors: still dynamic after all these years," Current opinion in physiology, 2, pp. 36–41. doi 10.1016/j.cophys.2017.12.003.*

*Wong, T. P. et al. (1999) "Reorganization of cholinergic terminals in the cerebral cortex and hippocampus in transgenic mice carrying mutated presenilin-1 and amyloid precursor protein transgenes," The Journal of neuroscience: the official journal of the Society for Neuroscience, 19(7), pp. 2706–2716. doi: 10.1523/jneurosci.19-0702706.1999.*

*Wyllie, D. J. A., Livesey, M. R. and Hardingham, G. E. (2013) "Influence of GluN2 subunit identity on NMDA receptor function," Neuropharmacology, 74, pp. 4–17. doi: 10.1016/j.neuropharm.2013.01.016.*

*Y. Shimada, H. Goto, T. Itoh, I. Sakakibara, M. Kubo, H. Sasaki, K. Terasawa Evaluation of the protective effects of alkaloids isolated from the hooks and stems of Uncaria sinensis on glutamate-induced neuronal death in cultured cerebellar granule cells from rats J. Pharm. Pharmacol., 51 (1999), pp. 715-722*

*Yang, Y. et al. (2013) "Nicotinic α7 receptors enhance NMDA cognitive circuits in the dorsolateral prefrontal cortex," Proceedings of the National Academy of Sciences of the United States of America, 110(29), pp. 12078–12083. doi 10.1073/pnas.1307849110.*

*Yeung, J. H. Y. et al. (2019) "The acute effects of amyloid-Beta1-42 on glutamatergic receptor and transporter expression in the mouse hippocampus," Frontiers in neuroscience, 13, p. 1427. doi: 10.3389/fnins.2019.01427.*

*Zhang J-M., Hu G-Y. Huperzine A, a nootropic alkaloid, inhibits N-methyl-Daspartate-induced current in rat-dissociated hippocampal neurons. Neurosci. 2011; 105:663–669*

*Zhang, X.-M. and Luo, J.-H. (2013) "GluN2A versus GluN2B: twins, but quite different," Neuroscience Bulletin, 29(6), pp. 761–772. doi 10.1007/s12264-013-1336-9.*